Kinetic modelling of steady-state CO fermentation by *Clostridium autoethanogenum*

Iris Kerkhof

TU Delft

Kinetic modelling of steady-state CO fermentation by *Clostridium autoethanogenum*

by

Iris Kerkhof

In partial fulfillment of the requirements for the degree of

Master of Science

in Life Science and Technology with an emphasis on Biochemical Engineering
and Cell Factory at the Delft University of Technology,
to be defended publicly on Tuesday May 28th, 2024 at 11:00 AM

Student number
5101956

Project duration
September 4th, 2023 - May 28th, 2024

Daily supervisors
Dr. ir. E. F. Almeida Benalcázar
Ir. Lars Puiman

Thesis committee
Dr.ir. A. J. J. Straathof, TU Delft, supervisor
Dr. L. Jourdin, TU Delft
Dr. D. Bajić, TU Delft

Faculty of Applied Sciences
Department of Biotechnology
Section Bioprocess Engineering

All models are wrong, but some are useful

- George Box

Abstract

The stability of our planet is threatened by climate change, necessitating a shift towards a circular economy in the (bio-)chemical industry to sustainably meet our increasing product demand. Syngas fermentation by acetogenic bacteria, such as *Clostridium autoethanogenum*, has been identified as a sustainable alternative for the production of biofuels and other chemicals. These bacteria harbour the Wood-Ljungdahl pathway (WLP), enabling them to convert carbon monoxide (CO), carbon dioxide (CO_2) and hydrogen (H_2) into acetate and ethanol. Several process parameters influence the outcome of syngas fermentation and their effects on the metabolic behaviour of syngas fermenting bacteria can be quantified through kinetic modelling.

This study aimed to build a simple quantitative model for steady-state CO fermentation by *C. autoethanogenum* using unstructured microbial kinetics and the current insights into the ATP production of the CO pathways to acetate and ethanol. To this aim, a dataset compromising 37 steady-state lab-scale syngas fermentations was compiled. Incomplete data was reconciled and recovery gaps were addressed through data reconciliation applied to the dataset. Furthermore, the growth kinetics of *C. autoethanogenum* was described by coupling ATP production in the catabolism to energy requirements for growth and maintenance through a modified Herbert-Pirt equation. Finally, a preliminary model for CO fermentation by *C. autoethanogenum* was presented, which given the gas inflow rate, gas inflow composition and liquid dilution rate should predict the consumption and production rates. Moreover, this study emphasizes the necessity for methodologies to measure dissolved gas concentrations and highlights the research gap concerning gas uptake kinetics in syngas fermentation.

Nomenclature

Abbreviations

General	
BCR	Bubble column reactor
CSTR	Continuous stirred tank reactor
PMF	Proton motive force
SLP	Substrate level phosphorylation
SST	Steady-state
WLP	Wood-Ljungdahl pathway

(Bio-)chemical compounds	
AcT	Total acetate
Ac	Acetate
Ac-CoA	Acetyl-CoA
ADH	Alcohol dehydrogenase
ADP	Adenosine diphosphate
AOR	Aldehyde:ferredoxin oxidoreductase
ATP	Adenosine triphosphate
ATPase	ATP synthase
BDO	2,3-butanediol
CO	Carbon monoxide
CO_2	Carbon dioxide
CODH	CO dehydrogenase
EtOH	Ethanol
Fd	Ferredoxin
H_2	Hydrogen
H^+	proton
HAc	Acetic acid
H_2O	Water
NADH	Nicotinamide adenine dinucleotide
NADHP	Nicotinamide adenine dinucleotide phosphate
NH_3	Ammonia
O_2	Oxygen
P(i)	Phosphate
X	Biomass

Symbols

Symbol	Description	Unit
a	Interfacial area	m^2
A	Cross-sectional area	m^2
c	Concentration	mol/L or g/L
c*	Solubility	mol/L
d_B	Bubble diameter	m
D	Dilution rate	h^{-1}
D_i	Stirrer diameter	m
D_L	Diffusivity constant	cm^2/s
f_{broth}	broth enhancement factor	-
F_g^N	Molar gas flow rate	mol/h
F_g^V	Volumetric gas flow rate	mL/min or m^3/s
F_L^V	Volumetric liquid flow rate	L/h
G	Gibbs free energy	kJ/mol
H	Reactor height	m
H	Enthalphy change	kJ/mol
k_L	Mass transfer coefficient	m/h
k_La	Volumetric mass transfer coefficient	h^{-1}
K	Affinity constant	mol/L
K_I	Inhibition constant	mol/L
m	Maintenance requirements	mol/(g_{DW} h) or h^{-1}
Mw	Molecular weight	g/mol
N	Agitation speed	rpm or s^{-1}
$N_{C,i}$	Number of carbons atoms in compound i	-
N_i	Number of stirrers	-
N_p	Power number	-
p	Pressure	atm or Pa
P	Permeability constant	dm/h
P	Gassed power input	W
P_0	Ungassed power input	W
pH	pH	-
pK_a	Acid dissociation constant	-
q	Biomass specific rate	mol/(g_{DW} h)
r	Diffusion rate	mol/(g_{DW} h)
R	Overall rate	mol/h
T	Temperature	K or ^oC
T	Reactor width	m
T_N	Gas-liquid transfer rate	mol/h
$u_{G,s}$	Superficial gas velocity	m/s
V_L	Liquid broth volume	L or m^3
V_R	Total reactor volume	L
y	Mole fraction	mol/mol_{gas}
$Y_{i/j}$	Yield	mol_i/mol_j or g_i/mol_j

Symbol	Description	Unit
α	Henry constant	mol/(m^3 Pa)
ε_g	Gas hold-up	-
μ	Growth rate	h^{-1}
γ_i	Degree of reduction of compound i	-
ρ	Density	kg/m^3

Superscripts and Subscripts

Symbol	Meaning
0	Coalescing broth
0	Standard conditions
01	Biochemical standard conditions
1	Non-coalescing broth
an	Anabolism
cat	Catabolism
DW	Dry weight (biomass)
f	Formation
g	Gas phase
i	Species
in	Incoming
L	Liquid phase
max	maximum
met	Metabolism
N	Molar
out	Outgoing
ox	Oxidized
p	Product
R	Reaction
s	Substrate
s	Standard
T	Temperature corrected
tot	total
V	Volume

Contents

1 Introduction

Climate change poses a profound threat to the stability and sustainability of our planet, impacting ecosystems, weather patterns, and global economies. As our demand for products grows, the (bio-)chemical industry must adapt by transitioning to a more circular economy. This involves rethinking product life cycles to prioritize renewable resources, enhancing energy efficiency, and reducing waste and emissions. By adopting innovative technologies and sustainable practices, the (bio-)chemical industry can help mitigate the effects of climate change while meeting consumer needs. Ultimately, this transformation is crucial for ensuring a healthier, more resilient environment for future generations (Ewing et al., 2022; Fackler et al., 2021).

Syngas, a blend of carbon monoxide (CO), hydrogen (H_2), and carbon dioxide (CO_2), has traditionally been produced by fossil fuel industries (Liew et al., 2016; Liew et al., 2017). However, recent advancements in novel methods, such as biomass and waste gasification, as well as CO_2 and water electroreduction, have enabled syngas production from renewable sources (Liew et al., 2016; Liew et al., 2017; Lu et al., 2020). Anaerobic carbon-fixating acetogenic bacteria are capable of converting syngas into ethanol (solventogenesis) and acetate (acetogenesis) (Figure 1.1a). Especially, the gas fermentation model organism *Clostridium autoethanogenum* (*C. autoethanogenum*) stands out as a robust and versatile platform for gas fermentation, having already been used in industrial processes (Abubackar et al., 2011; Marcellin et al., 2016). *C. autoethanogenum* uses the Wood-Ljungdahl pathway (WLP) for the reduction of CO and CO_2 (in the presence of H_2) into acetyl-CoA, which is a key intermediate compound for growth and the production of valuable metabolites, such as ethanol, acetic acid, and 2,3-butanediol (Abubackar et al., 2011; Arslan et al., 2019; Ljungdhal, 1986; Wood, 1991).

Microorganisms generate energy in the form of adenosine triphosphate (ATP) during catabolism. This energy is required for both cell growth and non-growth-related processes (Figure 1.1b). The latter is often termed cell maintenance and encompasses all energy-consuming processes unrelated to the synthesis of new cellular material. Examples of such processes are the continuous breakdown and synthesis of macromolecules and the maintenance of concentration gradients across cellular membranes (van Bodegom, 2007).

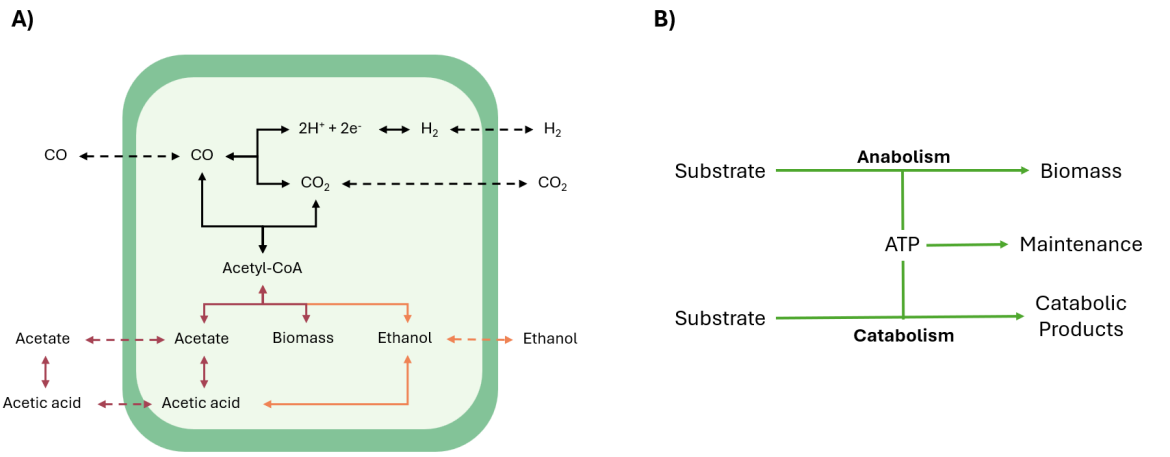

Figure 1.1: A) Schematic representation of the metabolism of anaerobic syngas fermenting acetogenic bacteria. With the reactions of the Wood-Ljungdahl pathway in black, acetogenesis and cell growth in red, and solventogenesis in orange. Adapted from Valgepea, de Souza Pinto Lemgruber, et al. (2017) and Puiman (2020). B) Schematic representation of the metabolism. ATP is generated during catabolism, which coincides with the formation of catabolic products. The generated ATP is used for maintenance, and biomass formation during anabolism.

Energy conservation in ATP can achieved through two methods: substrate level phosphorylation (SLP) and chemiosmotic ion gradient-drive phosphorylation (Figure 1.2). SLP involves coupling the energy released in a chemical reaction with the direct phosphorylation of ADP, thereby producing ATP. Chemiosmotic energy conservation is an indirect mechanism that links an exergonic reaction to the movement of ions across a membrane, leading to the formation of a transmembrane electrochemical ion gradient. In C. autoethanogenum, the Rnf complex generates this gradient, known as the proton motive force (PMF), by facilitating proton translocation across the membrane. Subsequently, the PMF drives ATP synthesis through the membrane-bound ATP synthase (ATPase) (Liew et al., 2016; Schuchmann and Müller, 2014). Since the WLP does not result in a net production of ATP, *C. autoethanogenum* relies on chemiosmotic energy conservation to conserve energy (Fernández-Blanco et al., 2023; Schuchmann and Müller, 2014).

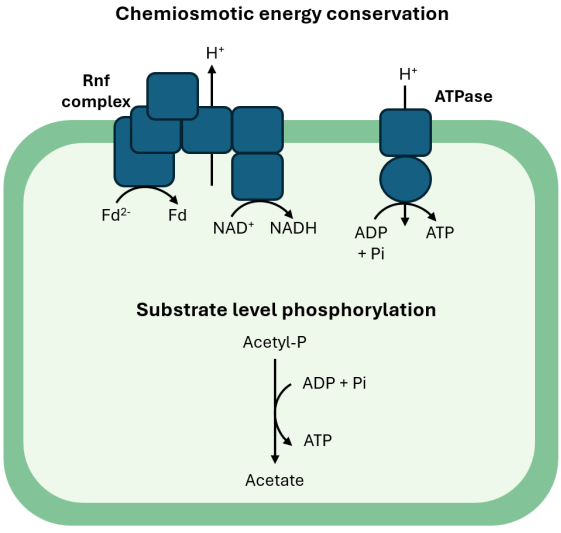

Figure 1.2: Schematic representation of the energy conservation methods in *Clostridium autoethanogenum*. The highly energetic phosphate-group (P) is transferred from acetyl-P to ADP, generating ATP directly through substrate level phosphorylation (SLP). ATP is indirectly formed through chemiosmotic energy conservation. Reduced ferredoxin (Fd) is oxidised and releases its electrons to the Rnf-complex. The electrons are transferred to NAD^+, forming NADH. The energy released during the electron transfer is used to pump protons (H^+) over the membrane. This generates a proton motive force (PMF) that drives ATP-synthesis by the membrane-bound ATP synthase (ATPase). Adapted from Schuchmann and Müller (2014).

Syngas fermentation by acetogenic microorganisms involves two distinct phases: acidogenesis and solventogenesis (Figure 1.1a). During acidogenesis, acetyl-CoA is converted into acetate and acetic acid. This reaction is favoured under optimal growth conditions and is coupled to biomass growth (Fernández-Blanco et al., 2023; Katsyv and Müller, 2020; Molitor et al., 2016). Ethanol is produced from acetyl-CoA and acetic acid reduction during solventogenesis (Fernández-Blanco et al., 2023). Acetogenic bacteria switch from acidogenesis to solventogenesis in response to stress factors, such as changes in pH and nutrient limitations, which hinder optimal growth (Abubackar et al., 2011; Fernández-Blanco et al., 2023). Other key parameters that influence the outcome of a syngas fermentation include the liquid dilution rate, gas-liquid mass transfer, pressure and product concentrations (Abubackar et al., 2011; Fernández-Blanco et al., 2023; Puiman et al., 2022; Sun et al., 2019). The effects of these parameters on the metabolic behaviour of syngas fermenting acetogenic bacteria can be described by kinetic modelling, enabling systematic process optimization and leading to more sustainable processes (de Medeiros et al., 2019; Greene et al., 2019). Nevertheless, the incorporation of microbial kinetics into syngas fermentation models has only started to gain traction in recent years (Almeida Benalcázar, 2023; Chen et al., 2015; de Medeiros et al., 2019; Greene et al., 2019; Jang et al., 2017; Puiman et al., 2023; Ruggiero et al., 2022).

Model structures range from complex to simple, depending on the modelling purpose. For process optimization, a simple unstructured kinetic model already suffices to predict product, substrate and biomass concentrations during fermentation (Almquist et al., 2014; Straathof, 2023b). Unstructured kinetic models focus on the apparent production and consumption rates from metabolic processes conducted by microorganisms, by setting up basic conservation relations over the studied system (González-Figueredo et al., 2018). In particular, unstructured kinetic models that include ATP availability are appealing, as insights into the energetic requirements of cellular processes allow for a more accurate representation of microbial growth and product formation (Heijnen and Kleerebezem, 2010; Straathof, 2023b).

This study aimed to develop a simple quantitative model for steady-state CO fermentation by *C. autoethanogenum* using unstructured microbial kinetics and the current insights in the ATP production of the CO pathways to ethanol and acetate. To this aim, a background literature review was performed to obtain an inventory of experimental steady-state syngas fermentation data. Subsequently, kinetic model equations that incorporate the ATP metabolism of *C. autoethanogenum* were derived and model parameters were fitted with the obtained dataset. The focus of this study is solely on CO fermentation, as CO serves as both a carbon and electron source for syngas-fermenting bacteria.

2

Methods

This chapter describes the methods and equations used in this study, including the underlying assumptions. First, the establishment of the experimental dataset will be discussed. Next, detailed descriptions of data reconciliation and calculation of missing parameters are provided, followed by an explanation of the methods employed for fitting the kinetic parameters.

2.1. Literature data

The experimental data obtained from literature included the process parameters, such as the agitation speed (N), process temperature (T), pressure (p), pH, and liquid broth volume (V_L). Additionally, the concentrations (c_i) of cell biomass (X), ethanol (EtOH), acetic acid (total of acetic acid in the dissociated and associated form) (AcT), and 2,3-butanediol (BDO) were provided. The gas inflow rate ($F^V_{g,in}$), as well as, the composition of the gas inflow ($y_{i,in}$) were specified. Though, the gas fraction in the off-gas ($y_{i,out}$) were only provided for the steady states by de Lima et al. (2022), Elisiário et al. (2023), Valgepea, de Souza Pinto Lemgruber, et al. (2017), and Valgepea et al. (2018) through personal correspondence (Straathof, 2023a; Valgepea, 2024). Additionally, the biomass-specific rates (q_i) and growth rate (μ) were stated. For hydrogen (H_2) and BDO production, the production rates were not always specified and therefore assumed to be zero in these cases. Furthermore, in cases where either the liquid dilution rate (D) or growth rate was specified, it was assumed that they were equal. The liquid outflow rate ($F^V_{L,out}$) was derived from the liquid dilution rate and the liquid broth volume (Eq. (2.1)). For the experimental dataset, it was assumed that the change in flow sizes due to gas-liquid mass transfer and the change in broth density due to the conversion of substrates into products were negligible, such that the liquid inflow rate ($F^V_{L,in}$) equals the liquid outflow rate. Additionally, technical bioreactor information, such as the total reactor volume (V_R), stirrer diameter (D_i) and number of stirrers (N_i) was either obtained from literature or assumed according to the reactor manuals (Applikon, 2008; Infors HT, 2023). While the standard deviations were reported for most parameters, a standard deviation of 5% was presumed when not explicitly stated.

$$F^V_{L,out} = V_L \cdot D \tag{2.1}$$

with $F^V_{L,out}$ the liquid inflow rate in L/h, V_L the liquid volume in L, and D the dilution rate in h^{-1}

2.2. Data Reconciliation

Data reconciliation was performed in Python (version 3.9.12), using the libraries listed below (Table 2.1). Furthermore, self-implemented functions are listed in Appendix A.

Table 2.1: Python libraries used for data reconciliation

Library	Version	Used for
pandas	1.4.2	Importing and exporting of Excel data
NumPy	1.21.5	Array operations and numerical computing
SciPy	1.7.3	Curve fitting
matplotlib	3.5.1	Data plotting

2.2.1. Elemental Recovery

The elemental recovery is defined as the amount of substrate elements that are recovered in the product (Wahl and Heijnen, 2021). Here, only the elemental recovery of carbon atoms ($N_{C,i}$) and degree of reduction (γ_i) were considered (Table 2.2). Since the composition of the gas feed varied between the steady-state fermentations in the dataset, the equation used to calculate the carbon and electron recoveries varied depending on the specific composition of the gas feed (Eq. (2.2)-(2.3)).

$$C\%_{recovery} = \frac{\sum N_{C,i} \cdot q_{i,in}}{\sum N_{C,i} \cdot q_{i,out}} \cdot 100\% \tag{2.2}$$

$$e^{-}\%_{recovery} = \frac{\sum \gamma_i \cdot q_{i,in}}{\sum \gamma_i \cdot q_{i,out}} \cdot 100\% \tag{2.3}$$

with $N_{C,i}$ the number of carbon atoms in compound i, γ_i the degree of reduction of compound i, $q_{i,in}$ the biomass-specific consumption rates in mol/(g_{DW} h), and $q_{i,out}$ the biomass-specific production rates in mol/(g_{DW} h)

Table 2.2: The molecular weight (Mw), number of carbon atoms ($N_{C,i}$) and degree of reduction (γ_i) of the compounds present in the fermentation broth, with γ_C = +4, γ_H = +1, γ_O = -2, γ_N = -3, γ_- = +1, and γ_+ = -1. a: From Norman et al. (2019).

Compound	Chemical formula	Abbreviation	Mw [g/mol]	$N_{C,i}$ [-]	γ_i [-]
Carbon monoxide	CO	CO	28.01	1	2
Carbon dioxide	CO_2	CO_2	44.01	1	0
Hydrogen	H_2	H_2	2.016	0	2
Ethanol	C_2H_5OH	EtOH	46.068	2	12
Acetate	$C_2H_3O_2^-$	Ac^-	59.044	2	8
Acetic acid	$C_2H_4O_2$	HAc	60.052	2	8
2,3-butanediol	$C_4H_{10}O_2$	BDO	90.121	4	22
Biomass	$CH_{1.52}O_{0.46}N_{0.28}S_{0.0059}P_{0.042}$ [a]	X	26.31	1	3.76

2.2.2. Rates and rate reconciliation

In order to find the biomass-specific rates that satisfy the principle of elemental conservation, the overall rates (R_i) were determined first (Eq. (2.4)).

$$R_i = q_i \cdot V_L \cdot c_X \tag{2.4}$$

with R_i the production or consumption rate for compound i in mol/h, q_i the biomass-specific rate for compound i in mol/(g_{DW} h), V_L the liquid broth volume in L, and c_X the biomass concentration in g_{DW}/L

The overall rates, liquid inflow rate, and liquid outflow rate were recalculated by establishing a weighted minimization problem with linear boundary conditions. The goal was to find new estimates that adhere to the principle of elemental and mass conservation (see Appendix B). In short, the optimization problem minimizes the error in the measured rates (ε) to find new rate estimates that satisfy the linear equality constraints (Eq. (2.5)-(2.6)). In this study, the linear equality constraints are defined as the carbon

balance (Eq. (2.7)), the degree of reduction balance (Eq. (2.8)), and the total liquid mass balance (Eq. (2.9)). The density of the liquid phase (ρ_L) was assumed to be 1000 kg/m^3.

$$R_i = R_{m,i} + \varepsilon \tag{2.5}$$
$$F_L^V = F_{L,m}^V + \varepsilon \tag{2.6}$$

with $R_{m,i}$ the measured overall rate for compound i in mol/h, R_i the new overall rate estimate for compound i in mol/h, ε the error in the measured rate in mol/h, $F_{L,m}^V$ the measured liquid inflow or outflow rate in L/h, and F_L^V the new liquid inflow or outflow rate estimate in L/h

$$N_{C,CO} \cdot R_{CO} + N_{C,CO_2} \cdot R_{CO_2} + N_{C,EtOH} \cdot R_{EtOH} + N_{C,AcT} \cdot R_{AcT} + N_{C,BDO} \cdot R_{BDO} + N_{C,X} \cdot R_X = 0 \tag{2.7}$$
$$\gamma_{CO} \cdot R_{CO} + \gamma_{H_2} \cdot R_{H_2} + \gamma_{EtOH} \cdot R_{EtOH} + \gamma_{AcT} \cdot R_{AcT} + \gamma_{BDO} \cdot R_{BDO} + \gamma_X \cdot R_X = 0 \tag{2.8}$$
$$-Mw_{CO} \cdot R_{CO} - Mw_{H_2} \cdot R_{H_2} - Mw_{CO_2} \cdot R_{CO_2} + \rho_L \cdot F_{L,in}^V - \rho_L \cdot F_{L,out}^V = 0 \tag{2.9}$$

with $N_{C,i}$ the number of carbons in compound i, R_i the overall rate for compound i in mol/h, γ_i the degree of reduction of compound i, Mw_i the molecular weight of compound i in g/mol, $F_{L,in}^V$ the liquid inflow rate in L/h, $F_{L,out}^V$ the liquid outflow rate in L/h, and ρ_L the density of the liquid phase in g/L

2.2.3. Gas outflow

The gas outflow rate ($F_{g,out}^N$) and off-gas composition were obtained from the estimated rates by solving a system of 5 equations, consisting of 4 mass balances for the compounds present in the gas phase (Eq. (2.10)-(2.13)), and the unity balance of the gas fractions in the off-gas (Eq. (2.14)). It was assumed that the dissolved gas concentrations in the liquid outflow are negligible, such that the gas-liquid mass transfer rates ($T_{N,i}$) of CO, H_2, and CO_2 are equal to the consumption (or production) rate of the respective gas.

$$F_{g,in}^N \cdot y_{CO,in} - F_{g,out}^N \cdot y_{CO,out} + R_{CO} = 0 \tag{2.10}$$
$$F_{g,in}^N \cdot y_{H_2,in} - F_{g,out}^N \cdot y_{H_2,out} + R_{H_2} = 0 \tag{2.11}$$
$$F_{g,in}^N \cdot y_{CO_2,in} - F_{g,out}^N \cdot y_{CO_2,out} + R_{CO_2} = 0 \tag{2.12}$$
$$F_{g,in}^N \cdot y_{inert,in} - F_{g,out}^N \cdot y_{inert,out} = 0 \tag{2.13}$$
$$y_{CO,out} + y_{H_2,out} + y_{CO_2,out} + y_{inert,out} = 1 \tag{2.14}$$

with $F_{g,in}^N$ the gas inflow rate in mol/h, $F_{g,out}^N$ the gas outflow rate in mol/h, $y_{i,in}$ the molar fraction of compound i in the gas inflow, $y_{i,out}$ the molar fraction of compound i in the gas outflow, R_i the overall rate for compound i in mol/h

2.2.4. Concentrations and biomass-specific rates

The new outflow concentrations estimates were calculated using the biomass, ethanol, total acetate, and 2,3-butanediol mass balances in the liquid phase (Eq. (2.15)-(2.18)). The biomass-specific rates and growth rate were recalculated with the new biomass concentration estimate (Eq. (2.19)-(2.20)).

$$c_{X,in} \cdot F_{L,in}^V - c_{X,out} \cdot F_{L,out}^V + R_X \tag{2.15}$$
$$c_{AcT,in} \cdot F_{L,in}^V - c_{AcT,out} \cdot F_{L,out}^V + R_{AcT} \tag{2.16}$$
$$c_{EtOH,in} \cdot F_{L,in}^V - c_{EtOH,out} \cdot F_{L,out}^V + R_{EtOH} \tag{2.17}$$
$$c_{BDO,in} \cdot F_{L,in}^V - c_{BDO,out} \cdot F_{L,out}^V + R_{BDO} \tag{2.18}$$

with $F_{L,in}^V$ the liquid inflow rate in L/h, $F_{L,out}^V$ the liquid outflow rate in L/h, $c_{i,in}$ the concentration of compound i in the inflow in mol/L, $c_{i,out}$ the concentration of compound i in the outflow in mol/L, and R_i the overall rate for compound i in mol/h

$$q_i = \frac{R_i}{c_X \cdot V_L} \tag{2.19}$$

$$\mu = \frac{R_X}{c_X \cdot V_L} \tag{2.20}$$

with q_i the biomass specific rate for compound i in mol/(g_{DW} h), R_i the overall rate for compound i in mol/h, c_X the biomass concentration in g_{DW}/L, V_L the liquid broth volume in L, and μ the growth rate in h^{-1}

2.3. Gas-liquid mass transfer

2.3.1. Continuous stirred tank reactor

For the steady-state fermentations performed in a continuous stirred tank reactor (CSTR), the volumetric mass transfer coefficients for CO, H_2 and CO_2 (k_La_i) were determined according the correlations proposed by Van't Riet (1979) for air in water at 20 ^oC in a coalescing and non-coalescing medium (Eq. (2.21)-(2.22)). As medium components and products in the fermentation broth affect the mass transfer (Puiman et al., 2022), it was assumed that the k_La lies between a minimum and maximum k_La, which are here defined as the k_La in a coalescence medium ($k_La_{O_2,0}$) and non-coalescence medium ($k_La_{O_2,1}$), respectively. The volumetric mass transfer coefficient for O_2 in water at 20 ^oC adjusted for the medium composition ($k_La_{O_2}$) was calculated as the weighted sum of the $k_La_{O_2,0}$ and $k_La_{O_2,1}$ (Eq. (2.23)). The weight was defined by the broth enhancement factor (f_{broth}) and had a value between 0 and 1, with 0 representing a coalescing broth and 1 a non-coalescing broth, respectively. Subsequently, the $k_La_{O_2}$ was corrected for the process temperature, and gas type (Eq. (2.24)) with to the compound-specific diffusion coefficient ($D_{L,i}$) (Table 2.3).

$$k_La_{O_2,0} = 3600 \cdot \left(0.026 \cdot \left(\frac{P}{V_L}\right)^{0.4} {u_{G,s}}^{0.5}\right) \tag{2.21}$$

$$k_La_{O_2,1} = 3600 \cdot \left(0.002 \cdot \left(\frac{P}{V_L}\right)^{0.7} {u_{G,s}}^{0.2}\right) \tag{2.22}$$

$$k_La_{O_2} = (1 - f_{broth}) \cdot k_La_{O_2,0} + f_{broth} \cdot k_La_{O_2,1} \tag{2.23}$$

$$k_La_i = k_La_{O_2} \cdot 1.022^{T-293.15} \cdot \sqrt{\frac{D_{L,i}}{D_{L,O_2}}} \tag{2.24}$$

with $k_La_{O_2,0}$ the volumetric mass transfer coefficient for O_2 in water at 20 ^oC for a coalescing broth in h^{-1}, $k_La_{O_2,1}$ the volumetric mass transfer coefficient for O_2 in water at 20 ^oC for a non-coalescing broth in h^{-1}, $k_La_{O_2}$ the volumetric mass transfer coefficient for O_2 in water at 20 ^oC corrected for broth composition in h^{-1}, k_La_i the volumetric mass transfer coefficient for compound i corrected for temperature in water in h^{-1}, P the gassed power input in W, V_L the liquid broth volume in m^3, $u_{G,s}$ the superficial gas velocity in m/s, f_{broth} the broth enhancement factor, T the process temperature in K, and $D_{L,i}$ the diffusivity of compound i in water in cm^2/s

Table 2.3: Diffusivity constant in water at 25 ^oC ($D_{L,i}$), Henry coefficient in water at 25 ^oC (α_i^0), and temperature dependency of $\alpha_i^0 \left(\frac{d(ln(\alpha_i))}{d(1/T)}\right)$. a: From Cussler (1997). b: From Sander (2023).

Compound	$D_{L,i}$ [a] [cm^2/s]	α_i^0 [b] [mol/(m^3 Pa)]	$\frac{d(ln(\alpha_i))}{d(1/T)}$ [b] [K]
CO	$2.03 \cdot 10^{-5}$	$9.7 \cdot 10^{-6}$	1300
H_2	$4.5 \cdot 10^{-5}$	$7.7 \cdot 10^{-6}$	490
CO_2	$1.92 \cdot 10^{-5}$	$3.4 \cdot 10^{-4}$	2300
O_2	$2.10 \cdot 10^{-5}$	$1.3 \cdot 10^{-5}$	1500

The volumetric mass transfer coefficient in a CSTR depends on the superficial gas velocity ($u_{G,s}$) (Eq. (2.25)) and the average power input per volume of the stirrer(s) (P/V_L). The superficial gas velocity was calculated assuming an aspect ratio (H/T) of 1.5 (Almeida Benalcázar, 2023). In aerated systems, the broth density is reduced by sparging of bubbles, such that the power consumption decreases. Therefore, the average power input per volume of the stirrer(s) was estimated from the ungassed power input (P_0) according to Eq. (2.26)-(2.28) (Cui et al., 1996; de Medeiros et al., 2019; Garcia-Ochoa and Gomez, 2009). Furthermore, a power number (N_p) of 6 (Noorman et al., 2018) and a liquid broth density of 1000 kg/m^3 were assumed.

$$u_{G,s} = \frac{F_{g,in}^V}{\frac{\pi}{4} \cdot \left(\frac{4 \cdot V_R}{(\pi \cdot H/T)^{\frac{1}{3}}} \right)^2} \tag{2.25}$$

$$P_0 = N_i \cdot N_p \cdot \rho_L \cdot N^3 \cdot {D_i}^5 \tag{2.26}$$

$$\frac{F_{g,in}^V \cdot N^{0.25}}{{D_i}^2} \leq 0.005, \ \left(1 - \frac{P}{P_0}\right) = 9.9 \cdot \left(\frac{F_{g,in}^V \cdot N^{0.25}}{{D_i}^2} \right) \tag{2.27}$$

$$\frac{F_{g,in}^V \cdot N^{0.25}}{{D_i}^2} \geq 0.005, \ \left(1 - \frac{P}{P_0}\right) = 0.52 + 0.62 \cdot \left(\frac{F_{g,in}^V \cdot N^{0.25}}{{D_i}^2} \right) \tag{2.28}$$

with $u_{G,s}$ the superficial gas velocity in m/s, $F_{g,in}^V$ the gas inflow rate in m^3/s, V_R the total reactor volume in m^3, H/T the reactor aspect ratio, P_0 the ungassed power input in W, P the gassed power input in W, N_i the number of impellers, N_p the power number, ρ_L the liquid density in kg/m^3, N the agitation speed in s^{-1}, and D_i the impeller diameter in m

2.3.2. Bubble column

The steady-state fermentations by Chen et al. (2018) (SST 25, 26 & 27) were performed in a bubble column reactor (BCR), of which the most important parameters are provided in Table 2.4. The volumetric mass transfer coefficient in BCRs was calculated according to Eq. (2.29)-(2.30). Here, a mass transfer coefficient (k_L) of $0.1 \cdot 10^{-3}$ m/s (for small rigid bubbles) and a bubble diameter (d_B) of $1.2 \cdot 10^{-3}$ m were assumed (Noorman et al., 2018; van der Lans, 2003).

$$a = \frac{6 \cdot \varepsilon_g}{d_B} \tag{2.29}$$

$$k_L a_{O_2} = k_L \cdot a \tag{2.30}$$

with a the interfacial area in m^2, ε_g the gas hold-up, d_B the bubble diameter in m, $k_L a_{O_2}$ the volumetric mass transfer coefficient of O_2 in water at 20 ^{o}C in h^{-1}, and k_L the mass transfer coefficient in m/h

Table 2.4: Parameters for gas-liquid mass transfer calculations in a bubble column reactor for the steady-state fermentations by Chen et al. (2018). a: Extracted from Figure 6 (Chen et al., 2018).

Parameter	Unit	SST 25	SST 26	SST 27
Reactor length (H)	[m]	1.06	1.06	1.06
Reactor cross-sectional area (A)	[m^2]	0.002436	0.002436	0.002436
Superficial gas velocity ($u_{G,s}$)	[m/s]	0.0033^a	0.0041^a	0.0048^a
Gas hold-up (ε_g)	[-]	0.309	0.356	0.378

2.3.3. Dissolved gas concentrations

The dissolved gas concentrations were calculated according to Eq. (2.31). Before the solubility (c_i^*) of CO, H_2 and CO_2 were calculated (Eq. (2.32)), the Henry coefficients (α_i) of the gasses were corrected for the process temperature according to Eq. (2.33). The Henry coefficients and the temperature dependencies of the gasses are listed in Table 2.3. It was assumed that the dissolved gas concentrations in the liquid outflow are negligible, such that the gas-liquid transfer rate of the gasses equals their respective overall rates.

$$T_{N,i} = R_i = k_L a_i \cdot V_L \cdot (c_i^* - c_i) \tag{2.31}$$

$$c_i^* = p \cdot y_{i,out} \cdot \alpha_i \tag{2.32}$$

$$\alpha_i = \alpha_i^0 \cdot \exp\left[\frac{d(ln(\alpha_i))}{d(1/T)} \cdot \left(\frac{1}{T} - \frac{1}{293.15}\right)\right] \tag{2.33}$$

with $T_{N,i}$ the gas-liquid transfer rate for compound i in mol/h, R_i the overall rate for compound i in mol/h, $k_L a_i$ the volumetric mass transfer coefficient for compound i corrected for temperature in water in h^{-1}, V_L the liquid broth volume in m^3, c_i^* the solubility of compound i in mol/m^3, c_i the dissolved gas concentration of compound i in mol/m^3, p the pressure in Pa, $y_{i,out}$ the gas outflow fraction of compound i, α_i^0 the Henry coefficient at 25 ^{o}C in mol/(m^3 Pa), α_i the temperature corrected Henry coefficient in mol/(m^3 Pa), $\frac{d(ln(\alpha_i))}{d(1/T)}$ the temperature dependency of the Henry coefficient in K, and T the process temperature in K

2.4. Parameter Fitting

Kinetic parameters were fitted with Python (version 3.9.12) using the curve fit function from SciPy's optimize module (version 1.7.3). This function uses non-linear least squares to fit the function to provided data. The fitted functions are included in Appendix A. Furthermore, an overview of used libraries is given below (Table 2.5).

Table 2.5: Python libraries used for parameter fitting

Library	Version	Used for
pandas	1.4.2	Importing and exporting of Excel data
NumPy	1.21.5	Array operations and numerical computing
SciPy	1.7.3	Curve fitting and hypothesis testing
matplotlib	3.5.1	Data plotting
scikit-learn	1.0.2	Model evaluation

3

Results and Discussion

This chapter discusses the results of building the experimental dataset and data reconciliation. Based on the ATP metabolism of *Clostridium autoethanogenum* (*C. autoethanogenum*), the growth and substrate uptake kinetic correlations are derived and form the basis of the model. Kinetic parameters are fitted with both the raw experimental data (see Appendix C) and the reconciled data (see Appendix D) to examine the effect of data reconciliation on the parameter fit. Finally, a preliminary model for CO fermentation by *C. autoethanogenum* is be presented, based on the kinetic correlations that most accurately explain the available steady-state data.

3.1. Dataset and data reconciliation

3.1.1. Literature data

A sufficiently large dataset is important to validate and fit a model for CO fermentation by *C. autoethanogenum*. Furthermore, such a dataset can help to discover relationships between variables and to gain a further quantitative understanding of syngas fermentation. Therefore, a dataset with a total of 37 steady-state syngas fermentations was created and includes work from Allaart et al. (2024), Chen et al. (2018), de Lima et al. (2022), Diender et al. (2019), Elisiário et al. (2023), Heffernan et al. (2020), Valgepea, de Souza Pinto Lemgruber, et al. (2017), and Valgepea et al. (2018). The raw experimental dataset is provided in Appendix C.

3.1.2. Data reconciliation

Measurement inaccuracies during experimentation can lead to gaps in elemental or mass balances, thus violating the general laws of conservation. Therefore, the experimental dataset was first qualitatively analysed by calculating the carbon and electron recoveries. As shown in Figure 3.1, the carbon and electron balances of most steady-state fermentations in the dataset did not close. To validate the success of the reconciliation, the carbon and electron balances were calculated after data reconciliation. The results confirmed that all carbon and electron balances closed. The reconciled dataset is provided in Appendix D.

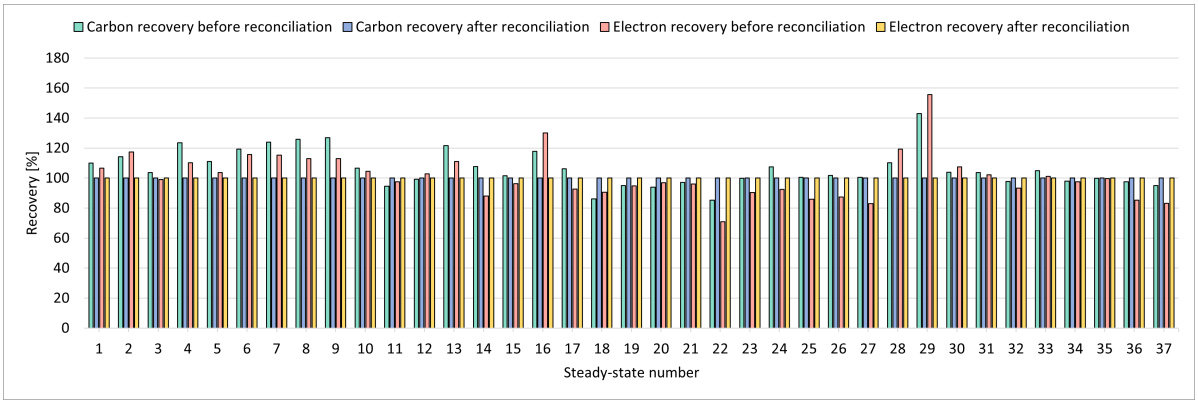

Figure 3.1: Carbon- and electron recoveries before and after data reconciliation for the 37 steady-state syngas fermentations in the dataset.

In Figure 3.2, the reconciled biomass-specific rates (q_i), concentrations (c_i), gas outflow fractions (y_i), and liquid in- and outflow (F_L^V) rates are plotted as a function of the raw experimental dataset. Overall, the reconciled data was closely aligned with the raw experimental data. Though, greater deviations were observed for steady states with larger carbon and/or electron recovery gaps. This occurs because the reconciliation process forces the carbon and electron balances to close. Consequently, steady states with larger recovery gaps must make more significant adjustments to the reconciled parameters to close the balances.

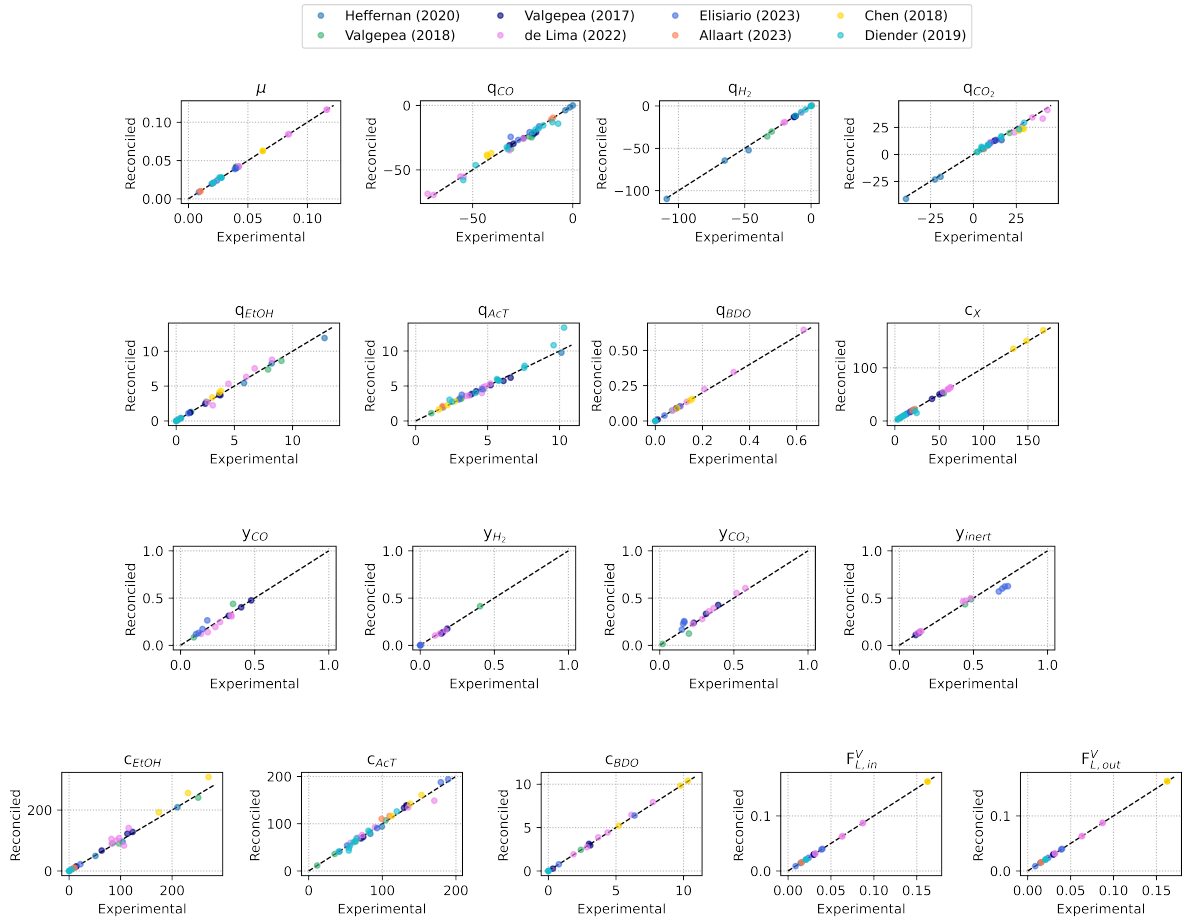

Figure 3.2: Parity plots of the biomass-specific rates (q_i), concentrations (c_i), gas fractions in the gas outflow (y_i), and liquid in- and outflow rates (F_L^V). Biomass-specific rates are in mmol/($g_{DW}h$), concentrations are in mM and in- and outflow rates are in L/h.

3.1.3. Gas-liquid mass transfer

Because the dissolved gas concentrations were not measured or specified for the steady states in the dataset, these concentrations were calculated according to general gas-liquid mass transfer correlations (Eq. (2.21)-(2.33)). The gas-liquid mass transfer data is provided in Appendix D.

The broth enhancement factor (f_{broth}) was used to correct for the broth composition of steady-state fermentations performed in a continuous stirred tank reactor (CSTR). To determine the appropriate value for f_{broth}, the dissolved gas concentrations were calculated for an f_{broth} ranging from 0 to 1. As the broth composition is different for each fermentation, it is preferable to scale each fermentation accordingly. However, the combined effect of different medium constituents is hard to quantify (Puiman et al., 2022). Therefore, it was assumed that the influence of the broth components on the gas-liquid mass transfer was equal for all fermentations. As shown in Figure 3.3, even at an f_{broth} of 1, a negative dissolved CO concentration was calculated for part of steady-state fermentations in the dataset. However, as this value was set as the upper boundary, an f_{broth} of 1 was assumed for gas-liquid mass transfer calculations.

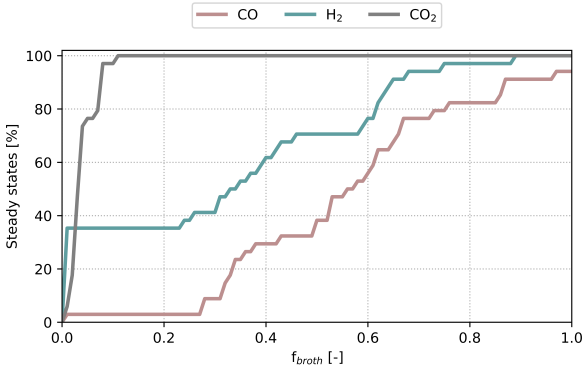

Figure 3.3: Percentage of steady-state syngas fermentations with a non-negative dissolved gas concentration performed in a continuous stirred tank reactor (CSTR). The steady states performed in a bubble column reactor (BCR) (SST 25, 26 & 27) were excluded from this analysis.

With the general as-liquid mass transfer correlations an estimation of the dissolved gas concentrations could be made. However, the validity of these estimations remains uncertain. The negative dissolved CO concentrations suggest that the volumetric mass transfer rate is underestimated by the used gas-liquid mass transfer correlations. Apparently, mass transfer is higher than anticipated for in lab-scale reactors with the low gas flow rates and gas fractions in the gas outflow as used by the steady states in the dataset (Puiman, 2024). The influence of broth constituents in this study was included through the f_{broth} correction factor, which had the same value for all steady-state fermentations in the dataset. However, variations in product, salt, and biomass concentrations between fermentation broths lead to different effects on gas-liquid mass transfer (Puiman et al., 2022). Furthermore, gas-liquid mass transfer appears to be sensitive to small differences in the reactor set-up. Specifically, the CO consumption rate for steady state 34 is three times higher than that of steady states 28 and 29, despite having similar setups and being operated under the same conditions (see Appendix C). However, this difference could be due to measurement uncertainties caused by low gas flow rates used in the study (Diender, 2024).

3.2. Derivation of kinetic model equations and parameter fitting

3.2.1. Metabolism and reaction stoichiometries

Catabolism

C. autoethanogenum uses the Wood-Ljungdahl pathway (WLP) to convert CO into acetyl-CoA (Ljungdhal, 1986; Sun et al., 2019; Wood, 1991). During catabolism, acetyl-CoA is reduced to fermentation byproducts such as ethanol (EtOH), acetate (AcT), and 2,3-butanediol (BDO), while simultaneously generating adenosine triphosphate (ATP) as an essential energy carrier for cellular growth and maintenance (Liew et al., 2016; Sun et al., 2019). Ethanol can be produced directly via acetyl-CoA or indirectly, using acetate as a precursor (Figure 3.4). In the direct route, acetyl-CoA is converted into ethanol via acetaldehyde by two alcohol dehydrogenases (ADH). In the indirect route, acetyl-CoA is initially converted into acetate. Next, acetate is reduced by aldehyde:ferredoxin oxidoreductase (AOR) and ADH into ethanol.

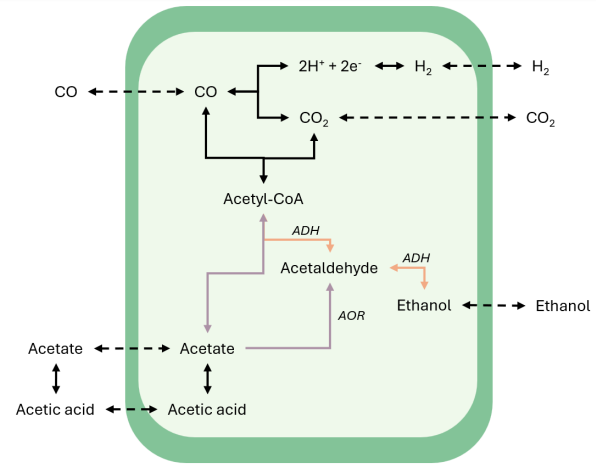

Figure 3.4: Schematic representation of the pathways for ethanol production. In the direct pathway (orange), acetyl-CoA is converted into ethanol via acetaldehyde by two alcohol dehydrogenases (ADH). Ethanol production via the indirect pathway (grey) involves reduction of acetate into acetaldehyde by aldehyde:ferredoxin oxidoreductase (AOR)

Through knockout studies and metabolomic analysis, it has been demonstrated that the indirect pathway is the preferred route for ethanol production by *C. autoethanogenum* (Diender, 2019; Liew et al., 2017; Valgepea, de Souza Pinto Lemgruber, et al., 2017). Therefore, the catabolism can be represented by two catabolic reactions, namely the production of acetate from CO (R1) (Eq. (3.1)), and the production of ethanol from acetate (R2) (Eq. (3.2)). Combining the two catabolic reactions yields the reaction for the production of ethanol from CO (R3) (Eq. (3.3)). As catabolic reaction R3 is the sum of catabolic reactions R1 and R2, it was not included in the model. Furthermore, 2,3-butanediol (BDO) and H_2 production was not always specified or low compared to the other fermentation products. Therefore, the catabolic reactions for BDO and H_2 production were not elaborated on.

$$4CO + 2H_2O \longrightarrow AcT + 2CO_2 + Y_{ATP,R1}ATP \tag{3.1}$$

$$2CO + AcT + H_2O \longrightarrow EtOH + 2CO_2 + Y_{ATP,R2}ATP \tag{3.2}$$

$$6CO + 3H_2O \longrightarrow EtOH + 4CO_2 + Y_{ATP,R3}ATP \tag{3.3}$$

In literature there exists a discrepancy between the reported ATP yields for the catabolic reactions. Katsyv and Müller (2020) reported ATP yields for catabolic reactions R1 ($Y_{ATP,R1}$) and R3 ($Y_{ATP,R3}$) of 1.5 mol/mol and 2.4 mol/mol, respectively, assuming the membrane-bound ATP synthase (ATPase) having an H^+/ATP-ratio of 3.6 and the methylene-THF reductase being electron bifurcating. Electron bifurcation by methylene-THF reductase has been supported by Munoz and Philips (2023), who reported an ATP yield for *C. autoethanogenum* grown on CO_2 and H_2 of 1.01 mol/mol, which is similar to the theoretical calculated yield of 1 mol/mol, assuming an electron bifurcating methylene-THF reductase (Katsyv and Müller, 2020). Because catabolic reaction R3 is the sum of reactions R1 and

R2, it can be deduced that the ATP yield for reaction R2 ($Y_{ATP,R2}$) is 0.9 mol/mol (2.4-1.5 = 0.9). Assuming the catabolic ATP yields reported by Katsyv and Müller (2020), the ATP yields per CO for catabolic reactions R1, R2 and R3 are 0.375, 0.45 and 0.4 mol/mol, respectively. When CO is limited, *C. autoethanogenum* will use the catabolic reaction with the highest ATP yield on CO, which is acetate reduction to ethanol (R2). However, acetate should first be produced up to a certain concentration in catabolic reaction R1. If there is an excess amount of CO, the bacterium might use its fastest catabolic reaction, which depends on the maximum reaction rate (q_R^{max}).

However, Allaart et al. (2023) reported a $Y_{ATP,R1}$, $Y_{ATP,R2}$ and $Y_{ATP,R3}$ of 1.5, 0.6 and 2.1, respectively. These ATP yields were also found in this study using the same enzymes as used by Katsyv and Müller (2020) (see Appendix E). Following these ATP yields, the ATP yields per CO for catabolic reactions R1, R2 and R3 are 0.375, 0.275 and 0.35 mol/mol, respectively. *C. autoethanogenum* will produce acetate in catabolic reaction R1 when CO is limited. When acetate becomes inhibiting, the acetate concentration will be decreased by acetate reduction into ethanol through catabolic reaction R2. In this scenario, the rate of reaction R2 would be equal to the rate of reaction R1, as using catabolic reaction R2 at a higher rate than R1 will provide an advantage towards neighbouring cells that will only keep using catabolic reaction R1. In case of an excess amount of CO, the fastest pathway might be used depending on the q_R^{max} of the catabolic reactions and the acetate concentration.

Allaart et al. (2023) proposed that *C. autoethanogenum* possesses an overflow mechanism. This term refers to a concept used to describe situations where microorganisms transition from efficiently utilizing a substrate to utilizing it inefficiently. An overflow metabolism is observed at high substrate concentrations and fast growth rates, and allows microorganisms to maintain high growth rates and adapt to fluctuations in substrate availability (Bachmann et al., 2016). Acetate production from CO in catabolic reaction R1 by *C. autoethanogenum* yields the highest ATP yield per CO and is therefore considered the longer, more efficient pathway. Allaart et al. (2023) argues that the observed increase in ethanol productivity at increasing growth rates (Figure 3.5) suggests a switch from acetate production to acetate reduction. Therefore, catabolic reaction R2 represents the shorter pathway, less efficient pathway.

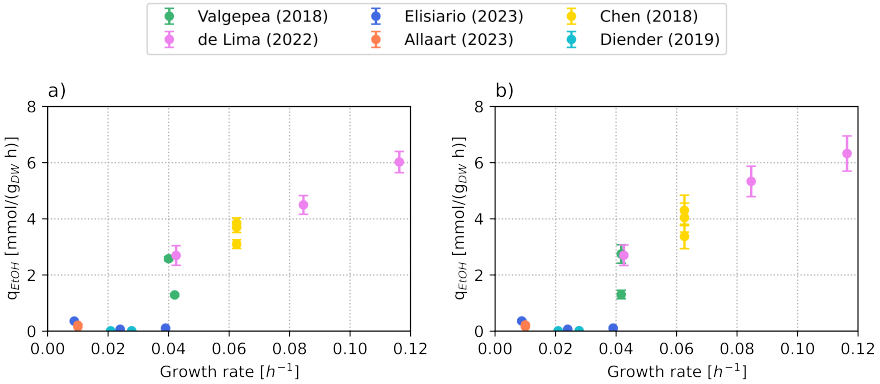

Figure 3.5: The biomass-specific ethanol production rate (q_{EtOH}) as a function of the growth rate (μ) for CO fermentation by *Clostridium autoethanogenum*. With a) the experimental data, and b) the reconciled data.

Anabolism

The energy harvested during catabolism is used for growth, which is described by the anabolic reaction (Eq. 3.4). In the anabolic reaction, CO and ammonia (NH_3) are the respective carbon and nitrogen source. Furthermore, a biomass composition of $CH_{1.52}O_{0.46}N_{0.28}$ was assumed (Norman et al., 2019). The theoretical ATP yield on biomass ($Y_{ATP/X}$) with CO as substrate for *C. autoethanogenum* has not been reported in literature. However, Valgepea, Loi, et al. (2017) reported a $Y_{ATP/X}$ of 0.042-0.056 mol/g_{DW} based on a literature study of several *Clostridial* species grown on glucose (Bahl et al., 1982; Canganella et al., 2002; Meyer Houston and Papoutsakis, 1989).

$$1.88CO + 0.34H_2O + 0.28NH_3 + Y_{ATP/X}ATP \longrightarrow CH_{1.52}O_{0.46}N_{0.28} + 0.88CO_2 \tag{3.4}$$

3.2.2. Growth kinetics

The growth kinetics of *C. autoethanogenum* are described by the Herbert-Pirt equation (Eq. (3.5)). The Herbert-Pirt equation demonstrates that consumed substrate (q_s) is distributed over growth (μ), product formation (q_p), and maintenance processes (m_s) (Pirt and Hinshelwood, 1997). When products are generated during catabolism, the rate of product formation is zero. The consumed substrate is then allocated to either growth or maintenance processes (Eq. (3.6)) (Heijnen, 2012; Straathof, 2023b).

$$-q_s = \frac{1}{Y_{x/s}^{max}}\mu + \frac{1}{Y_{p/s}^{max}}q_p + m_s \tag{3.5}$$

$$-q_s = \frac{1}{Y_{x/s}^{max}}\mu + m_s \tag{3.6}$$

with q_s the the biomass-specific substrate consumption rate in mol/(g_{DW} h), $Y_{x/s}^{max}$ the maximum biomass yield on substrate in g_{DW}/mol, μ the growth rate in h^{-1}, $Y_{p/s}^{max}$ the maximum product yield on substrate in mol/mol, q_p the the biomass-specific product rate in mol/(g_{DW} h), and m_s the maintenance coefficient in mol/(g_{DW} h)

Fitting the Herbirt-Pirt equation

For CO fermentation by *C. autoethanogenum*, CO serves as the substrate, while ethanol and acetate are the catabolic products, leading to Eq. (3.7). To determine the maximum biomass yield on CO ($Y_{x/CO}^{max}$) and the maintenance coefficient for growth on CO (m_{CO}), Eq. (3.7) was fitted with the experimental and reconciled steady-state CO fermentation data (Figure 3.6). This yielded an $Y_{x/CO}^{max}$ of 1.76 ±0.17 and 1.85 ±0.15 g_{DW}/mol for the experimental and reconciled data, respectively. Furthermore, the m_{CO} was 5.07 ±2.73 mmol/(g_{DW} h) for the experimental data and 6.42 ±2.20 mmol/(g_{DW} h) for the reconciled data. Both the $Y_{x/CO}^{max}$ and m_{CO} are considered apparent values, as the CO consumption depends on the produced catabolic products and the presence of undissociated acetic acid in the fermentation broth increases the ATP requirements for maintenance (Elisiário et al., 2023; Valgepea, de Souza Pinto Lemgruber, et al., 2017). Due to the inhibiting effect of acetic acid, the steady states with acetate added to the feed (SST 22, 35, 36 & 37) were excluded, as they could potentially skew the fit.

$$-q_{CO} = \frac{1}{Y_{x/CO}^{max}}\mu + m_{CO} \tag{3.7}$$

with q_{CO} the biomass-specific CO consumption rate in mol/(g_{DW} h), $Y_{x/CO}^{max}$ the maximum biomass yield on CO in g_{DW}/mol, μ the growth rate in h^{-1}, and m_{CO} the maintenance coefficient for growth on CO in mol/(g_{DW} h)

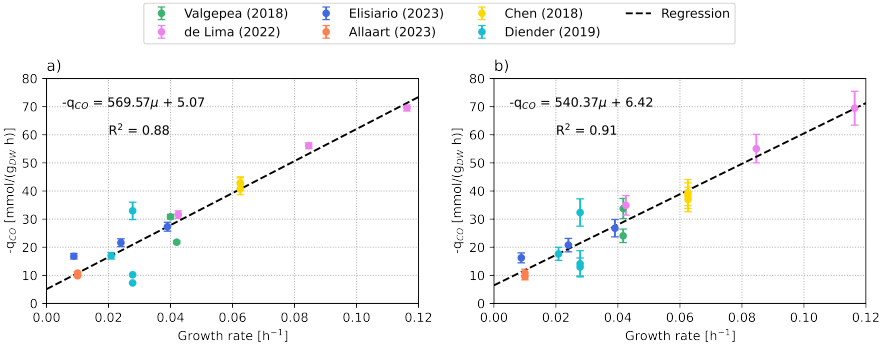

Figure 3.6: The biomass-specific CO consumption (q_{CO}) rate as a function of the growth rate (μ) for CO fermentation by *Clostridium autoethanogenum*. With a) the experimental data, and b) the reconciled data.

A thermodynamic analysis of the kinetic parameters yielded a $Y_{x/CO}^{max}$ and m_{CO} of 1.50-1.66 g_{DW}/mol and 12.16-13.30 mmol/(g_{DW} h), respectively (see Appendix F). The fitted $Y_{x/CO}^{max}$ is close to the thermodynamically determined range. However, the fitted m_{CO} is only half the thermodynamically determined m_{CO}, possibly stemming from assumptions made in the thermodynamic calculation. Elisiário et al. (2023) performed the same fit with a similar dataset and found an apparent $Y_{x/CO}^{max}$ and m_{CO} of 1.87 g_{DW}/mol and 7.92 mmol/(g_{DW} h), respectively. Differences between the fitted parameters by Elisiário et al. (2023) and this study are presumable due to the additional steady states included in this study. In particular, the three steady states from Diender et al. (2019) at μ = 0.028 h^{-1} deviate from the regression line. Gas outflow measurements of these steady-states proved difficult and might have introduced variability in the reported q_{CO} (Diender, 2024). Also, it was not specified whether biological replicates were used to obtain the reported steady-state data. In the case that only technical replicates were used, the variability in the data can be reduced by treating the three steady states as biological replicates, thereby improving the fit. Moreover, most steady-states in the dataset were operated at lower dilution rates. Therefore, the two steady-states by de Lima et al. (2022) at μ = 0.085 and 0.12 h^{-1} influence the model parameters considerably. Expanding the dataset with steady states at higher dilution rates could reduce this bias.

Incorporation of ATP production and consumption in growth kinetics

The rate at which CO is consumed is directly related to the production of acetate and ethanol in catabolic reactions R1 and R2, during which also ATP is produced. By rewriting the Herbert-Pirt equation in terms of ATP requirements, the produced ATP in catabolism was linked to the ATP requirements for growth and maintenance (Eq. (3.8)).

$$q_{R1}Y_{ATP,R1} + q_{R2}Y_{ATP,R2} = \frac{1}{Y_{x/ATP}^{max}}\mu + m_{ATP} \tag{3.8}$$

with q_R the reaction rate in mol/(g_{DW} h), $Y_{ATP,R}$ the ATP yield of the catabolic reaction in mol/mol $Y_{x/ATP}^{max}$ the maximum biomass yield on ATP in g_{DW}/mol, and m_{ATP} the ATP required for maintenance in mol/(g_{DW} h)

The left side of the equation describes the ATP production during catabolism. Namely, the produced amount of ATP depends on the rate (q_R) and ATP yield ($Y_{ATP,R}$) of catabolic reactions R1 and R2, respectively. Depicted on the right side of the equation is ATP consumption for maintenance processes (m_{ATP}) and growth (μ), of which the latter depends on the maximum biomass yield on ATP ($Y_{x/ATP}^{max}$). In catabolic reaction R1, CO is converted into acetate with at rate q_{R1} (Figure 3.7). As acetate is a product in itself and serves as a precursor for ethanol production, q_{R1} is the sum of the total acetate production rate (q_{AcT}) and the ethanol production rate (q_{EtOH}). In catabolic reaction R2, ethanol is produced with rate q_{R2}. Ethanol is not further converted into other products, such that q_{R2} equals q_{EtOH}.

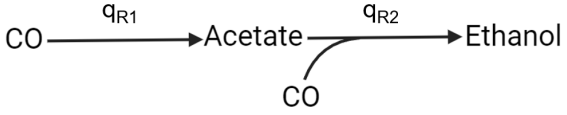

Figure 3.7: Schematic representation of catabolic reactions R1 and R2. In catabolic reaction R1, carbon monoxide (CO) is converted into acetate with reaction rate q_{R1}. Acetate and CO are converted into ethanol in catabolic reaction R2 at rate q_{R2}.

To obtain the parameter values for $Y_{x/ATP}^{max}$ and m_{ATP}, Eq. (3.8) was fitted with the experimental and reconciled data. Assuming the ATP yields reported by Katsyv and Müller (2020), a $Y_{x/ATP}^{max}$ of 6.10 ±0.65 and 5.61 ±0.51 g_{DW}/mol was obtained for the experimental and reconciled data, respectively. Furthermore, the m_{ATP} yielded 2.40 ±0.88 mmol/(g_{DW} h) for the experimental data and 2.28 ±0.81 mmol/(g_{DW} h) for the reconciled data (Figure 3.8a & 3.8b). However, with the ATP yields reported by Allaart et al. (2023), a $Y_{x/ATP}^{max}$ and m_{ATP} of 6.91 ±0.82 and 6.36 ±0.63 g_{DW}/mol, and 2.69 ±0.86 and 2.61 ±0.79 mmol/(g_{DW} h) were obtained for the experimental and reconciled data, respectively (Figure 3.8c & 3.8d). Despite the ATP yields reported by Katsyv and Müller (2020) giving a better fit for Eq. (3.8) for both the experimental and reconciled data, the ATP yields reported by Allaart et al. (2023) were used for further calculations, as these could be reproduced in this study (see Appendix E).

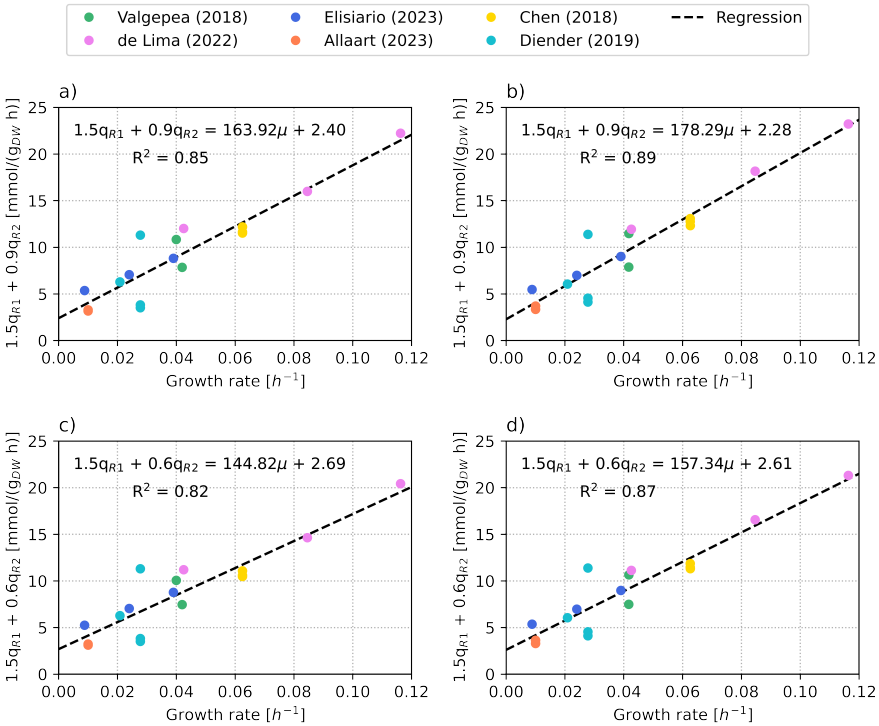

Figure 3.8: The total ATP production in catabolic reactions R1 and R2 rate as a function of the growth rate (μ) for CO fermentation by *Clostridium autoethanogenum*. Both the experimental (a & c) and reconciled (b & d) data were fitted. The ATP yields for catabolic reactions R1 ($Y_{ATP,R1}$) and R2 ($Y_{ATP,R2}$) were assumed 1.5 and 2.4 (a & b) (Katsyv and Müller, 2020), or 1.5 and 0.6 (c & d) (Allaart et al., 2023).

Valgepea, Loi, et al. (2017) assumed a $Y_{x/ATP}$ and m_{ATP} of 21.3 g_{DW}/mol and 8.4 mmol/(g_{DW} h) based on a literature study on *Clostridial* bacteria grown on glucose (Bahl et al., 1982; Canganella et al., 2002; Meyer Houston and Papoutsakis, 1989). This study highlighted that the $Y_{x/ATP}$ and m_{ATP} for *Clostridial* bacteria are within the range of 17.6-23.8 g_{DW}/mol and 3.5-14.5 mmol/(g_{DW} h). The difference between the found $Y^{max}_{x/ATP}$ range and the fitted $Y^{max}_{x/ATP}$ can be explained by the fact that more reduction steps and carbon-carbon coupling reactions are required with CO as the carbon source, compared to glucose. Specifically, glucose aligns more closely with the redox state of biomass and, with 6 carbon atoms, is also more similar to the typical biomass precursors, which have typically lengths of about 4 to 5 carbon atoms. Therefore, the synthesis of biomass from CO requires more work, resulting in a lower $Y^{max}_{x/ATP}$ (Heijnen and Van Dijken, 1992). Furthermore, the fitted m_{ATP} was only slightly below the found m_{ATP} range, and might be due to differences in strains and cultivation conditions (Meyer Houston and Papoutsakis, 1989).

Product inhibition

At elevated product concentrations, substrate conversion may decelerate due to product inhibition. Since the ethanol concentration of the steady states in the dataset appeared to be insufficient to cause inhibition, only acetate inhibition was considered (de Medeiros et al., 2019). Acetate inhibition occurs when undissociated extracellular acetic acid diffuses into the cell, thereby uncoupling the proton motive force (PMF) by importing an additional proton without the synthesis of ATP by the membrane-bound ATPase (Valgepea, de Souza Pinto Lemgruber, et al., 2017). Restoring the PMF costs energy, which increases the maintenance requirements of the cell (Elisiário et al., 2023). Hence, the m_{ATP} equals the ATP demands for maintenance in the absence of undissociated extracellular acetic acid in the broth ($m_{ATP,0}$), as a function of the acetic acid concentration (c_{HAc}) (Eq. 3.9).

$$q_{R1}Y_{ATP,R1} + q_{R2}Y_{ATP,R2} = \frac{1}{Y_{x/ATP}^{max}}\mu + m_{ATP,0} \cdot f(c_{HAc}) \tag{3.9}$$

with q_R the reaction rate in mol/(g_{DW} h), $Y_{ATP,R}$ the ATP yield of catabolic reaction R in mol/mol, $Y_{x/ATP}^{max}$ the maximum biomass yield on ATP in g_{DW}/mol, c_{HAc} the undissociated acetic acid concentration in M, $m_{ATP,0}$ the ATP required for maintenance at c_{HAc} = 0 in mol/(g_{DW} h), and $f(c_{HAc})$ the additional ATP requirement due to acetate inhibition

A method proposed to calculate the increase in maintenance due to acetate inhibition is by determining the undissociated acetic acid diffusion rate into the cell ($r_{HAc,in}$) (Almeida Benalcázar, 2023; Henriksen et al., 1998; Valgepea, de Souza Pinto Lemgruber, et al., 2017; Villadsen et al., 2011). The $r_{HAc,in}$ is regulated by the intra- and extracellular undissociated acetic acid concentration, and is influenced by the intra- and extracellular pH, as well as, the total concentration of undissociated and dissociated acetic acid (c_{AcT}) (Eq. 3.10-3.12). Subsequently, the increase in maintenance due to acetate inhibition can be determined given the $Y_{H^+/ATP}$ of the ATPase and the $Y_{H^+/HAc}$ (Eq. (3.13)). As one proton is imported per diffused molecule of undissociated acetic acid, $Y_{H^+/HAc}$ equals 1 mol/ mol. Furthermore, a $Y_{H^+/ATP}$ of 3.6 mol/mol was assumed (Elisiário et al., 2023; Katsyv and Müller, 2020).

$$r_{HAc,in} = P_{HAc} \cdot a_{cell} \cdot \left(c_{HAc,out} - c_{HAc,in}\right) \tag{3.10}$$

$$c_{AcT,in} = \frac{1 + 10^{pH_{out} - pK_a}}{1 + 10^{pH_{in} - pK_a}} \cdot c_{AcT,out} \tag{3.11}$$

$$c_{HAc} = c_{Ac^-} \cdot 10^{pK_a - pH} = \frac{c_{AcT}}{1 + 10^{pH - pK_a}} \tag{3.12}$$

$$q_{R1}Y_{ATP,R1} + q_{R2}Y_{ATP,R2} = \frac{1}{Y_{x/ATP}^{max}}\mu + m_{ATP,0} + r_{HAc,in}\frac{Y_{H^+/HAc}}{Y_{H^+/ATP}} \tag{3.13}$$

with $r_{HAc,in}$ the acetic acid diffusion rate in mol/(g_{DW} h), P_{HAc} the acetic acid permeability constant in dm/h, a_{cell} the cell surface in dm^2/g_{DW}, $c_{HAc,out}$ the extracellular undissociated acetic acid concentration in M, $c_{HAc,in}$ the intracellular undissociated acetic acid concentration in M, c_{HAc} the undissociated acetic acid concentration in the broth in M, c_{Ac^-} the dissociated acetic acid concentration in the broth in M, c_{AcT} the sum of the dissociated and undissociated acetic acid concentration in M, pH_{in} the intracellular pH, pH_{out} the extracellular pH, pK_a the acetic acid dissociation constant of 4.76, q_R the reaction rate in mol/(g_{DW} h), $Y_{ATP,R}$ the ATP yield of the catabolic reaction in mol/mol, $Y_{x/ATP}^{max}$ the maximum biomass yield on ATP in g_{DW}/mol, $m_{ATP,0}$ the ATP required for maintenance at c_{HAc} = 0 in mol/(g_{DW} h), $Y_{H^+/ATP}$ proton-to-ATP ratio of the ATPase in mol/mol, and $Y_{H^+/HAc}$ the amount of H^+ imported due to undissociated acetic acid diffusion into the cell in mol/mol

While the extracellular pH used for the steady-state CO fermentations was included in the dataset (see Appendix C), the intracellular pH was estimated using Eq. (3.14). Mock et al. (2015) reported an intracellular pH of 6 for *C. autoethanogenum* cultivated at an extracellular pH of 5, while Diender et al. (2019) assumed an intracellular pH of 6.8 for cultivation of *C. autoethanogenum* at pH 6.2. Since the extracellular pH in the dataset ranges from 5 to 6.2, it was assumed that the intracellular pH is a function of the extracellular pH (see Appendix H.1 for derivation).

$$pH_{in} = \frac{2}{3}pH_{out} + 2\frac{2}{3} \tag{3.14}$$

with pH_{in} the intracellular pH and pH_{out} the extracellular pH in the range of 5 to 6.2

In literature, there is a lack of consensus regarding the values of both the permeability constant (P_{HAc}) and the cell surface (a_{cell}). Valgepea, de Souza Pinto Lemgruber, et al. (2017) reported a cell surface of $3.9 \cdot 10^{-12}$ m^2 and a permeability constant of $6.9 \cdot 10^{-5}$ m/s that was determined for a bacterial phosphatidyl ethanolamine-squalane (Montal-Mueller) bilayer (Walter and Gutknecht, 1984). With these parameter values a m_{ATP} increase of 2.2 mmol/(g_{DW} h) for an extracellular acetate concentration of 8 g/L was reported. However, upon replicating this calculation, a significantly higher ATP cost of 25.41 mol/(g_{DW} h) was found (see Appendix H.2). Almeida Benalcázar (2023) estimated a permeability constant of $3.86 \cdot 10^{-5}$ m/h and $1.93 \cdot 10^{-5}$ m/h for acetate being exported via an uniport or antiport

transporter, respectively, using an integrated black box and metabolic model of *C. autoethanogenum*. Furthermore, a cell surface of 383 m^2/mol was used assuming *C. autoethanogenum* is cylindrical with a height, width and density of 2 μm, 1 μm and 1.1 g/mL, respectively. Due to the discrepancies in the reported values for P_{HAc} and a_{cell}, it was decided to merge them into one parameter (Eq. (3.15)). This parameter, referred to as P_{HAc}^{V}, reflects the volume of acetate that passes through the membrane per unit of time and biomass.

$$r_{HAc,in} = P_{HAc}^{V} \cdot \left(c_{HAc,out} - c_{HAc,in}\right) \tag{3.15}$$

with $r_{HAc,in}$ the acetic acid diffusion rate in mol/(g_{DW} h), P_{HAc}^{V} the volume of acetate that passes through the membrane per unit of time and biomass in L/(g_{DW} h), $c_{HAc,out}$ the extracellular undissociated acetic acid concentration in M, and $c_{HAc,in}$ the intracellular undissociated acetic acid concentration in M

Fitting Eq. (3.13) yielded a $Y_{x/ATP}^{max}$ of 6.97 ±1.00 g_{DW}/mol for the experimental data (R^2 =0.83) and 6.38 ±0.77 g_{DW}/mol for the reconciled data (R^2=0.87). Furthermore, a P_{HAc}^{V} and $m_{ATP,0}$ of 0.014 ±0.11 and 0.0063 ±0.10 L/(g_{DW} h), and 2.66 ±0.92 and 2.59 ±0.84 mmol/(g_{DW} h) were obtained for the experimental and reconciled data, respectively. Both the $Y_{x/ATP}^{max}$ and $m_{ATP,0}$ are in the range of the previously fitted values. However, the standard deviation of the P_{HAc}^{V} was significant, suggesting variability of the parameter. Therefore, an F-test was performed to test whether including acetate inhibition improves the fit of Eq. (3.8) significantly. The F-test (p>0.05) showed that including acetic acid inhibition according to Eq. (3.13) did not significantly improve the fit for both the experimental (p=0.90) and reconciled (p=0.95) data.

A different method to incorporate the increase in maintenance due to acetate inhibition is based on work by Straathof (2023b) (Eq. (3.16)). This method assumes a linear dependency between m_{ATP} and the undissociated acetic acid concentration, which is implemented through the parameter β_m that represents the undissociated acetic acid concentration at which m_{ATP} doubles.

$$q_{R1}Y_{ATP,R1} + q_{R2}Y_{ATP,R2} = \frac{1}{Y_{x/ATP}^{max}}\mu + m_{ATP,0}\left(1 + \frac{c_{HAc}}{\beta_m}\right) \tag{3.16}$$

with c_{HAc} the undissociated acetic acid concentration in M, q_R the reaction rate in mol/(g_{DW} h), $Y_{ATP,R}$ the ATP yield of catabolic reaction R in mol/mol, $Y_{x/ATP}^{max}$ the maximum biomass yield on ATP in g_{DW}/mol, $m_{ATP,0}$ the ATP required for maintenance at c_{HAc} = 0 in mol/(g_{DW} h), and β_m the undissociated acetic acid concentration at which m_{ATP} doubles in M

Fitting Eq. (3.16) with the experimental (R^2=0.83) and reconciled (R^2=0.87) data yielded a $Y_{x/ATP}^{max}$ and $m_{ATP,0}$ of 6.97 ±1.00 and 6.38 ±0.77 g_{DW}/mol, and 2.66 ±0.92 and 2.59 ±0.84 mmol/(g_{DW} h), respectively. Furthermore, β_m was 689.9 ±5603.3 mM for the experimental data and 1470.2 ±22987 mM for the reconciled data. The obtained values of β_m for the experimental and reconciled data are significantly different. Furthermore, their respective standard deviation suggests high variability of β_m. Again, an F-test (p>0.05) showed that including acetic acid inhibition as proposed by Straathof (2023b) did not significantly improve the fit of Eq. (3.8) for both the experimental (p=0.90) and reconciled (p=0.95) data.

Kinetic growth equation

Because incorporating acetate inhibition did not significantly improve the fit of Eq. (3.8), Eq. (3.8) was rewritten into Eq. (3.17) to predict the growth rate of *C. autoethanogenum* by subtracting the loss in growth due to ATP requirements for maintenance (m_x) from the gain in growth due to ATP production in the catabolism (see Appendix G for derivation).

$$\mu = \underbrace{4 \cdot Y^{max}_{x/CO,R1} \cdot q_{R1} + 2 \cdot Y^{max}_{x/CO,R2} \cdot q_{R2}}_{\text{gain in growth}} - \underbrace{m_x}_{\text{loss in growth}} \tag{3.17}$$

with μ the growth rate in h^{-1}, $Y^{max}_{x/CO,R}$ the maximum biomass yield on CO for catabolic reaction R in g_{DW}/mol, q_R the reaction rate in mol/(g_{DW} h), and m_x the loss of growth due to maintenance in h^{-1}

Fitting Eq. (3.17) with the experimental data (R^2=0.91) yielded a maximum biomass yield on CO for catabolic reaction R1 ($Y^{max}_{x/CO,R1}$) and R2 ($Y^{max}_{x/CO,R2}$) of 1.01 ±0.37 and 4.86 ±0.91 g_{DW}/mol. Furthermore, the m_x for the experimental data was -0.0045 ±0.006 h^{-1}. The $Y^{max}_{x/CO,R1}$, $Y^{max}_{x/CO,R2}$ and m_x for the reconciled data (R^2=0.92) were 1.15 ±0.35 g_{DW}/mol, 4.05 ±0.82 g_{DW}/mol and -0.0021 ±0.006 h^{-1}, respectively. To validate the accuracy of the predicted growth rates, the experimental and reconciled growth rates were compared with the predicted growth rates in parity plots (Figure 3.9). Overall, the data points scatter around the equality line (y=x), indicating that the growth rate predictions by the modified Herbert-Pirt equation (Eq. 3.17) agree with the observed growth rates. An F-test (p>0.05) showed that Eq. (3.17) gives a significantly better fit to the experimental data (p=0.02) compared to Eq. (3.7). However, this was not the case for the reconciled data (p=0.09). Therefore, it remains unsure whether the proposed model is significantly better than Eq. (3.7) for estimating the growth rate of *C. autoethanogenum*.

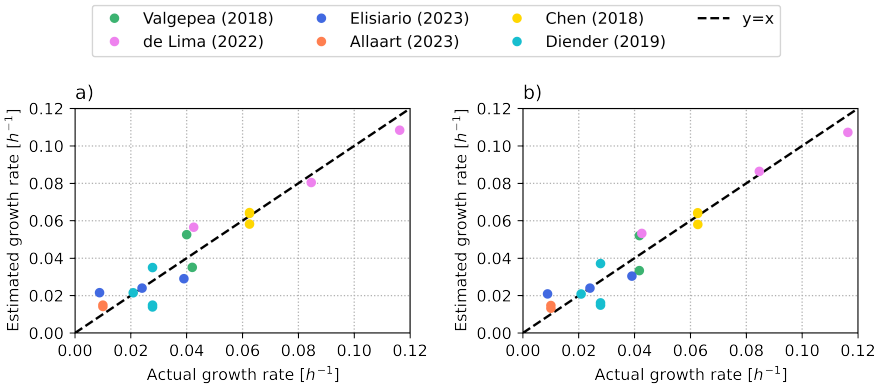

Figure 3.9: Parity plot comparing the actual growth rate (μ) and predicted growth rate for a) the experimental and b) reconciled dataset.

The variability in m_x suggests that the loss of growth is negligible compared to the gain in growth, such that Eq. (3.17) can be rewritten into Eq. (3.18). Fitting Eq. (3.18) yielded an $Y^{max}_{x/CO,R1}$ of 1.25 ±0.18 g_{DW}/mol for the experimental data and 1.27 ±0.16 g_{DW}/mol for the reconciled data. The $Y^{max}_{x/CO,R2}$ was 4.57 ±0.80 and 3.90 ±0.68 g_{DW}/mol for the experimental data and reconciled data, respectively. While no significant changes were visible between the parity plots for Eq. (3.17) (Figure 3.9) and Eq. (3.18) (Figure 3.10), a better fit was observed with Eq. (3.18) for both the experimental (R^2=0.97) and reconciled data (R^2=0.98).

$$\mu = 4 \cdot Y^{max}_{x/CO,R1} \cdot q_{R1} + 2 \cdot Y^{max}_{x/CO,R2} \cdot q_{R2} \tag{3.18}$$

with μ the growth rate in h^{-1}, $Y^{max}_{x/CO,R}$ the maximum biomass yield on CO for catabolic reaction R in g_{DW}/mol, and q_R the reaction rate in mol/(g_{DW} h)

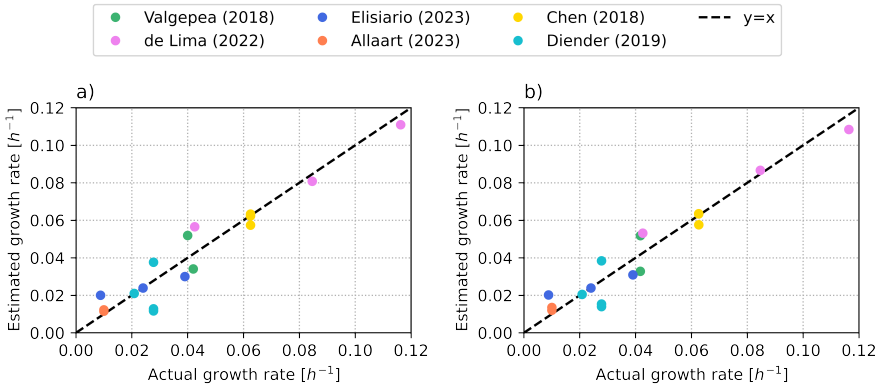

Figure 3.10: Parity plot comparing the actual growth rate (μ) and predicted growth rate for a) the experimental and b) reconciled dataset.

Despite catabolic reaction R1 having a higher ATP yield than catabolic reaction R2, a higher biomass yield on CO was observed for catabolic reaction R2. As illustrated in Figure 3.11, CO is converted into acetyl-CoA in catabolic reaction R1. Subsequently, acetyl-CoA serves as a precursor for both acetate production and biomass synthesis. In catabolic reaction R2, acetate is imported from outside the cell and directly serves as precursor for ethanol production. Therefore, more acetyl-CoA might be used for biomass synthesis, thus explaining why the maximum biomass yield on CO is higher for catabolic reaction R2 than for catabolic reaction R1.

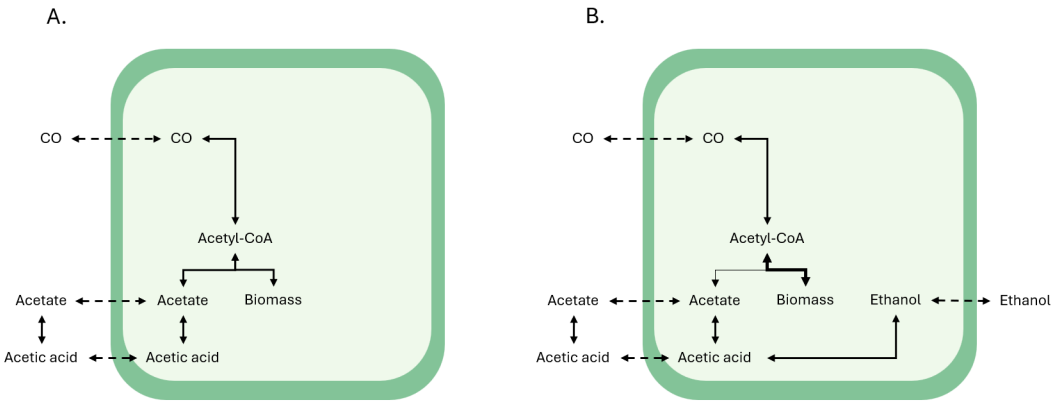

Figure 3.11: Schematic representation of acetyl-CoA distribution in catabolic reaction R1 and R2. A) In catabolic reaction R1, CO is converted into acetyl-CoA. Acetyl-CoA is the precursor for both acetate and biomass synthesis. B) In catabolic reaction R2, acetate serves as precursor for ethanol production. More acetyl-CoA might be used for biomass synthesis, rather than serve as precursor for acetate production.

3.2.3. Substrate uptake kinetics

The substrate uptake kinetics of *C. autoethanogenum* were described by the hyperbolic substrate equation (Eq. (3.19)), which relates the biomass-specific substrate consumption rate (q_s) to the concentration of the growth-limiting substrate (c_s) by the maximal biomass-specific consumption rate (q_s^{max}) of the microorganism and its affinity for the substrate (K_s) (Kuenen, 2019). The hyperbolic substrate equation is preferred over the Monod equation (Eq. (3.20)) (Monod, 1949), as the latter predicts μ = 0 when the substrate is depleted (c_s=0), while there should still be substrate uptake due to maintenance according to the Herbert-Pirt equation (Eq. (3.6)) (Straathof, 2023b).

$$-q_s = -q_s^{max} \frac{c_s}{K_s + c_s} \tag{3.19}$$

$$\mu = \mu^{max} \frac{c_s}{K_s + c_s} \tag{3.20}$$

with q_s the biomass-specific substrate consumption rate in mol/(g_{DW} h), q_s^{max} the maximum biomass-specific substrate consumption rate in mol/(g_{DW} h), c_s the substrate concentration in M, K_s the substrate affinity constant in M, μ the growth rate in h^{-1}, and μ^{max} the maximum growth rate in h^{-1}

Fitting the substrate uptake equation

During CO fermentation, the CO consumption rate (q_{CO}) depends on the dissolved CO concentration (c_{CO}), the CO affinity constant (K_{CO}), and the maximum CO consumption rate (q_{CO}^{max}) (Eq. (3.21)). Compared to Eq. (3.19), Eq. (3.21) has an additional parameter, $K_{I,CO}$, accounting for CO inhibition. To obtain the model parameters, Eq. (3.21) was fitted with the experimental and reconciled data. However, due to the data scatter at lower dissolved CO concentrations (Figure 3.12), the model parameters could not be obtained.

$$-q_{CO} = -q_{CO}^{max} \frac{c_{CO}}{K_{CO} + c_{CO} + \frac{{c_{CO}}^2}{K_{I,CO}}} \tag{3.21}$$

with q_{CO} the biomass-specific CO consumption rate in mol/(g_{DW} h), q_{CO}^{max} the maximum biomass-specific CO consumption rate in mol/(g_{DW} h), c_{CO} the dissolved CO concentration in M, K_{CO} the CO affinity constant in M, and $K_{I,CO}$ the CO inhibition constant in M.

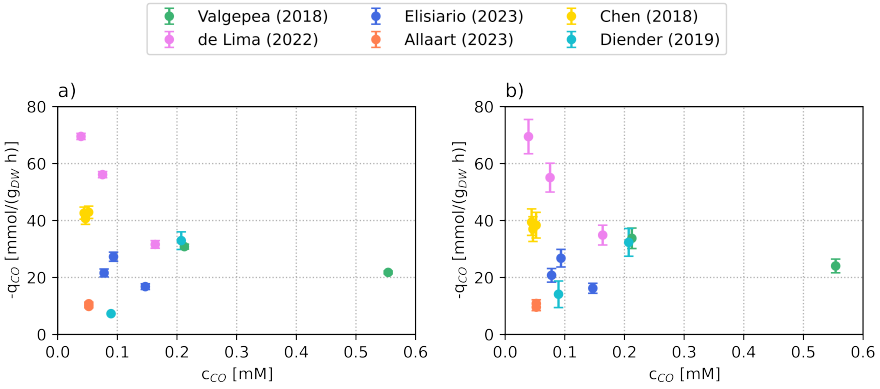

Figure 3.12: The biomass-specific CO consumption rate (q_{CO}) plotted as a function of the dissolved CO concentration (c_{CO}). With a) the experimental and b) reconciled data.

Reported values for K_{CO} and $K_{I,CO}$ in literature for various *Clostridium* species range from 0.0115 to 0.536 mM and 0.107 to 1.607 mM, respectively (Table 3.1). Furthermore, Allaart et al. (2024) reported a q_{CO} of -119 ±1 mmol/(g_{DW} h), which is higher compared to the previously reported estimates and experimental values for q_{CO}^{max}. In Figure 3.13, Eq. (3.21) is plotted with the reported K_{CO} and $K_{I,CO}$ values and an assumed q_{CO}^{max} of -119 mmol/(g_{DW} h) (Allaart et al., 2024). None of the resulting curves appeared to capture the entire dataset. However, the plots with the K_{CO} and $K_{I,CO}$ reported by de Medeiros et al. (2019) for *Clostridium ljungdahlii* and Lanzillo et al. (2020) for *Clostridium carboxidivorans* seem to capture part of the dataset. Assuming the parameters found by de Medeiros et al. (2019), q_{CO}^{max} is already reached at a CO concentration below 0.1 mM, which aligns with the highest q_{CO} value in the dataset. Subsequently, the q_{CO} decreases due to CO inhibition, which aligns with the q_{CO} found for the highest CO concentration in the dataset. Overall, this suggests that CO inhibition occurs to some extent in most of the steady states within the dataset. The parameters found by Lanzillo et al. (2020) suggest another scenario, where there is no CO inhibition for the range of dissolved CO concentrations used in the steady states. Therefore, the relationship between q_{CO} and c_{CO} resembles more of a hyperbolic curve within the plotted dissolved CO concentration range.

Table 3.1: CO affinity constants (K_{CO}) and CO inhibition constants ($K_{I,CO}$) reported in literature.

Source	K_{CO} [mM]	$K_{I,CO}$ [mM]	Organism
de Medeiros et al., 2019	0.0115	0.136	*Clostridium ljungdahlii*
de Medeiros et al., 2019	0.0454	0.827	*Clostridium* strain P11
Almeida Benalcázar, 2023	0.042	0.496	*Clostridium autoethanogenum*
Ruggiero et al., 2022	0.393	0.107	*Clostridium carboxidivorans*
Lanzillo et al., 2020	0.536	1.607	*Clostridium carboxidivorans*

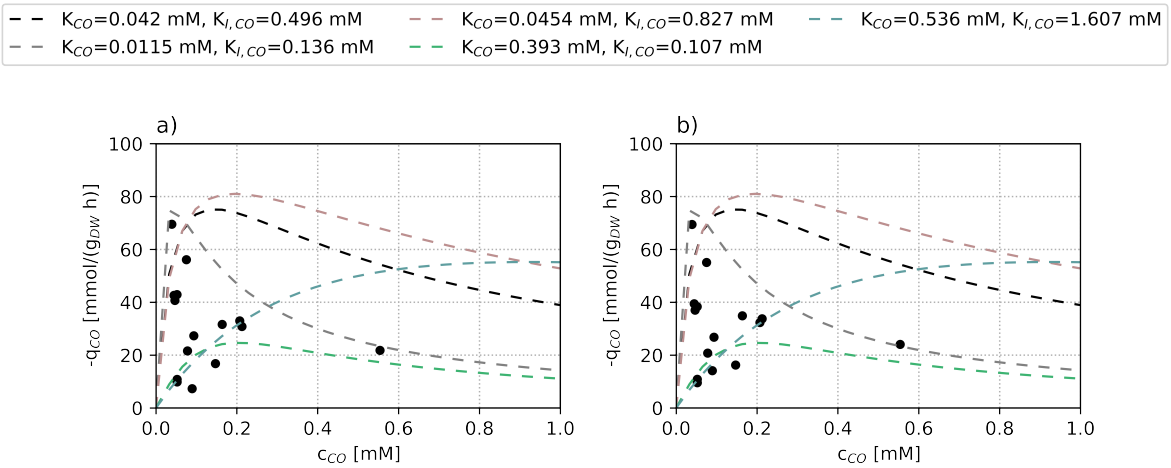

Figure 3.13: The biomass-specific consumption rate (q_{CO}) plotted as function of the dissolved CO concentration (c_{CO}). With a) the experimental and b) the reconciled data. The hyperbolic CO uptake curves are plotted according to Eq. (3.21) with the CO affinity constant (K_{CO}) and CO inhibition constant ($K_{I,CO}$) values reported by de Medeiros et al. (2019) for *Clostridium ljungdahlii* (grey) and *Clostridium* strain P11 (brown), Almeida Benalcázar (2023) for *Clostridium autoethanogenum* (black), Ruggiero et al. (2022) for *Clostridium carboxidivorans* (green), Lanzillo et al. (2020) for *Clostridium carboxidivorans* (blue). The maximum CO uptake rate (q_{CO}^{max}) was assumed as -119 ±1 mmol/(g_{DW} h) (Allaart et al. (2024)).

Substrate uptake equations for the catabolic reactions

To describe the uptake of the growth-limiting substrate in catabolic reactions R1 and R2, Eq (3.21) was rewritten in terms of the catabolic reaction rates q_{R1} and q_{R2}. Given that CO acts as the limiting substrate in catabolic reaction R1, the rate of catabolic reaction R1 is influenced by three parameters: the dissolved CO concentration, the CO affinity constant, and the maximum rate of reaction R1 (q_{R1}^{max}) (Eq. 3.22). The rate of catabolic reaction R2 depends on two limiting substrates: CO and acetate. Therefore, q_{R2} is influenced by the concentration of CO and its affinity constant, as well as, the total acetate concentration, the acetate affinity constant (K_{AcT}), and the maximum rate of reaction R2 (q_{R2}^{max}) (Eq. (3.23)). Eq. (3.22) and (3.23) were fitted with the experimental and reconciled data to obtain the model parameters. However, scattering of the data prevented fitting the model parameters (Figure 3.14).

$$q_{R1} = q_{R1}^{max} \frac{c_{CO}}{K_{CO} + c_{CO}} \tag{3.22}$$

$$q_{R2} = q_{R2}^{max} \frac{c_{CO}}{K_{CO} + c_{CO}} \frac{c_{AcT}}{K_{AcT} + c_{AcT}} \tag{3.23}$$

with q_R the biomass-specific reaction rate in mol/(g_{DW} h), q_R^{max} the maximum reaction rate in mol/(g_{DW} h), c_i the concentration of compound i in M, and K_i the affinity constant for compound i in M

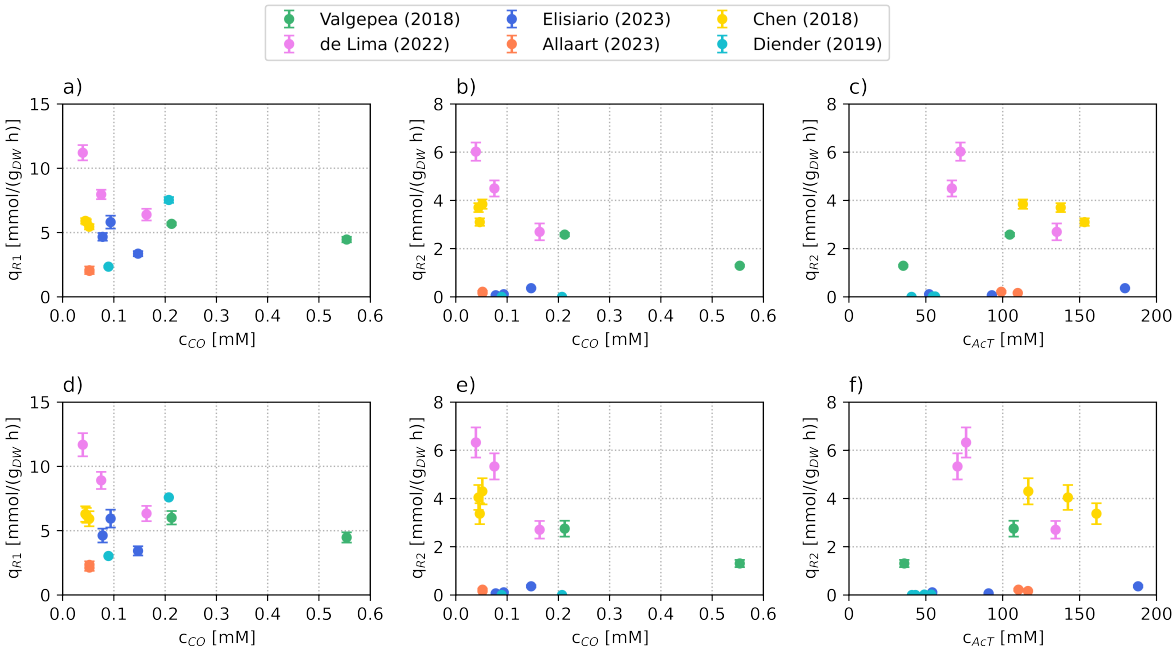

Figure 3.14: The rate of catabolic reaction R1 (q_{R1}) (a & d) and R2 (q_{R2}) (b & e) as a function of the dissolved CO concentration (c_{CO}). Additionally, q_{R2} was plotted against the total acetate concentration (c_{AcT}) (c & f). Both the experimental (a, b & c) and reconciled (d, e & f) data were plotted.

The observed scatter in the plots of q_{CO}, q_{R1} and q_{R2} as a function of the dissolved CO concentration might be due to variability in the dissolved CO concentrations. Various factors influence gas-liquid mass transfer, complicating the estimation of dissolved gas concentration from process parameters and off-gas measurements in small-scale bioreactors. Furthermore, the steady-state CO fermentations in the dataset used low gas flow rates, potentially leading to a degree of uncertainty in the off-gas measurements. The scatter in the plots of q_{R2} as a function of c_{AcT} could have been caused by the co-dependency of q_{R2} on CO. Alternatively, q_{R2} may be dependent on the undissociated acetic acid concentration (Eq. (3.24)), rather than the total acetate concentration. Namely, undissociated acetic acid can diffuse back into the cell and is converted into ethanol to prevent uncoupling of the PMF (Elisiário et al., 2023; Valgepea, de Souza Pinto Lemgruber, et al., 2017). In Figure 3.15, q_{R2} is plotted as a function of the undissociated acetic acid concentration. The curve follows the expected hyperbolic trend, where q_{R2} increases with higher concentrations of undissociated acetic acid. After reaching the maximum, q_{R2} decreases, which might be due to acetate inhibition or co-dependency on CO.

$$q_{R2} = q_{R2}^{max} \frac{c_{CO}}{K_{CO} + c_{CO}} \frac{c_{HAc}}{K_{HAc} + c_{HAc}} \tag{3.24}$$

with q_R the reaction rate in mol/(g_{DW} h), q_R^{max} the maximum reaction rate in mol/(g_{DW} h), c_i the concentration of compound i in M, and K_i the affinity constant for compound i in M

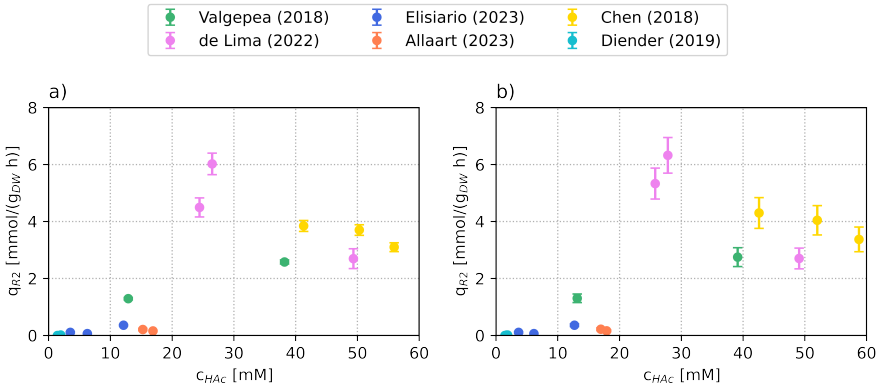

Figure 3.15: The rate of catabolic reaction R2 (q_{R2}) as a function of the undissociated acetic acid concentration (c_{HAc}). With a) the experimental and b) reconciled data.

Because the estimated dissolved CO concentration did not appear to capture the true dissolved CO concentrations, the substrate uptake kinetic parameters were decoupled from the dissolved CO concentrations by dividing Eq. (3.24) with Eq. (3.22), yielding Eq. (3.25). By doing so, it was assumed that the K_{CO} is the same in both catabolic reactions. However, this assumption might be incorrect as *C.autoethanogenum* harbours more than one CO dehydrogenase (CODH) enzyme, which catalyzes CO oxidation into CO_2. According to Eq. (3.25), the ratio of q_{R2} to q_{R1} (q_{R2}/q_{R1}) is hyperbolic dependent on the maximal ratio of q_{R2} to q_{R1} ($q_{R2}^{max}/q_{R1}^{max}$), the undissociated acetic acid concentration, and the undissociated acetic acid affinity constant.

$$\frac{q_{R2}}{q_{R1}} = \frac{q_{R2}^{max}}{q_{R1}^{max}} \frac{c_{HAc}}{K_{HAc} + c_{HAc}} \tag{3.25}$$

with q_R the reaction rate in mol/(g_{DW} h), q_R^{max} the maximum reaction rate in mol/(g_{DW} h), c_{HAc} the undissociated acetic acid concentration in M, and K_{HAc} the undissociated acetic acid affinity constant in M

Fitting Eq. (3.25) with the experimental and reconciled data yielded a $q_{R2}^{max}/q_{R1}^{max}$ ratio of 1.5 ±1.02 an 1.64 ±1.26, respectively (Figure 3.16). Furthermore, the K_{HAc} was 79.38 ±80.06 mM for the experimental data and 91.03 ±101.01 mM for the reconciled data. While Eq. (3.25) demonstrates a decent fit with both datasets, the standard deviations linked to the kinetic parameters suggest variability, ultimately failing to capture the trend of the data. Namely, the data presented in Figure 3.16 suggest a $q_{R2}^{max}/q_{R1}^{max}$ ratio of 0.6 and a K_{HAc} around 20 mM, respectively.

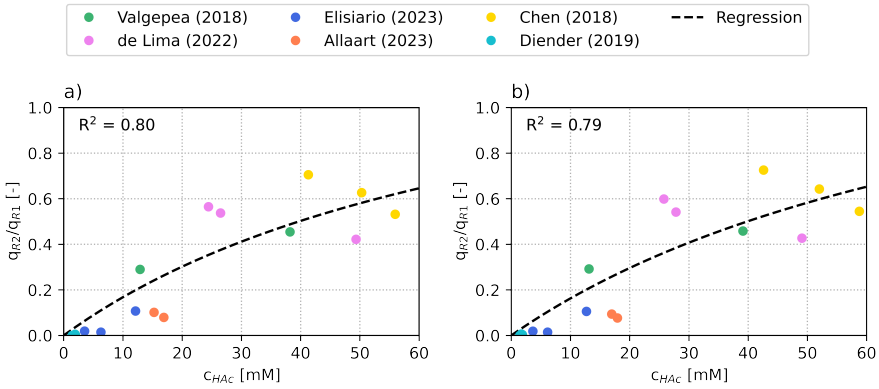

Figure 3.16: The ratio of the catabolic reaction R2 and R1 rate (q_{R2}/q_{R1}) plotted as a function of the undissociated acetic acid concentration (c_{HAc}). With a) the experimental and b) reconciled data.

No literature was available on the catabolic reaction rates q_{R1} and q_{R2}. However, Ruggiero et al. (2022) reported a K_{HAc} of 54.95 mM for *Clostridium carboxidivorans* (*C. carboxidivorans*) grown on CO. The difference of this values with the observed K_{HAc} may arise from differences in process conditions and intracellular differences with *C. autoethanogenum*. With the observed $q_{R2}^{max}/q_{R1}^{max}$ ratio the maximum q_{R1}^{max} and q_{R2}^{max} were estimated. Therefore, the maximal growth rate (μ^{max}) was determined first using Eq. (3.21) and assuming a q_{CO}^{max} of -119 mmol/(g_{DW} h) (Allaart et al., 2024). This yielded a μ^{max} of 0.20 h^{-1} for the experimental data and 0.21 h^{-1} for the reconciled data. With the observed $q_{R2}^{max}/q_{R1}^{max}$ ratio of 0.6, a q_{R1}^{max} and q_{R2}^{max} of 19.1 and 21.4 mmol/(g_{DW} h) and 11.5 and 12.8 mmol/(g_{DW} h) were obtained for the experimental and reconciled data, respectively (see Appendix I).

Various μ^{max} values for batch growth of *C. autoethanogenum* have been reported in literature. For batch growth of *C. autoethanogenum* on syngas (50% N_2, 20% CO, 20% CO_2 and 10% H_2) at pH 6.8 (uncontrolled) with mainly acetate production, Cotter et al. (2009) published data from which a μ^{max} of 0.093 h^{-1} was calculated from the exponential growth phase (Appendix I). Though, Oliveira et al. (2022) reported a μ^{max} of 0.065 h^{-1} for batch growth on syngas (60% CO, 20% CO_2 and 20% H_2) at pH 6 (controlled) with mainly ethanol production. Valgepea, Loi, et al. (2017) published a doubling time of 7.3 h for batch growth of *C. autoethanogenum* on syngas (29% N_2, 50% CO, 18% CO_2 and 3% H_2) at pH 5.7 with slight acetate production from which a μ^{max} of 0.095 h^{-1} was calculated. The μ^{max} estimated in this study is significantly higher than the experimental values. For gas fermentation, it is challenging to determine whether the observed rates are constrained by either gas-liquid mass transfer, biological capacity or CO inhibition. Furthermore, changes in the fermentation broth during batch fermentation influence the gas-liquid mass transfer (Allaart et al., 2024; Puiman et al., 2022). Therefore, the experimentally reported μ^{max} values might not be the maximum, due to other limitations. Lanzillo et al. (2020) reported a μ^{max} of 0.22 h^{-1} for batch growth of *C. carboxidivorans* on CO, which suggests that acetogenic bacteria are capable of reaching the maximum growth rates estimated in this study.

3.3. Preliminary model description

In this section, a preliminary model is suggested based on the kinetic equations derived in the previous sections. Given the gas inflow rate ($F_{g,in}^{N}$), fraction of CO in the gas inflow ($y_{CO,in}$), and dilution rate (D), the model can predict the consumption and production rates (q_i) for a steady-state CO-fermentation by *C. autoethanogenum* at 37 ^{o}C and a pressure of 1 atm.

The growth kinetics of *C. autoethanogenum* were described by coupling ATP production in the catabolism to energy requirements for growth and maintenance processes through a modified Herbert-Pirt equation. Eq. (3.18) proved best at estimating the growth rate (Table 3.2), and was therefore incorporated into the final model. Furthermore, Eq. (3.7) was incorporated into the model to estimate the CO uptake rate. Overall, a better fit was obtained when parameters were fitted with the reconciled data. This suggests that closing carbon and electron balances provides more accurate representation of the underlying processes, thereby enhancing the overall model fit and the reliability of the predictions. Therefore, the parameters fitted with the reconciled data were used in the final model.

Table 3.2: Summary of model equations fitted to both experimental and reconciled data.

Equation	R^2 experimental	R^2 reconciled
(3.7)	0.88	0.91
(3.8)	0.82	0.87
(3.18)	0.97	0.98

Assuming the dilution rate is equal to the growth rate (μ), combining the two kinetic equations (Eq. (3.26)-(3.27)) with the carbon balance (Eq. (3.28)), degree of reduction balance (Eq. (3.29)), and the definitions for catabolic reaction rates q_{R1} (Eq. (3.30)) and q_{R2} (Eq. (3.31)) allows calculating the consumption and production rates. Without access to the dissolved CO concentrations, it was not possible to describe the substrate uptake kinetics and, consequently, determine the dissolved CO concentrations. Without the dissolved CO concentrations, there are more unknowns than equations, making it impossible to predict the product concentrations.

Kinetic equations:

$$\mu = 4 \cdot Y_{x/CO,R1}^{max} \cdot q_{R1} + 2 \cdot Y_{x/CO,R2}^{max} \cdot q_{R2} \tag{3.26}$$

with $Y_{x/CO,R1}^{max}$ = 1.27 g_{DW} /mol and $Y_{x/CO,R1}^{max}$ = 3.90 g_{DW} /mol

$$-q_{CO} = \frac{1}{Y_{x/CO}^{max}} + m_{CO} \tag{3.27}$$

with $Y_{x/CO}^{max}$ = 1.85 g_{DW} /mol and m_{CO} = 6.42 mmol/(g_{DW} h)

Elemental balances:

$$q_{CO} + q_{CO_2} + \mu + 2q_{AcT} + 2q_{EtOH} = 0 \tag{3.28}$$

$$2q_{CO} + 3.76\mu + 8q_{AcT} + 12q_{EtOH} = 0 \tag{3.29}$$

Rate definitions:

$$q_{R1} = q_{EtOH} + q_{AcT} \tag{3.30}$$

$$q_{R2} = q_{EtOH} \tag{3.31}$$

4

Conclusions

This study aimed to develop a simple quantitative model for steady-state CO fermentation by *Clostridium autoethanogenum* (*C. autoethanogenum*) using unstructured microbial kinetics and the current insights into the ATP production of the CO to ethanol and acetate pathways. The main conclusions of the study are summarized below:

- Data reconciliation improves data quality, such that model parameters can be estimated more precisely.
- The maximum biomass yield on ATP ($Y_{x/ATP}^{max}$) and ATP requirements for maintenance (m_{ATP}) for CO fermentation by *C. autoethanogenum* are estimated as 6.36 ±0.63 g_{DW}/mol and 2.61 ±0.79 mmol/(g_{DW} h), respectively.
- The maximal growth rate (μ^{max}), maximal rate of catabolic reaction R1 (q_{R1}^{max}) and maximal rate for catabolic reaction R2 (q_{R2}^{max}) are estimated as 0.21 h^{-1}, 21.4 mmol/(g_{DW} h) and 12.8 mmol/(g_{DW} h), respectively.
- The growth kinetics of *C. autoethanogenum* can be described by coupling ATP production in the catabolism to energy requirements for growth through a modified Herbert-Pirt equation. In this equation, the maximum biomass yield on CO for catabolic reactions R1 ($Y_{x/CO,R1}^{max}$) and R2 ($Y_{x/CO,R2}^{max}$) are 1.27 ±0.16 and 3.90 ±0.68 g_{DW}/mol_{CO}, respectively. Moreover, the effect of maintenance on growth is negligible, and acetate inhibition is insignificant.

$$\mu = 4 \cdot Y_{x/CO,R1}^{max} \cdot q_{R1} + 2 \cdot Y_{x/CO,R2}^{max} \cdot q_{R2}$$

- A preliminary model was suggested that, given the gas inflow rate, gas inflow composition and liquid dilution rate, predicts the consumption and production rates for CO fermentation by *C. autoethanogenum* at 37 ^{o}C and 1 atm pressure.
- The gas uptake kinetics for syngas fermentation is a research gap that should be explored further in the upcoming years.
- The development of dissolved CO measurement methods is essential to gain a better understanding of gas-liquid mass transfer in lab-scale bioreactors with low gas flows.

5

Future perspectives

In this study, new insights were gained into the kinetic modelling of steady-state CO fermentations by *Clostridium autoethanogenum*. While the findings outlined in this study are not groundbreaking, they highlight some important issues that should be addressed and improvements that can be made.

To start, the development of the model was constrained by the availability of dissolved CO concentrations. Given that gas-liquid mass transfer in lab-scale gas fermentations with low gas flows remains an area in need of further research, developing online CO sensors, such as presented by Mann et al. (2021), is crucial in bridging the knowledge gap (Puiman, 2024). Additionally, novel dissolved gas measurement methods could provide a better understanding of the influence of different broth components on the mass transfer.

In this study, it was not possible to determine the substrate uptake kinetics for CO-fermentation by *C. autoethanogenum*. Uptake kinetic parameters have been obtained for syngas fermenting bacteria through either experimentation or modelling (Allaart et al., 2023; Almeida Benalcázar, 2023; de Medeiros et al., 2019; Lanzillo et al., 2020; Ruggiero et al., 2022). Obtaining substrate uptake kinetics through batch cultivation poses challenges for gas fermentations, as it is difficult to discern whether the observed rates are limited by gas-liquid mass transfer, biological capacity, or CO inhibition (Allaart et al., 2024). In light of this problem, Allaart et al. (2024) proposed a novel method to study the CO uptake kinetics in gas-fermenting bacteria by exposing them to pulses of increasing CO partial pressures. Together with novel online dissolved CO measuring methods, this method could be used to determine the maximum CO uptake rate (q_{CO}^{max}) in gas fermentations. Additionally, the affinity constant (K_{CO}) and inhibition constant ($K_{I,CO}$) might be approached in steady-state chemostat experiments, during which the amount of CO in the inflow is stepwise increased (Puiman, 2024).

Because putting together the experimental dataset, including data reconciliation, was more time-consuming than anticipated, there are still some model extensions that should be implemented. To start, the production of 2,3-butanediol and hydrogen was not accounted for in this model. With an ATP yield of 0.14 and 0.136 ATP per CO for 2,3-butanediol and hydrogen (Norman et al., 2019), respectively, it is still not fully understood why they are produced. It has been suggested that the production of both might be essential in the regeneration of co-factors (Celińska and Grajek, 2009; Hermann et al., 2020; Norman et al., 2019). Including hydrogen and 2,3-butanediol production could provide greater insight into the reasons behind their production.

Additionally, industrial syngas fermentation often uses mixtures of CO, H_2 and CO_2 (Stoll et al., 2020). Therefore, H_2 and CO_2 consumption should be incorporated into the model, such that the model is not only relevant for CO-fermentation. Furthermore, increasing the extracellular acetic acid and biomass concentration have been identified as a strategy to increase ethanol productivity in *C. autoethanogenum* (Elisiário et al., 2023; Valgepea, de Souza Pinto Lemgruber, et al., 2017). Therefore, incorporating a recycle loop for biomass and acetate into the model would enable the analysis of the impacts of both strategies.

6

Acknowledgements

This last chapter marks the end of this thesis and, simultaneously, the end of the academic part of the Master's program. The MSc LST Delft has been a roller coaster that was exciting, stressful, challenging, fun and rewarding at once. This thesis represents the culmination of everything I have learned during this period. However, I could not have accomplished this by myself. Therefore, this chapter is dedicated to all the people who contributed, either directly or indirectly, to my thesis.

First of all, I would like to thank my supervisor **Adrie Straathof** for all the insightful conversations and guidance. Additionally, I would like to thank **Lars Puiman** and **Eduardo Almeida Benalcázar** for their guidance and support as my daily supervisors throughout the various stages of this thesis. Furthermore, I would like to thank **Adrie Straathof**, **Ludovic Jourdin**, and **Djordje Bajić** for participating in my thesis committee.

To my fellow students and friends **Daniëlle**, **Eline**, **Jesús**, **Mehrab**, **Stijn** and **Thomas**, thank you for keeping me (somewhat) sane during this time. Not only did I enjoy the time we spent together during the breaks and mental health walks, but you guys also encouraged me to participate in fun activities (i.e. the weekly borrels, Oktoberfest etc.) I would most certainly have skipped without you being there. Also, **Ruby**, whom I became friends with during the first year of the Bachelor LST, and reintroduced me into the magical world of reading throughout the duration of this project.

I would also like to give a shout-out to **Martijn Diender**, **Kaspar Valgepea** and **James Heffernan** for taking the time to gather and share some of their data.

Last but certainly not least, I would like to thank my **parents** and **family** for their continuous support throughout the entire duration of my studies.

Bibliography

Abrini, J., Naveau, H., & Nyns, E.-J. (1994). Clostridium autoethanogenum, sp. nov., an anaerobic bacterium that produces ethanol from carbon monoxide. *Archives of Microbiology*, *161*(4), 345–351. https://doi.org/10.1007/BF00303591

Abubackar, H. N., Veiga, M. C., & Kennes, C. (2011). Biological conversion of carbon monoxide: Rich syngas or waste gases to bioethanol. *Biofuels, Bioproducts and Biorefining*, *5*(1), 93–114. https://doi.org/10.1002/bbb.256

Allaart, M. T. (2023). *Poison to products: On harnessing the power of microorganisms to convert waste streams into new chemicals* [Doctoral dissertation, TU Delft]. https://repository.tudelft.nl/islandora/object/uuid%3Abbf1eb72-9cc7-4e64-adf0-d869954c1750

Allaart, M. T., Diender, M., Sousa, D. Z., & Kleerebezem, R. (2023). Overflow metabolism at the thermodynamic limit of life: How carboxydotrophic acetogens mitigate carbon monoxide toxicity. *Microbial Biotechnology*, *16*(4), 697–705. https://doi.org/10.1111/1751-7915.14212

Allaart, M. T., Korkontzelos, C., Sousa, D. Z., & Kleerebezem, R. (2024). A novel experimental method to determine substrate uptake kinetics of gaseous substrates applied to the carbon monoxide-fermenting clostridium autoethanogenum. *Biotechnology and Bioengineering*, *121*(4), 1324–1334. https://doi.org/https://doi.org/10.1002/bit.28652

Almeida Benalcázar, E. F. (2023). *Modeling the anaerobic fermentation of co, h2 and co2 mixtures at large and micro-scales* [Doctoral dissertation, TU Delft]. https://repository.tudelft.nl/islandora/object/uuid%3Aa152e57f-1c21-4941-b298-55f7b133e2e4

Almquist, J., Cvijovic, M., Hatzimanikatis, V., Nielsen, J., & Jirstrand, M. (2014). Kinetic models in industrial biotechnology – improving cell factory performance. *Metabolic Engineering*, *24*, 38–60. https://doi.org/10.1016/j.ymben.2014.03.007

Applikon. (2008, September). Autoclavable bioreactors 1 - 20 l.

Arslan, K., Bayar, B., Nalakath Abubackar, H., Veiga, M. C., & Kennes, C. (2019). Solventogenesis in Clostridium aceticum producing high concentrations of ethanol from syngas. *Bioresource Technology*, *292*, 121941. https://doi.org/10.1016/j.biortech.2019.121941

Bachmann, H., Bruggeman, F. J., Molenaar, D., Branco dos Santos, F., & Teusink, B. (2016). Public goods and metabolic strategies. *Current Opinion in Microbiology*, *31*, 109–115. https://doi.org/10.1016/j.mib.2016.03.007

Bahl, H., Andersch, W., Braun, K., & Gottschalk, G. (1982). Effect of ph and butyrate concentration on the production of acetone and butanol by clostridium acetobutylicum grown in continuous culture. *European journal of applied microbiology and biotechnology*, *14*(1), 17–20. https://doi.org/10.1007/BF00507998

Canganella, F., Kuk, S.-U., Morgan, H., & Wiegel, J. (2002). Clostridium thermobutyricum: Growth studies and stimulation of butyrate formation by acetate supplementation. *Microbiological Research*, *157*(2), 149–156. https://doi.org/10.1078/0944-5013-00140

Celińska, E., & Grajek, W. (2009). Biotechnological production of 2,3-butanediol—current state and prospects. *Biotechnology Advances*, *27*(6), 715–725. https://doi.org/10.1016/j.biotechadv.2009.05.002

Chen, J., Daniell, J., Griffin, D., Li, X., & Henson, M. A. (2018). Experimental testing of a spatiotemporal metabolic model for carbon monoxide fermentation with Clostridium autoethanogenum. *Biochemical Engineering Journal*, *129*, 64–73. https://doi.org/10.1016/j.bej.2017.10.018

Chen, J., Gomez, J. A., Höffner, K., Barton, P. I., & Henson, M. A. (2015). Metabolic modeling of synthesis gas fermentation in bubble column reactors. *Biotechnology for Biofuels*, *8*(1), 89. https://doi.org/10.1186/s13068-015-0272-5

Cotter, J. L., Chinn, M. S., & Grunden, A. M. (2009). Influence of process parameters on growth of clostridium ljungdahlii and clostridium autoethanogenum on synthesis gas. *Enzyme and Microbial Technology*, *44*(5), 281–288. https://doi.org/10.1016/j.enzmictec.2008.11.002

Cui, Y. Q., van der Lans, R. G. J. M., & Luyben, K. C. A. M. (1996). Local power uptake in gas-liquid systems with single and multiple rushton turbines. *Chemical Engineering Science*, *51*(11), 2631–2636. https://doi.org/10.1016/0009-2509(96)00128-5

Cussler, E. L. (1997, February). *Diffusion: Mass transfer in fluid systems* [Google-Books-ID: TGRmfTrsPTQC]. Cambridge University Press.

de Lima, L. A., Ingelman, H., Brahmbhatt, K., Reinmets, K., Barry, C., Harris, A., Marcellin, E., Köpke, M., & Valgepea, K. (2022). Faster growth enhances low carbon fuel and chemical production through gas fermentation. *Frontiers in Bioengineering and Biotechnology*, *10*. https://doi.org/10.3389/fbioe.2022.879578

de Medeiros, E. M., Posada, J. A., Noorman, H., & Filho, R. M. (2019). Dynamic modeling of syngas fermentation in a continuous stirred-tank reactor: Multi-response parameter estimation and process optimization. *Biotechnology and Bioengineering*, *116*(10), 2473–2487. https://doi.org/10.1002/bit.27108

Diender, M. (2024, March). Personal communication [March 1, 2024].

Diender, M. (2019). *Exploration of microbial systems as biocatalysts for conversion of synthesis gas to bio-based chemicals* [Doctoral dissertation, Wageningen University]. https://doi.org/10.18174/466065

Diender, M., Parera Olm, I., Gelderloos, M., Koehorst, J. J., Schaap, P. J., Stams, A. J. M., & Sousa, D. Z. (2019). Metabolic shift induced by synthetic co-cultivation promotes high yield of chain elongated acids from syngas. *Scientific Reports*, *9*(11), 18081. https://doi.org/10.1038/s41598-019-54445-y

Elisiário, M. P., Van Hecke, W., De Wever, H., Noorman, H., & Straathof, A. J. J. (2023). Acetic acid, growth rate, and mass transfer govern shifts in co metabolism of Clostridium autoethanogenum. *Applied Microbiology and Biotechnology*, *107*(17), 5329–5340. https://doi.org/10.1007/s00253-023-12670-6

Ewing, T. A., Nouse, N., van Lint, M., van Haveren, J., Hugenholtz, J., & van Es, D. S. (2022). Fermentation for the production of biobased chemicals in a circular economy: A perspective for the period 2022–2050. *Green Chemistry*, *24*(17), 6373–6405. https://doi.org/10.1039/d1gc04758b

Fackler, N., Heijstra, B. D., Rasor, B. J., Brown, H., Martin, J., Ni, Z., Shebek, K. M., Rosin, R. R., Simpson, S. D., Tyo, K. E., Giannone, R. J., Hettich, R. L., Tschaplinski, T. J., Leang, C., Brown, S. D., Jewett, M. C., & Köpke, M. (2021). Stepping on the gas to a circular economy: Accelerating development of carbon-negative chemical production from gas fermentation. *Annual Review of Chemical and Biomolecular Engineering*, *12*(1), 439–470. https://doi.org/10.1146/annurev-chembioeng-120120-021122

Fernández-Blanco, C., Robles-Iglesias, R., Naveira-Pazos, C., Veiga, M. C., & Kennes, C. (2023). Production of biofuels from C1-gases with Clostridium and related bacteria-recent advances. *Microbial Biotechnology*, *16*(4), 726–741. https://doi.org/10.1111/1751-7915.14220

Garcia-Ochoa, F., & Gomez, E. (2009). Bioreactor scale-up and oxygen transfer rate in microbial processes: An overview. *Biotechnology Advances*, *27*(2), 153–176. https://doi.org/10.1016/j.biotechadv.2008.10.006

González-Figueredo, C., Flores-Estrella, R. A., Rojas-Rejón, O. A., González-Figueredo, C., Flores-Estrella, R. A., & Rojas-Rejón, O. A. (2018, November). Fermentation: Metabolism, kinetic models, and bioprocessing. In *Current topics in biochemical engineering*. IntechOpen. https://doi.org/10.5772/intechopen.82195

Greene, J., Daniell, J., Köpke, M., Broadbelt, L., & Tyo, K. E. J. (2019). Kinetic ensemble model of gas fermenting clostridium autoethanogenum for improved ethanol production. *Biochemical Engineering Journal*, *148*, 46–56. https://doi.org/10.1016/j.bej.2019.04.021

Heffernan, J. K., Valgepea, K., de Souza Pinto Lemgruber, R., Casini, I., Plan, M., Tappel, R., Simpson, S. D., Köpke, M., Nielsen, L. K., & Marcellin, E. (2020). Enhancing CO2-valorization using Clostridium autoethanogenum for sustainable fuel and chemicals production. *Frontiers in Bioengineering and Biotechnology*, *8*. https://www.frontiersin.org/articles/10.3389/fbioe.2020.00204

Heijnen, J. J. (2012). Black box (bb) model of microorganisms: Stoichiometry.

Heijnen, J. J., & Kleerebezem, R. (2010, April). Bioenergetics of microbial growth. https://doi.org/10.1002/9780470054581.eib084

Heijnen, J. J., & Van Dijken, J. P. (1992). In search of a thermodynamic description of biomass yields for the chemotrophic growth of microorganisms. *Biotechnology and Bioengineering*, *39*(8), 833–858. https://doi.org/10.1002/bit.260390806

Heijnen, J. J., & Verheijen, P. J. T. (2011). How to obtain true and accurate rate-values. *Methods in enzymology*, *500*, 457–508. https://doi.org/10.1016/b978-0-12-385118-5.00023-2

Henriksen, C. M., Nielsen, J., & Villadsen, J. (1998). Modelling of the protonophoric uncoupling by phenoxyacetic acid of the plasma membrane potential of Penicillium chrysogenum. *Biotechnology and Bioengineering*, *60*(6), 761–767. https://doi.org/10.1002/(SICI)1097-0290(19981220)60:6<761::AID-BIT12>3.0.CO;2-N

Hermann, M., Teleki, A., Weitz, S., Niess, A., Freund, A., Bengelsdorf, F. R., & Takors, R. (2020). Electron availability in co2, co and h2 mixtures constrains flux distribution, energy management and product formation in clostridium ljungdahlii. *Microbial Biotechnology*, *13*(6), 1831–1846. https://doi.org/10.1111/1751-7915.13625

Infors HT. (2023, October). Multifors 2 bench-top bioreactor - version for microorganisms.

Jang, N., Yasin, M., Park, S., Lovitt, R. W., & Chang, I. S. (2017). Determination of volumetric gas–liquid mass transfer coefficient of carbon monoxide in a batch cultivation system using kinetic simulations. *Bioresource Technology*, *239*, 387–393. https://doi.org/10.1016/j.biortech.2017.05.023

Katsyv, A., & Müller, V. (2020). Overcoming energetic barriers in acetogenic C1 conversion. *Frontiers in Bioengineering and Biotechnology*, *8*. https://www.frontiersin.org/articles/10.3389/fbioe.2020.621166

Kleerebezem, R. (2022, November). Kinetics [Presentation slides for LM3741 Fermentation Technology and Environmental Biotechnology, November 29th 2022, TU Delft].

Kleerebezem, R., & Van Loosdrecht, M. C. M. (2010). A generalized method for thermodynamic state analysis of environmental systems. *Critical Reviews in Environmental Science and Technology*, *40*(1), 1–54. https://doi.org/10.1080/10643380802000974

Korkontzelos, H. (2022). *Estimation of kinetic parameters of the acetogen clostridium autoethanogenum on carbon monoxide*. https://repository.tudelft.nl/islandora/object/uuid%3Ad7b7e6d4-c38d-42a2-8c7b-3d44bad427c1

Kuenen, G. (2019). Continuous cultures (chemostats). In T. M. Schmidt (Ed.), *Encyclopedia of microbiology* (pp. 743–761). Elsevier. https://doi.org/10.1016/B978-0-12-801238-3.02490-9

Lanzillo, F., Ruggiero, G., Raganati, F., Russo, M. E., & Marzocchella, A. (2020). Batch syngas fermentation by clostridium carboxidivorans for production of acids and alcohols. *Processes*, *8*(99), 1075. https://doi.org/10.3390/pr8091075

LibreTexts. (2022, December). Lagrange multipliers. https://math.libretexts.org/@go/page/2607

Liew, F., Henstra, A. M., K□pke, M., Winzer, K., Simpson, S. D., & Minton, N. P. (2017). Metabolic engineering of clostridium autoethanogenum for selective alcohol production. *Metabolic Engineering*, *40*, 104–114. https://doi.org/10.1016/j.ymben.2017.01.007

Liew, F., Martin, M. E., Tappel, R. C., Heijstra, B. D., Mihalcea, C., & Köpke, M. (2016). Gas fermentation—a flexible platform for commercial scale production of low-carbon-fuels and chemicals from waste and renewable feedstocks. *Frontiers in Microbiology*, *7*. https://doi.org/10.3389/fmicb.2016.00694

Ljungdhal, L. G. (1986). The autotrophic pathway of acetate synthesis in acetogenic bacteria. *Annual Review of Microbiology*, *40*(1), 415–450. https://doi.org/10.1146/annurev.mi.40.100186.002215

Lu, S., Shi, Y., Meng, N., Lu, S., Yu, Y., & Zhang, B. (2020). Electrosynthesis of syngas via the co-reduction of co2 and h2o. *Cell Reports Physical Science*, *1*(11), 100237. https://doi.org/10.1016/j.xcrp.2020.100237

Mann, M., Miebach, K., & Büchs, J. (2021). Online measurement of dissolved carbon monoxide concentrations reveals critical operating conditions in gas fermentation experiments. *Biotechnology and Bioengineering*, *118*(1), 253–264. https://doi.org/10.1002/bit.27567

Marcellin, E., Behrendorff, J. B., Nagaraju, S., DeTissera, S., Segovia, S., Palfreyman, R. W., Daniell, J., Licona-Cassani, C., Quek, L.-e., Speight, R., Hodson, M. P., Simpson, S. D., Mitchell, W. P., Köpke, M., & Nielsen, L. K. (2016). Low carbon fuels and commodity chemicals from waste gases – systematic approach to understand energy metabolism in a model acetogen. *Green Chemistry*, *18*(10), 3020–3028. https://doi.org/10.1039/c5gc02708j

Meyer Houston, C. L., & Papoutsakis, E. T. (1989). Continuous and biomass recycle fermentations of clostridium acetobutylicum. *Bioprocess Engineering*, *4*(2), 49–55. https://doi.org/10.1007/BF00373731

Mock, J., Zheng, Y., Mueller, A. P., Ly, S., Tran, L., Segovia, S., Nagaraju, S., Köpke, M., Dürre, P., & Thauer, R. K. (2015). Energy conservation associated with ethanol formation from H2 and CO2 in Clostridium autoethanogenum involving electron bifurcation. *Journal of Bacteriology*, *197*(18), 2965–2980. https://doi.org/10.1128/JB.00399-15

Molitor, B., Richter, H., Martin, M. E., Jensen, R. O., Juminaga, A., Mihalcea, C., & Angenent, L. T. (2016). Carbon recovery by fermentation of co-rich off gases – turning steel mills into biorefineries. *Bioresource Technology*, *215*, 386–396. https://doi.org/10.1016/j.biortech.2016.03.094

Monod, J. (1949). The growth of bacterial cultures. *Annual Review of Microbiology*, *3*(1), 371–394. https://doi.org/10.1146/annurev.mi.03.100149.002103

Munoz, L., & Philips, J. (2023). No acetogen is equal: Strongly different h2 thresholds reflect diverse bioenergetics in acetogenic bacteria. *Environmental Microbiology*, *25*(10), 2032–2040. https://doi.org/10.1111/1462-2920.16429

Noorman, H. J., van Winden, W., Heijnen, J. J., & van der Lans, R. G. J. M. (2018). Intensified fermentation processes and equipment. https://doi.org/10.1039/9781788010320-00001

Norman, R. O., Millat, T., Schatschneider, S., Henstra, A. M., Breitkopf, R., Pander, B., Annan, F. J., Piatek, P., Hartman, H. B., Poolman, M. G., Fell, D. A., Winzer, K., Minton, N. P., & Hodgman, C. (2019). Genome-scale model of C. autoethanogenum reveals optimal bioprocess conditions for high-value chemical production from carbon monoxide. *Engineering Biology*, *3*(2), 32–40. https://doi.org/10.1049/enb.2018.5003

Oliveira, L., Rückel, A., Nordgauer, L., Schlumprecht, P., Hutter, E., & Weuster-Botz, D. (2022). Comparison of syngas-fermenting clostridia in stirred-tank bioreactors and the effects of varying syngas impurities. *Microorganisms*, *10*(44), 681. https://doi.org/10.3390/microorganisms10040681

Pirt, S. J., & Hinshelwood, C. N. (1997). The maintenance energy of bacteria in growing cultures. *Proceedings of the Royal Society of London. Series B. Biological Sciences*, *163*(991), 224–231. https://doi.org/10.1098/rspb.1965.0069

Puiman, L. (2024). *From bioreactors to bubbles to bacteria: On multi-scale interactions in gas fermentations* [Dissertation]. TU Delft. https://doi.org/10.4233/uuid:e68fcc5d-f349-4f52-ad66-89f1a5e6187d

Puiman, L. (2020). *Modelling syngas fermentation in hollow fibre membrane reactors* [Master Thesis]. TU Delft. http://resolver.tudelft.nl/uuid:bf2f8373-4953-44b1-b584-ce7746ca8d40

Puiman, L., Almeida Benalcázar, E., Picioreanu, C., Noorman, H. J., & Haringa, C. (2023). Downscaling industrial-scale syngas fermentation to simulate frequent and irregular dissolved gas concentration shocks. *Bioengineering*, *10*(55), 518. https://doi.org/10.3390/bioengineering10050518

Puiman, L., Elisiário, M. P., Crasborn, L. M. L., Wagenaar, L. E. C. H., Straathof, A. J. J., & Haringa, C. (2022). Gas mass transfer in syngas fermentation broths is enhanced by ethanol. *Biochemical Engineering Journal*, *185*, 108505. https://doi.org/10.1016/j.bej.2022.108505

Ruggiero, G., Lanzillo, F., Raganati, F., Russo, M. E., Salatino, P., & Marzocchella, A. (2022). Bioreactor modelling for syngas fermentation: Kinetic characterization. *Food and Bioproducts Processing*, *134*, 1–18. https://doi.org/10.1016/j.fbp.2022.04.002

Sander, R. (2023). Compilation of Henry's law constants (version 5.0.0) for water as solvent. *Atmospheric Chemistry and Physics*, *23*(19), 10901–12440. https://doi.org/10.5194/acp-23-10901-2023

Schuchmann, K., & Müller, V. (2014). Autotrophy at the thermodynamic limit of life: A model for energy conservation in acetogenic bacteria. *Nature Reviews Microbiology*, *12*(12), 809–821. https://doi.org/10.1038/nrmicro3365

Stoll, I. K., Boukis, N., & Sauer, J. (2020). Syngas fermentation to alcohols: Reactor technology and application perspective. *Chemie Ingenieur Technik*, *92*(1–2), 125–136. https://doi.org/10.1002/cite.201900118

Straathof, A. J. J. (2023a, September). Personal communication [September 6, 2023].

Straathof, A. J. J. (2023b). Modelling of end-product inhibition in fermentation. *Biochemical Engineering Journal*, *191*, 108796. https://doi.org/10.1016/j.bej.2022.108796

Sun, X., Atiyeh, H. K., Huhnke, R. L., & Tanner, R. S. (2019). Syngas fermentation process development for production of biofuels and chemicals: A review. *Bioresource Technology Reports*, *7*, 100279. https://doi.org/10.1016/j.biteb.2019.100279

Valgepea, K. (2024, January). Personal communication [January 2, 2024].

Valgepea, K., de Souza Pinto Lemgruber, R., Abdalla, T., Binos, S., Takemori, N., Takemori, A., Tanaka, Y., Tappel, R., Köpke, M., Simpson, S. D., Nielsen, L. K., & Marcellin, E. (2018). H2 drives metabolic rearrangements in gas-fermenting Clostridium autoethanogenum. *Biotechnology for Biofuels*, *11*(1), 55. https://doi.org/10.1186/s13068-018-1052-9

Valgepea, K., de Souza Pinto Lemgruber, R., Meaghan, K., Palfreyman, R. W., Abdalla, T., Heijstra, B. D., Behrendorff, J. B., Tappel, R., Köpke, M., Simpson, S. D., Nielsen, L. K., & Marcellin, E. (2017). Maintenance of ATP homeostasis triggers metabolic shifts in gas-fermenting acetogens. *Cell Systems*, *4*(5), 505–515.e5. https://doi.org/10.1016/j.cels.2017.04.008

Valgepea, K., Loi, K. Q., Behrendorff, J. B., Lemgruber, R. d. S. P., Plan, M., Hodson, M. P., Köpke, M., Nielsen, L. K., & Marcellin, E. (2017). Arginine deiminase pathway provides atp and boosts growth of the gas-fermenting acetogen clostridium autoethanogenum. *Metabolic Engineering*, *41*, 202–211. https://doi.org/10.1016/j.ymben.2017.04.007

van der Lans, R. G. J. M. (2003). Gas-liquid interphase transport. chapter 19. In *Course book advanced course on environmental biotechnology*. Delft University of Technology.

van Bodegom, P. (2007). Microbial maintenance: A critical review on its quantification. *Microbial Ecology*, *53*(4), 513–523. https://doi.org/10.1007/s00248-006-9049-5

Van't Riet, K. (1979). Review of measuring methods and results in nonviscous gas-liquid mass transfer in stirred vessels. *Industrial & Engineering Chemistry Process Design and Development*, *18*(3), 357–364. https://doi.org/10.1021/i260071a001

Villadsen, J., Nielsen, J., & Lidén, G. (2011). *Bioreaction engineering principles*. Springer US. https://doi.org/10.1007/978-1-4419-9688-6

Wahl, A., & Heijnen, J. J. (2021). *AMN module 1: Rates, recovery, reconciliation, black-box modeling* (T. Páez Watson, Ed.). TU Delft.

Walter, A., & Gutknecht, J. (1984). Monocarboxylic acid permeation through lipid bilayer membranes. *The Journal of Membrane Biology*, *77*(3), 255–264. https://doi.org/10.1007/BF01870573

Wood, H. G. (1991). Life with CO or CO2 and H2 as a source of carbon and energy. *The FASEB Journal*, *5*(2), 156–163. https://doi.org/10.1096/fasebj.5.2.1900793

A

Overview of Python functions

A.1. Data reconciliation

A.1.1. Elemental Recovery

```
    def recoveries(yCO_in, yH2_in, yCO2_in, R, Emat):
    '''Calculates the carbon and electron recoveries

    Parameters
    ----------
    y_CO_in    : CO inflow fraction
    y_H2_in    : H2 inflow fraction
    y_CO2_in   : CO2 inflow fraction
    R : vector R containing the rates in mmol/h
    Emat: E matrix containing the elemental relations of rates in R.

    Returns:
        MB: an array containing the carbon recovery and electron recovery
    '''

    # Unpack  the rates
    RCO, RH2, RCO2, REtOH, RAcT, RBDO, Rx = R
    MB = [0, 0]

    ### CO/H2/CO2 fermentation ###
    if yCO_in > 0 and yH2_in > 0 and yCO2_in > 0:

        # Define the consumption- (in) and production rates (out)
        Rin = np.array([RCO, RH2, RCO2])
        Rout = np.array([REtOH, RAcT, RBDO, Rx])

        # Define the amount of carbons and electrons of the consumed (in) and produced (out)
    compounds
        Ein = Emat[:, 0:3]
        Eout = Emat[:, 3::]

        # Calculate the Carbon and Electron recoveries
        MB = Eout@Rout / (Ein@Rin) * -100

    ### CO fermentation ###
    elif yCO_in > 0 and yH2_in == 0 and yCO2_in == 0:

        # Define the consumption- (in) and production rates (out)
        Rin = np.array([RCO])
        Rout = np.array([RH2, RCO2, REtOH, RAcT, RBDO, Rx])

        # Define the amount of carbons and electrons of the consumed (in) and produced (out)
    compounds
        Ein = Emat[:, 0:1]
        Eout = Emat[:, 1::]

```

```
        # Calculate the Carbon and Electron recoveries
        MB = Eout@Rout / (Ein@Rin) * -100

    ### CO/H2 fermentation ###
    elif yCO_in > 0 and yH2_in > 0 and yCO2_in == 0:

        # Define the consumption- (in) and production rates (out)
        Rin = np.array([RCO, RH2])
        Rout = np.array([RCO2, REtOH, RAcT, RBDO, Rx])

        # Define the amount of carbons and electrons of the consumed (in) and produced (out)
    compounds
        Ein = Emat[:, 0:2]
        Eout = Emat[:, 2::]

        # Calculate the Carbon and Electron recoveries
        MB = Eout@Rout / (Ein@Rin) * -100

    ### H2/CO2 fermentation ###
    elif yCO_in == 0 and yH2_in > 0 and yCO2_in > 0:

        # Define the consumption- (in) and production rates (out)
        Rin = np.array([RH2, RCO2])
        Rout = np.array([RCO, REtOH, RAcT, RBDO, Rx])

        # Define the amount of carbons and electrons of the consumed (in) and produced (out)
    compounds
        Ein = Emat[:, 1:3]
        Eout = np.vstack((Emat[:,0:1].T, Emat[:, 3::].T)).T

        # Calculate the Carbon and Electron recoveries
        MB = Eout@Rout / (Ein@Rin) * -100

    ### CO/CO2 fermentation ###
    elif yCO_in > 0 and yH2_in == 0 and yCO2_in > 0:

        # Define the consumption- (in) and production rates (out)
        Rin = np.array([RCO])
        Rout = np.array([RH2, RCO2, REtOH, RAcT, RBDO, Rx])

        # Define the amount of carbons and electrons of the consumed (in) and produced (out)
    compounds
        Ein = Emat[:, 0:1]
        Eout = Emat[:, 1::]

        # Calculate the Carbon and Electron recoveries
        MB = Eout@Rout / (Ein@Rin) * -100

    return MB
```

A.1.2. Rate reconciliation

```
import numpy as np

def lagrange_solve_w( E, M, Rm, std_dev_Rm ):
    '''Solves an optimization problem using the Lagrange multipliers.
    Takes into consideration linear constraints and standard deviation
    of measured rates.

    Parameters
    ----------
    E          : E matrix containing the elemental relations of rates in R.
                 Linearity constraints (m balance equations E . R = 0)
    M          : M matrix containing the for the k measurements
                 (M . R = Rm +/-)
    Rm         : vector Rm containing the measurement values
    std_dev_Rm : standard deviations of the measurement in Rm

    Returns:
        R        : an array containing the estimated rates that
```

```
                    satisfy the linear constraints
        std_dev_r: an array containing the estimated standard deviation
                    of estimated rates'''

    # Rescale equation according to std_dev_Rm: gives different weights to
    # the measurements based on their uncertainty
    M_w = np.diag( std_dev_Rm ** -1 ) @ M

    # Construction of the Augmented Lagrangian Matrix to solve the
    # constrained optimization problem
    L1 = np.hstack( (M_w.T @ M_w, E.T) )
    L2 = np.hstack( (E, np.zeros( (E.shape[0], E.shape[0]) ) ) )
    L = np.vstack( (L1, L2) )

    # Construction of the right-hand side vector that incorporates
    # information from both measurements and constraints.
    b = np.concatenate( (M_w.T @ (Rm/std_dev_Rm), np.zeros((E.shape[0]))))

    # Solve the linear system and extract the estimated rates that satisfy
    # the constraints from the Rl vector
    Rl = np.linalg.solve(L, b)
    R = Rl[0:E.shape[1]]

    # Error propagation
    M = np.pad( M_w, ((0,0),(0,b.shape[0]-M_w.shape[1])), mode='constant')
    J = np.linalg.inv(L) @ M.T
    S_R = J @ J.T
    std_dev_R = np.diag(S_R) ** 0.5
    std_dev_R = std_dev_R[0:E.shape[1]]

    return (R, std_dev_R)
```

A.1.3. Gas outflow

```
    def gas_outflow(SST_data):
    '''Calculates the gas outflow rate and gas outflow fractions given
    the gas inflow rate and production/consumption rates

    Parameters
    ----------
    Fg_in     : Gas inflow rate in mmol/h
    y_CO_in   : CO inflow fraction
    y_H2_in   : H2 inflow fraction
    y_CO2_in  : CO2 inflow fraction
    y_inert_in: inert gas inflow fraction
    R_CO      : CO production/consumption rate in mmol/h
    R_H2      : H2 production/consumption rate in mmol/h
    R_CO2     : CO2 production/consumption rate in mmol/h

    Returns:
        y_CO  : CO outflow fraction
        y_H2  : H2 outflow fraction
        y_CO2 : CO2 outflow fraction
        Fg_out: Gas outflow rate in mmol/h
    '''

    # Mass balances in the gas phase
    def solve(x, *args):
        '''Optimization function'''

        # Unpack all variables
        Fg_in, y_CO_in, y_H2_in, y_CO2_in, y_inert_in, R_CO, R_H2, R_CO2 = args
        y_CO, y_H2, y_CO2, y_inert, Fg_out = x

        # Solve the gas-phase balances
        eq1 = Fg_in*y_CO_in - Fg_out*y_CO + R_CO     # CO balance in the gas-phase
        eq2 = Fg_in*y_H2_in - Fg_out*y_H2 + R_H2     # H2 balance in the gas-phase
        eq3 = Fg_in*y_CO2_in - Fg_out*y_CO2 + R_CO2  # CO2 balance in the gas-phase
        eq4 = Fg_in*y_inert_in - Fg_out*y_inert      # inert gas balance in the gas-phase
        eq5 = y_CO + y_H2 + y_CO2 + y_inert - 1      # Unity balance
```

```
        return [eq1, eq2, eq3, eq4, eq5]

    # Initial guesses
    x0 = [SST_data[1], SST_data[2], SST_data[3], SST_data[4], SST_data[0]]

    # Solve the system of equations
    solution = spo.least_squares(solve, x0, args=SST_data, bounds=([0, 0, 0, 0, 0], [1, 1, 1,
     1, np.inf]) )
    y_CO, y_H2, y_CO2, y_inert, Fg_out = solution.x

    return [y_CO, y_H2, y_CO2, y_inert, Fg_out]
```

A.1.4. Dissolved gas concentrations

```
    def gas_concentrations(args):
    '''Returns the dissolved gas concentrations of CO, H2, and CO2 in the liquid phase and
    their respective kLa's

    Parameters
    ----------
    fbroth : broth enhancement factor
    VL     : Worjing volume in m3
    T      : Temperature in K
    rhoL   : Density of the liquid phase in kg/m3
    N      : Agitation speed in 1/s
    Vr     : Total reactor volume in m3
    No_i   : Number of impellers
    Di     : Impeller diameter in m
    FG_in  : Gas inflow rate in m3/s
    FG_out : Gas outflow rate in m3/s
    y_CO   : CO outflow fraction
    y_H2   : H2 outflow fraction
    y_CO2  : CO2 outflow fraction
    T_CO   : CO transfer rate in mmol/h
    T_H2   : H2 transfer rate in mmol/h
    T_CO2  : CO2 transfer rate in mmol/h
    e_G    : Gas hold-up
    ugs    : Superficial gas velocity in m/s

    Returns:
        C_CO   : Dissolved CO concentration in mmol/L
        C_H2   : Dissolved H2 concentration in mmol/L
        C_CO2  : Dissolved CO2 concentration in mmol/L
        kLa_CO : kLa of CO in 1/h
        kLa_H2 : kLa of H2 in 1/h
        kLa_CO2: kLa of CO2 in 1/h
    '''
    # Unpack the variables
    fbroth, VL, T, P, rhoL, N, Vr, No_i, Di, FG_in, FG_out, y_CO, y_H2, y_CO2, T_CO, T_H2,
    T_CO2, e_G, ugs = args

    # Henry's correction constants (R. Sander)
    dHR_H2  = 490    # K
    dHR_CO  = 1300   # K
    dHR_CO2 = 2300   # K

    # Henry coefficients (R. Sander)
    H_CO  = (9.7e-6) * np.exp( -dHR_CO*((1/(T))  - (1/298.15)) ) * 101325 # mol/m3/atm
    H_H2  = (7.7e-6) * np.exp( -dHR_H2*((1/(T))  - (1/298.15)) ) * 101325 # mol/m3/atm
    H_CO2 = (3.4e-4) * np.exp( -dHR_CO2*((1/(T)) - (1/298.15)) ) * 101325 # mol/m3/atm

    # Diffusivity constants (Cussler et al., )
    Df_CO   = 2.03e-5   # Diffusivity CO in water at 25C, cm2/s
    Df_H2   = 4.5e-5    # Diffusivity H2 in water at 25C, cm2/s
    Df_CO2  = 1.92e-5   # Diffusivity CO2 in water at 25C, cm2/s
    Df_O2   = 2.10e-5   # Diffusivity O2 in water at 25C, cm2/s

    # Calculate the reactor diameter
    HT = 1.5 # Height over diameter ratio, -
```

```
    Dr = (Vr*4/(np.pi*HT))**(1/3) # vessel diameter, m

    ### Bubble Column ###
    if np.isnan(Di):

        # Constants
        kL = 0.1e-3 # m/s for small rigid bubbles at 20 oC
        db = 1.2e-3 # bubble size, m

        # Calculate the kLa for O2
        a = 6*e_G/db
        kLa_o2 = kL * a * 3600

    ### Stirred tank reactor ###
    else:
        # Calculate the ungassed power input
        Np = 6 # Power number, -
        Pug = No_i * Np * rhoL * N**3 * Di**5 # Ungassed power input, W

        # Calculate the gassed power number(de Meideros, 2019)
        x = (FG_in * N**0.25) / Di**2
        if x <= 0.055:
            Pg = (-9.9*x + 1)*Pug
        else:
            Pg = (-0.52-0.62*x + 1)*Pug

        # Calculate the superficial gas velocity
        ugs = (FG_in)/(np.pi/4 * Dr**2) # Superficial gas velocity, m/s

        # Calculate the kla for O2
        kLa_o2_col  = fbroth*1.022**(T-298.15) * 3600 * (0.026 * (Pg/VL)**0.4 * ugs**0.5) # kLa oxygen, 1/h
        kLa_o2_noncol  = fbroth*1.022**(T-298.15) * 3600 * (0.002 * (Pg/VL)**0.7 * ugs**0.2) # kLa oxygen, 1/h (non-coalescing = upper boundary)
        kLa_o2         = (1-fbroth) * kLa_o2_col + (fbroth) * kLa_o2_noncol

    # Correct for type of gas
    kLa_CO  = kLa_o2 * (Df_CO/Df_O2)**0.5  # kLa CO, 1/h
    kLa_H2  = kLa_o2 * (Df_H2/Df_O2)**0.5  # kLa H2, 1/h
    kLa_CO2 = kLa_o2 * (Df_CO2/Df_O2)**0.5 # kLa CO2, 1/h

    # Calculate the solubilities with Henry's Law
    C_COsol  = H_CO  * y_CO  * P # Solubility CO,  mol/m3 (=mmol/L)
    C_H2sol  = H_H2  * y_H2  * P # Solubility H2,  mol/m3 (=mmol/L)
    C_CO2sol = H_CO2 * y_CO2 * P # Solubility CO2, mol/m3 (=mmol/L)

    # Calculate the dissolved concentrations
    C_CO  = - abs(T_CO) /(VL * kLa_CO)  + C_COsol  # Dissolved CO concentration, mol/m3 (=mmol/L)
    C_H2  = - abs(T_H2) /(VL * kLa_H2)  + C_H2sol  # Dissolved H2 concentration, mol/m3 (=mmol/L)
    C_CO2 = - abs(T_CO2)/(VL * kLa_CO2) + C_CO2sol # Dissolved CO2 concentration, mol/m3 (=mmol/L)

    return C_CO, C_H2, C_CO2, kLa_CO, kLa_H2, kLa_CO2
```

A.2. Parameter Fitting

A.2.1. Growth kinetics

```
    def Herbert_Pirt(mu, a, b):
    '''Function for fitting all variations of the Herbert-Pirt equation

    Parameters:
    mu: growth rate in 1/h
    a : maximum yield on biomass in mol/gDW
    b : maintenance coefficient in mol/(gDW h)
    '''
    return a*mu + b
```

```python
def Herbert_Pirt_modified(x, a, b, c):
'''Function for fitting the modified Herbert-Pirt equation

Parameters:
qR1: reaction rate of catabolic reaction R1 in mol/(gDW h)
qR2: reaction rate of catabolic reaction R2 in mol/(gDW h)
a  : maximum biomass yield for catabolic reaction R1 in gDW/mol
b  : maximum biomass yield for catabolic reaction R2 in gDW/mol
c  : loss in growth due to maintenance in 1/h
'''

# unpack variables
qR1, qR2 = x

return a*qR1 + b*qR2 + c
```

```python
def Herbert_Pirt_modified_no_mx(x, a, b):
'''Function for fitting the modified Herbert-Pirt equation
   without the loss in growth due to maintenance

Parameters:
qR1: reaction rate of catabolic reaction R1 in mol/(gDW h)
qR2: reaction rate of catabolic reaction R2 in mol/(gDW h)
a  : maximum biomass yield for catabolic reaction R1 in gDW/mol
b  : maximum biomass yield for catabolic reaction R2 in gDW/mol
'''

# unpack variables
qR1, qR2 = x

return a*qR1 + b*qR2
```

```python
def Herbert_Pirt_HAc_inhibition1(x, a, b, c):
'''Function for fitting the Herbert-Pirt equation with HAc inhibition
   according to method 1

   Parameters:
   mu: growth rate in 1/h
   cHAc_out: extracellular undissociated acetic acid concentration in mol/L
   cHAc_in : intracellular undissociated acetic acid concentration in mol/L
   a       : maximum yield on biomass in mol/gDW
   b       : maintenance coefficient at cHAc = 0 in mol/(gDW h)
   c       : volume of acetate passing through the membrane per unit of time
             and biomass in L/(gDW h)
   '''

# unpack variables
mu, cHAc_out, cHAc_in = x

# proton-to-ATP ratio of the ATPase
Y_H_ATP = 3.6 # mol H+/mol ATP

return a*mu + b + (c*(cHAc_out-cHAc_in))/Y_H_ATP
```

```python
def Herbert_Pirt_HAc_inhibition2(x, a, b, c):
'''Function for fitting the Herbert-Pirt equation with HAc inhibition
   according to method 2

   Parameters:
   mu  : growth rate in 1/h
   cHAc: extracellular undissociated acetic acid concentration in mol/L
   a   : maximum yield on biomass in mol/gDW
   b   : maintenance coefficient at cHAc = 0 in mol/(gDW h)
   c   : undissociated acetic acid concentration at which m$_{ATP}$ doubles
         in mol/L
   '''
# unpack variables
mu, cHAc = x

return mu*a + b*(1 + cHAc/c)
```

A.2.2. Substrate uptake kinetics

```
    def Hyperbolic(x, a, b):
    '''Function for fitting the hyperbolic curve

       Parameters:
       x   : concentration in M
       a   : the maximum rate in mol/(gDW h)
       b   : the affinity constant in mol/L
    '''
    return (a*x) / (b + x)
```

```
    def Hyperbolic_inh(x, a, b, c):
        '''Function for fitting the hyperbolic curve with substrate inhibition

       Parameters:
       x   : concentration in mol/L
       a   : the maximum rate in mol/(gDW h)
       b   : the affinity constant in mol/L
       c   : the inhibition constant in mol/L
    '''
    return (a*x) / (b + x + x**2/c)
```

B

Rate reconciliation

Overall rates (R_i) and liquid inflow ($F^V_{L,in}$) and outflow rates ($F^V_{L,out}$) were reconciled by setting up a weighted minimization problem with linear boundary conditions, aiming to find new estimates ($\hat{R}$) that satisfy the principle of elemental and mass conservation while staying closely aligned with the observed rates (R_m). In other words, the absolute difference between the observations and estimations (R) should be minimized ($|R_m - R|$) (Eq. (B.1)). To account for the accuracy of each measurement, the rates were rescaled according to their standard deviation (σ). This ensures that more accurate rates have a higher contribution to the new rate estimates than less accurate rates. The new rate estimates were found by solving two sets of equations, the linear equality constraints and the optimization equations, using the Lagrangian multipliers (Wahl and Heijnen, 2021).

$$\hat{R} = \underset{\mathbf{ER=0}}{\arg\min} \left(\frac{\|R_m - R\|}{\sigma} \right) \tag{B.1}$$

B.1. Linear equality constraints

The linear equality constraints for this problem are the principle of elemental and mass conservation in the system (Eq. (B.2)). Here, the constraint matrix (E) specifies the constraint relations between the known rates, which are stored in the rate vector (R), such that the residuals of the balances can be determined. The first seven columns of the E-matrix represent the rates of the seven compounds in the system (R_{CO}, R_{H_2}, R_{CO_2}, R_{EtOH}, R_{AcT}, R_{BDO}, R_X), while the last 2 columns represent the liquid inflow ($F^V_{L,in}$) and outflow rate ($F^V_{L,out}$) (Eq. (B.2)). To add, the first two rows of the E-matrix represent the conservation of carbon atoms ($N_{c,i}$) and the degree of reduction (γ_i) in the system. The last row represents the total mass conservation in the liquid phase, which is determined by the liquid inflow and outflow rates and the transfer of gaseous species to- and from the gas phase. Here, the constraint relations are the carbon balance, the degree of reduction balance, and the total mass balance. Ideally, when all balances close, the residual of all balances is equal to zero. However, the residuals are not expected to be zero because of errors in the measured rates (Heijnen and Verheijen, 2011; Wahl and Heijnen, 2021).

$$E \cdot R = 0 \quad \begin{cases} \text{Carbon Balance} \\ \text{Degree of Reduction Balance} \\ \text{Total Liquid Phase Mass Balance} \end{cases} \tag{B.2}$$

with,

$$E = \begin{pmatrix} 1 & 0 & 1 & 2 & 2 & 4 & 1 & 0 & 0 \\ 2 & 2 & 0 & 12 & 8 & 22 & 3.76 & 0 & 0 \\ -Mw_{CO} & -Mw_{H_2} & -Mw_{CO_2} & 0 & 0 & 0 & 0 & \rho_L & -\rho_L \end{pmatrix}$$

$$R = \begin{pmatrix} R_{CO} & R_{H_2} & R_{CO_2} & R_{EtOH} & R_{AcT} & R_{BDO} & R_X & F^V_{L,in} & F^V_{L,out} \end{pmatrix}$$

B.2. Optimization equation

During optimization, the errors in the measured rates (ε) are minimized to find new rate estimates (R) that satisfy the principle of elemental and mass conservation imposed by the linear equality constraints (Eq. (B.3)). Here, the measurement matrix (M) is an eye matrix indicating the relationship between measurements and rate estimates (Heijnen and Verheijen, 2011; Wahl and Heijnen, 2021).

$$R_m = M \cdot R + \varepsilon \quad \begin{cases} R_{m,CO} = R_{CO} + \varepsilon_{CO} \\ R_{m,H_2} = R_{H_2} + \varepsilon_{H_2} \\ R_{m,CO2} = R_{CO2} + \varepsilon_{CO2} \\ R_{m,EtOH} = R_{EtOH} + \varepsilon_{EtOH} \\ R_{m,AcT} = R_{AcT} + \varepsilon_{AcT} \\ R_{m,BDO} = R_{BDO} + \varepsilon_{BDO} \\ R_{m,X} = R_X + \varepsilon_X \\ F^V_{L,m,in} = F^V_{L,in} + \varepsilon_{F^V_{L,in}} \\ F^V_{L,m,out} = F^V_{L,out} + \varepsilon_{F^V_{L,out}} \end{cases} \tag{B.3}$$

with,

$$M = \begin{pmatrix} 1 & 0 & 0 & 0 & 0 & 0 & 0 & 0 & 0 \\ 0 & 1 & 0 & 0 & 0 & 0 & 0 & 0 & 0 \\ 0 & 0 & 1 & 0 & 0 & 0 & 0 & 0 & 0 \\ 0 & 0 & 0 & 1 & 0 & 0 & 0 & 0 & 0 \\ 0 & 0 & 0 & 0 & 1 & 0 & 0 & 0 & 0 \\ 0 & 0 & 0 & 0 & 0 & 1 & 0 & 0 & 0 \\ 0 & 0 & 0 & 0 & 0 & 0 & 1 & 0 & 0 \\ 0 & 0 & 0 & 0 & 0 & 0 & 0 & 1 & 0 \\ 0 & 0 & 0 & 0 & 0 & 0 & 0 & 0 & 1 \end{pmatrix}$$

$$R = \begin{pmatrix} R_{CO} & R_{H_2} & R_{CO_2} & R_{EtOH} & R_{AcT} & R_{BDO} & R_X & F^V_{L,in} & F^V_{L,out} \end{pmatrix}$$

B.3. Lagrangian multipliers

The Lagrange multipliers (λ) allow for the weighted optimization of functions with multiple variables and additional constraints (LibreTexts, 2022). The implementation of the Lagrangian multipliers to calculate the new rate estimates (R) in Python is obtained from Wahl and Heijnen (2021).

$$\begin{pmatrix} M_w^T \frac{R_m}{\sigma} \\ 0 \end{pmatrix} = \underbrace{\begin{pmatrix} M_w^T M_w & E^T \\ E & 0 \end{pmatrix}}_{L} \begin{pmatrix} R \\ \lambda \end{pmatrix}$$

Solve for R, λ : (B.4)

$$\begin{pmatrix} R \\ \lambda \end{pmatrix} = L^{-1} \begin{pmatrix} M_w^T \frac{R_m}{\sigma} \\ 0 \end{pmatrix}$$

with,

$$M_w = \begin{pmatrix} \frac{1}{\sigma_{R_{CO}}} & 0 & 0 & 0 & 0 & 0 & 0 & 0 & 0 \\ 0 & \frac{1}{\sigma_{R_{H_2}}} & 0 & 0 & 0 & 0 & 0 & 0 & 0 \\ 0 & 0 & \frac{1}{\sigma_{R_{CO_2}}} & 0 & 0 & 0 & 0 & 0 & 0 \\ 0 & 0 & 0 & \frac{1}{\sigma_{R_{EtOH}}} & 0 & 0 & 0 & 0 & 0 \\ 0 & 0 & 0 & 0 & \frac{1}{\sigma_{R_{AcT}}} & 0 & 0 & 0 & 0 \\ 0 & 0 & 0 & 0 & 0 & \frac{1}{\sigma_{R_{BDO}}} & 0 & 0 & 0 \\ 0 & 0 & 0 & 0 & 0 & 0 & \frac{1}{\sigma_{R_X}} & 0 & 0 \\ 0 & 0 & 0 & 0 & 0 & 0 & 0 & \frac{1}{\sigma_{F^V_{L,in}}} & 0 \\ 0 & 0 & 0 & 0 & 0 & 0 & 0 & 0 & \frac{1}{\sigma_{F^V_{L,out}}} \end{pmatrix}$$

$$\sigma = \begin{pmatrix} \sigma_{R_{CO}} & \sigma_{R_{H_2}} & \sigma_{R_{CO_2}} & \sigma_{R_{EtOH}} & \sigma_{R_{AcT}} & \sigma_{R_{BDO}} & \sigma_{R_X} & \sigma_{F^V_{L,in}} & \sigma_{F^V_{L,out}} \end{pmatrix}$$

$$R = \begin{pmatrix} R_{CO} & R_{H_2} & R_{CO_2} & R_{EtOH} & R_{AcT} & R_{BDO} & R_X & F^V_{L,in} & F^V_{L,out} \end{pmatrix}$$

$$R_m = \begin{pmatrix} R_{m,CO} & R_{m,H_2} & R_{m,CO_2} & R_{m,EtOH} & R_{m,AcT} & R_{m,BDO} & R_{m,X} & F^V_{L,m,in} & F^V_{L,m,out} \end{pmatrix}$$

$$E = \begin{pmatrix} 1 & 0 & 1 & 2 & 2 & 4 & 1 & 0 & 0 \\ 2 & 2 & 0 & 12 & 8 & 22 & 3.76 & 0 & 0 \\ -Mw_{CO} & -Mw_{H_2} & -Mw_{CO_2} & 0 & 0 & 0 & 0 & \rho_L & -\rho_L \end{pmatrix}$$

C

Experimental dataset

C.1. Process parameters

Table C.1: Overview of experimental data. Sources: Heffernan et al., 2020 [1], Valgepea et al., 2018 [2], Valgepea, de Souza Pinto Lemgruber, et al., 2017 [3], de Lima et al., 2022 [4], Elisiário et al., 2023 [5], Allaart, 2023 [6], Chen et al., 2018 [7], and Diender et al., 2019 [8]. Abbreviations: Temperature (T), pressure (p), agitation speed (N), liquid broth volume (V_L), dilution rate (D), reactor volume (V_R), impeller diameter (D_i), liquid inflow rate ($F^V_{L,in}$), total acetate concentration in the inflow ($c_{AcT,in}$), and not applicable (N/A). a: Standard deviation assumed as 5%. b: Not specified, assumed as zero. c: Calculated. d: Experiments performed in bubble column.

SST Number	T [°C]	p [atm]	pH [-]	N [rpm]	V_L [L]	D [h^{-1}]	V_R [L]	N_i [-]	D_i [mm]	$F^V_{L,in}$ [L/h]	$c_{AcT,in}$ [g/L]
1 [1]	37	1	5	1200	0.75 ±0.04[a]	0.042 ±0.0004	1.4	2	38	0.031 ±0.002	0
2 [1]	37	1	5	500	0.75 ±0.04[a]	0.020 ±0.0004	1.4	2	38	0.015 ±0.0008	0
3 [1]	37	1	5	800	0.75 ±0.04[a]	0.021 ±0.0004	1.4	2	38	0.016 ±0.0008	0
4 [2]	37	1	5	510	0.75 ±0.04[a]	0.04 ±0.0004	1.4	2	38	0.031 ±0.002	0
5 [2]	37	1	5	665	0.75 ±0.04[a]	0.04 ±0.0004	1.4	2	38	0.031 ±0.002	0
6 [2]	37	1	5	650	0.75 ±0.04[a]	0.04 ±0.0004	1.4	2	38	0.031 ±0.002	0
7 [2]	37	1	5	1000	0.75 ±0.04[a]	0.04 ±0.0004	1.4	2	38	0.031 ±0.002	0
8 [3]	37	1	5	500	0.75 ±0.04[a]	0.04 ±0.0001	1.4	2	38	0.030 ±0.002	0
9 [3]	37	1	5	500	0.75 ±0.04[a]	0.04 ±0.0001	1.4	2	38	0.030 ±0.002	0
10 [3]	37	1	5	590	0.75 ±0.04[a]	0.04 ±0.0001	1.4	2	38	0.030 ±0.002	0
11 [3]	37	1	5	650	0.75 ±0.04[a]	0.04 ±0.0001	1.4	2	38	0.030 ±0.002	0
12 [3]	37	1	5	650	0.75 ±0.04[a]	0.04 ±0.0001	1.4	2	38	0.030 ±0.002	0
13 [4]	37	1	5	690	0.75 ±0.04[a]	0.043 ±0.0004	1.4	2	38	0.032 ±0.002	0
14 [4]	37	1	5	815	0.75 ±0.04[a]	0.085 ±0.003	1.4	2	38	0.063 ±0.004	0
15 [4]	37	1	5	1175	0.75 ±0.04[a]	0.12 ±0.001	1.4	2	38	0.087 ±0.004	0
16 [4]	37	1	5	675	0.75 ±0.04[a]	0.042 ±0.0008	1.4	2	38	0.032 ±0.002	0

Table C.1: Continued

SST Number	T [^{o}C]	p [atm]	pH [-]	N [rpm]	V_L [L]	D [h^{-1}]	V_R [L]	N_i [-]	D_i [mm]	$F^V_{L,in}$ [L/h]	$c_{AcT,in}$ [g/L]
17 [4]	37	1	5	800	0.75 ±0.04[a]	0.0084 ±0.003	1.4	2	38	0.063 ±0.004	0
18 [4]	37	1	5	1160	0.75 ±0.04[a]	0.12 ±0.003	1.4	2	38	0.087 ±0.005	0
19 [5]	37	1	5.9	500	1 ±0.05	0.0088 ±0.0004	1.5	2	46	0.0088 ±0	0
20 [5]	37	1	5.9	500	1 ±0.05	0.024 ±0.001	1.5	2	46	0.024 ±0	0
21 [5]	37	1	5.9	500	1 ±0.05	0.039 ±0.002	1.5	2	46	0.040 ±0	0
22 [5]	37	1	5.9	500	1 ±0.05	0.04 ±0.002	1.5	2	46	0.040 ±0	10.15 ±0.11
23 [6]	37	1	5.5	600	1.6 ±0.08[a]	0.01 ±0.0005[a]	3	2	46	0.016 ±0.001	0
24 [6]	37	1	5.5	600	1.6 ±0.08[a]	0.01 ±0.0005[a]	3	2	46	0.016 ±0.001	0
25 [7]	37	1	5	N/A[d]	2.6 ±0.13[a]	0.063 ±0.003[a]	4	2	N/A[d]	0.16 ±0.01	0
26 [7]	37	1	5	N/A[d]	2.6 ±0.13[a]	0.063 ±0.003[a]	4	2	N/A[d]	0.16 ±0.01	0
27 [7]	37	1	5	N/A[d]	2.6 ±0.13[a]	0.063 ±0.003[a]	4	2	N/A[d]	0.16 ±0.01	0
28 [8]	37	1	6.2	400	0.75 ±0.04[a]	0.028 ±0.001[a]	1.5	2	46	0.021 ±0.001	0
29 [8]	37	1	6.2	400	0.75 ±0.04[a]	0.028 ±0.001[a]	1.5	2	46	0.021 ±0.001	0
30 [8]	37	1	6.2	400	1 ±0.05[a]	0.021 ±0.001[a]	1.5	2	46	0.021 ±0.001	0
31 [8]	37	1	6.2	400	1 ±0.05[a]	0.021 ±0.001[a]	1.5	2	46	0.021 ±0.001	0
32 [8]	37	1	6.2	400	1 ±0.05[a]	0.021 ±0.001[a]	1.5	2	46	0.021 ±0.001	0
33 [8]	37	1	6.2	400	1 ±0.05[a]	0.021 ±0.001[a]	1.5	2	46	0.021 ±0.001	0
34 [8]	37	1	6.2	400	0.75 ±0.04[a]	0.028 ±0.001[a]	1.5	2	46	0.021 ±0.001	0
35 [8]	37	1	6.2	400	0.75 ±0.04[a]	0.028 ±0.001[a]	1.5	2	46	0.021 ±0.001	1.5 ±0.08[a]
36 [8]	37	1	6.2	400	0.75 ±0.04[a]	0.028 ±0.001[a]	1.5	2	46	0.021 ±0.001	3 ±0.15[a]
37 [8]	37	1	6.2	400	0.75 ±0.04[a]	0.028 ±0.001[a]	1.5	2	46	0.021 ±0.001	5.4 ±0.27[a]

C.2. Gas inflow and liquid outflow data

Table C.2: Overview of experimental data. Sources: Heffernan et al., 2020 [1], Valgepea et al., 2018 [2], Valgepea, de Souza Pinto Lemgruber, et al., 2017 [3], de Lima et al., 2022 [4], Elisiário et al., 2023 [5], Allaart, 2023 [6], Chen et al., 2018 [7], and Diender et al., 2019 [8]. Abbreviations: Gas inflow rate ($F^V_{g,in}$), fraction CO in the gas feed ($y_{CO,in}$), fraction H_2 in the gas feed ($y_{H_2,in}$), fraction CO_2 in the gas feed ($y_{CO_2,in}$), fraction inert gas in the gas feed ($y_{inert,in}$), liquid outflow rate ($F^V_{L,out}$), biomass concentration in the broth ($c_{X,out}$), ethanol concentration in the broth ($c_{EtOH,out}$), total acetate concentration in the broth ($c_{AcT,out}$), and 2,3-butanediol concentration in the broth ($c_{BDO,out}$). a: Standard deviation assumed as 5%. b: Not specified, assumed as zero. c: Calculated. d: Experiments performed in bubble column.

SST Number	$F^V_{g,in}$ [mL/min]	$y_{CO,in}$ [-]	$y_{H_2,in}$ [-]	$y_{CO_2,in}$ [-]	$y_{inert,in}$ [-]	$F^V_{L,out}$ [L/h]	$c_{X,out}$ [g/L]	$c_{EtOH,out}$ [g/L]	$c_{AcT,out}$ [g/L]	$c_{BDO,out}$ [g/L]
1 [1]	30	0.02	0.65	0.23	0.1	0.031 ±0.002	0.34 ±0.02	4.79 ±0.43	5.03 ±0.34	0^b
2 [1]	32	0	0.67	0.23	0.1	0.015 ±0.0008	0.18 ±0.02	2.36 ±0.25	2.51 ±0.42	0^b
3 [1]	30	0.02	0.65	0.23	0.1	0.016 ±0.0008	0.54 ±0.01	9.69 ±0.39	5.97 ±0.98	0^b
4 [2]	46.5	0.6	0	0	0.4	0.031 ±0.002	0.47 ±0.02	0.63 ±0.05	2.12 ±0.18	0
5 [2]	46.5	0.6	0	0	0.4	0.031 ±0.002	1.43 ±0.08	3.88 ±0.15	6.28 ±0.43	0.2 ±0.01
6 [2]	46.5	0.15	0.45	0	0.4	0.031 ±0.002	0.46 ±0.04	4.46 ±0.41	0.69 ±0.07	0
7 [2]	110	0.15	0.45	0	0.4	0.031 ±0.002	1.45 ±0.04	11.55 ±0.41	3.84 ±0.33	0
8 [3]	46.5	0.5	0.2	0.2	0.1	0.030 ±0.002	0.45 ±0.02[a]	0.58 ±0.03[a]	4.27 ±0.21[a]	0
9 [3]	46.5	0.5	0.2	0.2	0.1	0.030 ±0.002	0.51 ±0.03[a]	0.66 ±0.03[a]	4.45 ±0.22[a]	0
10 [3]	46.5	0.5	0.2	0.2	0.1	0.030 ±0.002	1.1 ±0.06[a]	2.92 ±0.15[a]	8.03 ±0.40	0.03 ±0.001[a]
11 [3]	46.5	0.5	0.2	0.2	0.1	0.030 ±0.002	1.32 ±0.07[a]	5.21 ±0.26[a]	7.97 ±0.40[a]	0.28 ±0.01[a]
12 [3]	46.5	0.5	0.2	0.2	0.1	0.030 ±0.002	1.4 ±0.07[a]	5.68 ±0.28[a]	7.77 ±0.39[a]	0.27 ±0.01[a]
13 [4]	50	0.6	0	0	0.4	0.032 ±0.002	1.58 ±0.06	4.27 ±0.39	8.12 ±0.79	0.26 ±0.05
14 [4]	72	0.6	0	0	0.4	0.063 ±0.004	1.65 ±0.01	3.79 ±0.30	4.02 ±0.13	0.39 ±0.06
15 [4]	72	0.6	0	0	0.4	0.087 ±0.004	1.65 ±0.02	3.81 ±0.24	4.35 ±0.38	0.17 ±0.03
16 [4]	50	0.5	0.2	0.2	0.1	0.032 ±0.002	1.59 ±0.03	4.92 ±0.62	10.25 ±0.68	0.33 ±0.08
17 [4]	72	0.5	0.2	0.2	0.1	0.063 ±0.004	1.57 ±0.08	5.33 ±0.56	5.40 ±0.37	0.55 ±0.1
18 [4]	72	0.5	0.2	0.2	0.1	0.087 ±0.005	1.43 ±0.03	4.46 ±0.19	3.42 ±0.28	0.70 ±0.07
19 [5]	10	0.5	0	0	0.5	0.0088 ±0.0006	0.54 ±0.01	1.01 ±0.02	10.76 ±0.09	0.58 ±0.01
20 [5]	10	0.5	0	0	0.5	0.024 ±0.002	0.48 ±0.02	0.06 ±0.004	5.58 ±0.06	0.07 ±0.03
21 [5]	10	0.5	0	0	0.5	0.039 ±0.002	0.36 ±0.01	0.05 ±0.009	3.13 ±0.17	0
22 [5]	10	0.5	0	0	0.5	0.040 ±0.003	0.26 ±0.01	0.32 ±0.006	11.38 ±0.11	0
23 [6]	100	0.1	0	0	0.9	0.016 ±0.001	0.52 ±0.02	0.51 ±0.09	5.95 ±0.93	0
24 [6]	100	0.1	0	0	0.9	0.016 ±0.001	0.59 ±0.03	0.43[c] ±0.02[a]	6.59[c] ±0.33[a]	0
25 [7]	500	0.5	0	0.2	0.3	0.16	3.51	8.02	9.2	0.47

Table C.2: Continued

SST Number	$F^{V}_{g,in}$ [mL/min]	$y_{CO,in}$ [-]	$y_{H_2,in}$ [-]	$y_{CO_2,in}$ [-]	$y_{inert,in}$ [-]	$F^{V}_{L,out}$ [L/h]	$c_{X,out}$ [g/L]	$c_{EtOH,out}$ [g/L]	$c_{AcT,out}$ [g/L]	$c_{BDO,out}$ [g/L]
						±0.01	±0.18[a]	±0.40[a]	±0.5[a]	±0.02[a]
26 [7]	600	0.5	0	0.2	0.3	0.16	3.9	10.64	8.27	0.88
						±0.01	±0.20[a]	±0.53[a]	±0.41[a]	±0.04[a]
27 [7]	700	0.5	0	0.2	0.3	0.16	4.4	12.47	6.79	0.93
						±0.01	±0.22[a]	±0.62[a]	±0.34[a]	±0.05[a]
28 [8]	2.97	0.66	0	0	0.34	0.021	0.6	0.009	3.28	0[b]
						±0.001	±0.03[a]	±0.0005[a]	±0.054	
29 [8]	2.97	0.66	0	0	0.34	0.021	0.65[c]	0	3.27[c]	0[b]
						±0.001	±0.03[a]		±0.08[c]	
30 [8]	1.97	1	0	0	0	0.021	0.28	0.009	3.36	0[b]
						±0.001	±0.01[a]	±0.0005[a]	±0.17[a]	
31 [8]	2.36	0.83	0.17	0	0	0.021	0.22	0.009	3.66	0[b]
						±0.001	±0.01[a]	±0.0005[a]	±0.18[a]	
32 [8]	2.77	0.71	0.29	0	0	0.021	0.24	0.018	3.90	0[b]
						±0.001	±0.01[a]	±0.0009[a]	±0.20[a]	
33 [8]	3.55	0.56	0.44	0	0	0.021	0.3	0.28	4.98	0[b]
						±0.001	±0.02[a]	±0.014[a]	±0.25[a]	
34 [8]	2.97	0.66	0	0	0.34	0.021	0.15	0.009	2.44	0[b]
						±0.001	±0.01[a]	±0.0005[a]	±0.12[a]	
35 [8]	2.97	0.66	0	0	0.34	0.021	0.14	0.012	3.80	0[b]
						±0.001	±0.01[a]	±0.0006[a]	±0.19[a]	
36 [8]	2.97	0.66	0	0	0.34	0.021	0.09	0.025	4.87	0[b]
						±0.001	±0.004[a]	±0.0013[a]	±0.24[a]	
37 [8]	2.97	0.66	0	0	0.34	0.021	0.08	0.052	7.19	0[b]
						±0.001	±0.004[a]	±0.0026[a]	±0.36[a]	

C.3. Biomass-specific rates

Table C.3: Overview of experimental data. Consumption is specified with negative rates and production with positive rates. Sources: Heffernan et al., 2020 [1], Valgepea et al., 2018 [2], Valgepea, de Souza Pinto Lemgruber, et al., 2017 [3], de Lima et al., 2022 [4], Elisiário et al., 2023 [5], Allaart, 2023 [6], Chen et al., 2018 [7], and Diender et al., 2019 [8]. Abbreviations: Growth rate (μ), biomass-specific CO consumption/production rate (q_{CO}), biomass-specific H_2 consumption/production rate (q_{H_2}),biomass-specific CO_2 consumption/production rate (q_{CO_2}), biomass-specific ethanol production rate (q_{EtOH}),biomass-specific total acetate production rate (q_{AcT}),biomass-specific 2,3-butanediol production rate (q_{BDO}). a: Standard deviation assumed as 5%. b: Not specified, assumed as zero. c: Calculated. d: Experiments performed in bubble column.

SST Number	μ [h^{-1}]	q_{CO} [mmol/(g_{DW} h)]	q_{H_2} [mmol/(g_{DW} h)]	q_{CO_2} [mmol/(g_{DW} h)]	q_{EtOH} [mmol/(g_{DW} h)]	q_{AcT} [mmol/(g_{DW} h)]	q_{BDO} [mmol/(g_{DW} h)]
1 [1]	0.042	-3.71	-108.79	-39.33	12.75	10.13	0^b
	±0.0008	±0.08	±2.38	±0.96	±1.13	±0.67	
2 [1]	0.0196	0	-47.08	-19.13	5.83	4.71	0^b
	±0.0004		±6.58	±3.21	±0.50	±0.38	
3 [1]	0.021	-1.50	-65.08	-22.42	8.21	3.79	0^b
	±0.0004	±0.17	±1	±0.83	±0.33	±0.63	
4 [2]	0.04	-21.8	0.58	16.42	1.29	3.17	0
	±0.001	±0.5	±0.04	±0.25	±0.04	±0.2	
5 [2]	0.04	-30.8	0.43	21.12	2.58	3.1	0.071
	±0.001	±0.9	±0.1	±0.47	±0.07	±0.09	±0.01
6 [2]	0.04	-20.0	-33.0	2.13	9.04	1.08	0
	±0.001	±1.3	±3	±0.17	±0.2	±0.13	
7 [2]	0.04	-20.6	-29.6	4.42	7.9	1.9	0
	±0.001	±0.8	±1.7	±0.07	±0.5	±0.16	
8 [3]	0.04	-19.3	-13	5.7	1.2	6.6	0
	±0.001	±0.97^a	±0.7^a	±0.3^a	±0.06^a	±0.3^a	
9 [3]	0.04	-18.3	-12.2	5.6	1.2	6.1	0
	±0.001	±0.92^a	±0.6^a	±0.3^a	±0.06^a	±0.3^a	
10 [3]	0.04	-24.6	-12.5	8.7	2.5	5.2	0.01
	±0.001	±1.2^a	±0.6^a	±0.4^a	±0.1^a	±0.3^a	±0.0005^a
11 [3]	0.04	-31.6	-12.3	12.9	3.7	4.2	0.09
	±0.001	±1.6^a	±0.6^a	±0.6^a	±0.2^a	±0.2^a	±0.005^a
12 [3]	0.04	-29.6	-11.5	12.2	3.8	3.9	0.09
	±0.001	±1.5^a	±0.6^a	±0.6^a	±0.2^a	±0.2^a	±0.005^a
13 [4]	0.043	-31.61	0.28	23.72	2.70	3.70	0.07
	±0.0004	±1.34	±0.07	±1.42	±0.35	±0.29	±0.02
14 [4]	0.085	-56.11	0.21	40.41	4.50	3.47	0.21
	±0.003	±1.06	±0.18	±1	±0.33	±0.16	±0.04
15 [4]	0.12	-69.53	0.27	43.18	6.02	5.19	0.13
	±0.001	±1.07	±0.15	±0.85	±0.38	±0.46	±0.03
16 [4]	0.042	-24.67	-7.23	9.78	3.15	4.60	0.11
	±0.0008	±0.37	±0.80	±2.41	±0.49	±0.49	±0.03
17 [4]	0.084	-54.53	-20.66	28.39	6.75	4.87	0.33
	±0.003	±2.33	±1.24	±1.83	±0.70	±0.22	±0.08
18 [4]	0.12	-72.48	-19.71	34.38	8.24	4.69	0.63
	±0.003	±1.53	±1.31	0.8	±0.50	±0.38	±0.08
19 [5]	0.0088	-16.8	0	8.5	0.36	3.0	0.10
	±0.0004	±1.0		±0.6	±0.02	±0.2	±0.006
20 [5]	0.024	-21.6	0	9.9	0.067	4.6	0.039
	±0.001	±1.4		±0.7	±0.006	±0.3	±0.02
21 [5]	0.039	-27.3	0	13.4	0.11	5.7	0
	±0.002	±1.6		±0.8	±0.02	±0.5	
22 [5]	0.04	-31.0	0	16.4	1.05	3.2	0
	±0.002	±2		±1.6	±0.07	±0.3	
23 [6]	0.01	-10.8	0.35	6.26	0.21	1.86	0
	±0.0005^a	±0.54	±0.08	±0.35	±0.04	±0.29	
24 [6]	0.01	-9.85	0	6.16	0.16	1.86	0
	±0.0005^a	±0.46		±0.76	±0.02	±0.09	
25 [7]	0.063	-40.7	0^b	26.5	3.1^c	2.7^c	0.09^c
	±0.003^a	±2.0^a		±1.3^a	±0.2^a	±0.1^a	±0.005^a

Table C.3: Continued

SST Number	μ [h^{-1}]	q_{CO} [mmol/(g_{DW}h)]	q_{H_2} [mmol/(g_{DW}h)]	q_{CO_2} [mmol/(g_{DW}h)]	q_{EtOH} [mmol/(g_{DW}h)]	q_{AcT} [mmol/(g_{DW}h)]	q_{BDO} [mmol/(g_{DW}h)]
26 [7]	0.063	-42.6	0[b]	28.6	3.7[c]	2.2[c]	0.16[c]
	±0.003[a]	±2.1[a]		±1.4[a]	±0.2[a]	±0.1[a]	±0.008[a]
27 [7]	0.063	-42.9	0[b]	29.3	3.8[c]	1.6[c]	0.15[c]
	±0.003[a]	±2.1[a]		±1.5[a]	±0.2[a]	±0.08[a]	±0.007[a]
28 [8]	0.028	-10.21	0	5.11[c]	0.014	2.53	0
	±0.006	±0.04		±0.23	±0.0006[a]	±0.04	
29 [8]	0.028	-7.30	0	4.69[c]	0	2.34	0
	±0.006	±0.06		±0.25		±0.06	
30 [8]	0.021	-16.96	0	8.48	0.015	4.17	0
	±0.001	±1.16		±0.42[a]	±0.013	±0.14	
31 [8]	0.021	-20.07	-4.12	8.43	0.019	5.78	0
	±0.002	±1.0	±0.21	±0.42[a]	±0.0006	±0.13	
32 [8]	0.021	-18.47	-7.56	5.91	0.035	5.64	0
	±0.002	±1.16	±0.49	±0.30[a]	±0.0005	±0.34	
33 [8]	0.021	-14.79	-11.93	2.37	0.42	5.76	0
	±0.001	±0.82	±0.67	±0.12[a]	±0.01	±0.05	
34 [8]	0.028	-32.94	0	16.14	0	7.54	0
	±0.003	±3.09		±0.81[a]		±0.23	
35 [8]	0.027	-32.56	0	16.28	0.036	7.57	0
	±0.003	±0.85		±0.81[a]	±0.02	±0.14	
36 [8]	0.028	-48.44	0	26.64	0.17	9.59	0
	±0.002	±1.85		±1.33[a]	±0.02	±0.57	
37 [8]	0.026	-54.68	0	29.53	0.39	10.32	0
	±0.003	±2.05		±1.48[a]	±0.01	±1.74	

C.4. Gas fractions in the off gas

Table C.4: Overview of gas fractions in the off gas. Sources: Valgepea et al., 2018 [2], Valgepea, de Souza Pinto Lemgruber, et al., 2017 [3], de Lima et al., 2022 [4], Elisiário et al., 2023 [5]. Abbreviations: Fraction CO in the gas outflow ($y_{CO,out}$), fraction H_2 in the gas outflow ($y_{H_2,out}$), fraction CO_2 in the gas outflow ($y_{CO_2,out}$), fraction inert gas in the gas outflow ($y_{inert,out}$), average (avg). Data was obtained through personal correspondence (Straathof, 2023a; Valgepea, 2024).

SST Number		$y_{CO,out}$ [-]	$y_{H_2,out}$ [-]	$y_{CO_2,out}$ [-]	$y_{inert,out}$ [-]
4 + 5 (avg)	[2]	0.354	0.005	0.197	0.443
6 + 7 (avg)	[2]	0.089	0.404	0.019	0.484
8 + 9 (avg)	[3]	0.476	0.183	0.229	0.110
10	[3]	0.409	0.151	0.312	0.126
11 + 12 (avg)	[3]	0.325	0.144	0.394	0.135
13	[4]	0.344	0.001	0.224	0.429
14	[4]	0.266	0.002	0.286	0.443
15	[4]	0.183	0.001	0.332	0.481
16	[4]	0.340	0.172	0.364	0.121
17	[4]	0.235	0.101	0.518	0.139
18	[4]	0.138	0.132	0.577	0.148
19	[5]	0.148	0	0.158	0.695
20	[5]	0.104	0	0.164	0.732
21	[5]	0.121	0	0.167	0.712
22	[5]	0.180	0	0.149	0.671

D

Reconciled data

D.1. Gas and liquid outflow data

Table D.1: Overview of reconciled data. Sources: Heffernan et al., 2020 [1], Valgepea et al., 2018 [2], Valgepea, de Souza Pinto Lemgruber, et al., 2017 [3], de Lima et al., 2022 [4], Elisiário et al., 2023 [5], Allaart, 2023 [6], Chen et al., 2018 [7], and Diender et al., 2019 [8]. Abbreviations: Gas outflow rate ($F^V_{g,out}$), fraction CO in the gas outflow ($y_{CO,out}$), fraction H_2 in the gas outflow ($y_{H_2,out}$), fraction CO_2 in the gas outflow ($y_{CO_2,out}$), fraction inert gas in the gas outflow ($y_{inert,out}$), liquid outflow rate ($F^V_{L,out}$), biomass concentration in the broth ($c_{X,out}$), ethanol concentration in the broth ($c_{EtOH,out}$), total acetate concentration in the broth ($c_{AcT,out}$), and 2,3-butanediol concentration in the broth ($c_{BDO,out}$). a: Standard deviation assumed as 5%. b: Not specified, assumed as zero. c: Calculated. d: Experiments performed in bubble column.

SST Number	$F^V_{g,out}$ [mL/min]	$y_{CO,out}$ [-]	$y_{H_2,out}$ [-]	$y_{CO_2,out}$ [-]	$y_{inert,out}$ [-]	$F^V_{L,in}$ [L/h]	$F^V_{L,out}$ [L/h]	$c_{X,out}$ [g/L]	$c_{EtOH,out}$ [g/L]	$c_{AcT,out}$ [g/L]	$c_{BDO,out}$ [g/L]
1 [1]	14.0	0.02	0.58	0.19	0.21	0.031 ±0.001	0.032 ±0.001	0.34 ±0.03	4.42 ±0.41	4.73 ±0.48	0
2 [1]	28.0	0	0.66	0.22	0.11	0.015 ±0.001	0.015 ±0.001	0.18 ±0.02	2.28 ±0.32	2.47 ±0.36	0
3 [1]	15.4	0.02	0.58	0.20	0.20	0.015 ±0.001	0.016 ±0.001	0.54 ±0.04	9.63 ±0.62	5.65 ±0.83	0
4 [2]	45.1	0.54	0	0.04	0.41	0.031 ±0.001	0.031 ±0.001	0.47 ±0.04	0.68 ±0.05	2.16 ±0.17	0
5 [2]	40.9	0.33	0	0.2	0.46	0.031 ±0.001	0.031 ±0.001	1.37 ±0.1	4.17 ±0.31	6.43 ±0.53	0.22 ±0.04
6 [2]	38.9	0.10	0.41	0.01	0.48	0.031 ±0.001	0.031 ±0.001	0.44 ±0.05	4.16 ±0.35	0.70 ±0.11	0
7 [2]	88.9	0.07	0.41	0.02	0.5	0.031 ±0.001	0.032 ±0.001	1.37 ±0.10	11.08 ±0.73	3.75 ±0.42	0
8 [3]	42.5	0.48	0.18	0.24	0.11	0.030 ±0.001	0.030 ±0.001	0.45 ±0.04	0.61 ±0.06	4.13 ±0.30	0
9 [3]	42.2	0.47	0.18	0.24	0.11	0.030 ±0.001	0.030 ±0.001	0.51 ±0.04	0.70 ±0.06	4.33 ±0.32	0
10 [3]	36.6	0.40	0.14	0.33	0.13	0.030 ±0.001	0.030 ±0.001	1.09 ±0.09	3.10 ±0.27	8.34 ±0.69	0.02 ±0.002
11 [3]	34.4	0.31	0.13	0.42	0.14	0.030 ±0.001	0.030 ±0.001	1.31 ±0.11	5.63 ±0.44	8.34 ±0.73	0.27 ±0.03
12 [3]	34.2	0.31	0.12	0.43	0.14	0.030 ±0.001	0.030 ±0.001	1.39 ±0.12	5.90 ±0.46	8.02 ±0.72	0.28 ±0.03
13 [4]	43.1	0.31	0	0.23	0.46	0.032 ±0.001	0.032 ±0.001	1.57 ±0.12	4.61 ±0.50	8.07 ±0.81	0.25 ±0.06
14 [4]	60.9	0.25	0	0.28	0.47	0.063 ±0.003	0.063 ±0.003	1.67 ±0.12	4.85 ±0.33	4.24 ±0.32	0.40 ±0.08
15 [4]	57.8	0.14	0	0.36	0.5	0.087 ±0.003	0.087 ±0.003	1.65 ±0.10	4.14 ±0.28	4.57 ±0.44	0.17 ±0.04
16 [4]	39.3	0.32	0.16	0.39	0.13	0.031	0.032	1.57	3.84	8.93	0.35

Table D.1: Continued

SST Number	$F^V_{g,out}$ [mL/min]	$y_{CO,out}$ [-]	$y_{H_2,out}$ [-]	$y_{CO_2,out}$ [-]	$y_{inert,out}$ [-]	$F^V_{L,in}$ [L/h]	$F^V_{L,out}$ [L/h]	$c_{X,out}$ [g/L]	$c_{EtOH,out}$ [g/L]	$c_{AcT,out}$ [g/L]	$c_{BDO,out}$ [g/L]
						±0.001	±0.001	±0.11	±0.60	±1.10	±0.09
17 [4]	48.4	0.19	0.1	0.55	0.15	0.063	0.063	1.57	6.49	5.56	0.58
						±0.003	±0.003	±0.14	±0.55	±0.51	±0.14
18 [4]	48.6	0.12	0.12	0.61	0.15	0.087	0.087	1.43	4.98	3.59	0.72
						±0.003	±0.003	±0.10	±0.33	±0.35	±0.10
19 [5]	8.3	0.17	0	0.23	0.6	0.0088	0.0088	0.54	1.02	11.29	0.58
						±0.0004	±0.0004	±0.05	±0.09	±0.86	±0.05
20 [5]	8.0	0.12	0	0.26	0.63	0.024	0.024	0.48	0.06	5.45	0.07
						±0.001	±0.001	±0.04	±0.01	±0.41	±0.03
21 [5]	8.0	0.13	0	0.25	0.62	0.039	0.039	0.36	0.05	3.25	0
						±0.002	±0.002	±0.03	±0.01	±0.25	
22 [5]	8.8	0.26	0	0.17	0.57	0.040	0.040	0.27	0.34	11.66	0
						±0.002	±0.002	±0.03	±0.03	±0.79	
23 [6]	98.4	0.06	0	0.02	0.92	0.016	0.016	0.52	0.53	6.62	0
						±0.001	±0.001	±0.05	±0.10	±0.60	
24 [6]	98.2	0.06	0	0.02	0.92	0.016	0.016	0.59	0.45	6.99	0
						±0.001	±0.001	±0.06	±0.07	±0.56	
25 [7]	442.7	0.25	0	0.41	0.34	0.16	0.16	3.57	8.87	9.66	0.47
						±0.008	±0.008	±0.35	±0.74	±0.90	±0.05
26 [7]	534.5	0.25	0	0.41	0.34	0.16	0.16	3.96	11.79	8.55	0.89
						±0.008	±0.008	±0.39	±0.95	±0.82	±0.09
27 [7]	629.5	0.26	0	0.4	0.33	0.16	0.16	4.49	14.21	7.00	0.94
						±0.008	±0.008	±0.44	±1.12	±0.68	±0.09
28 [8]	2.0	0	0	0.5	0.5	0.021	0.021	0.50	0.01	2.94	0
						±0.001	±0.001	±0.12	±0.001	±0.22	
29 [8]	2.1	0.12	0	0.4	0.47	0.021	0.021	0.40	0	2.60	0
						±0.001	±0.001	±0.13		±0.21	
30 [8]	1.0	0	0	1	0	0.021	0.021	0.28	0.009	3.22	0
						±0.001	±0.001	±0.03	±0.008	±0.23	
31 [8]	0.9	0.13	0.03	0.84	0	0.021	0.021	0.22	0.009	3.66	0
						±0.001	±0.001	±0.03	±0.0001	±0.24	
32 [8]	0.8	0.18	0.12	0.7	0	0.021	0.021	0.24	0.018	4.16	0
						±0.001	±0.001	±0.03	±0.002	±0.29	
33 [8]	0.5	0.14	0.32	0.54	0	0.021	0.021	0.30	0.28	4.96	0
						±0.001	±0.001	±0.03	±0.025	±0.35	
34 [8]	2.2	0.22	0	0.33	0.45	0.021	0.021	0.15	0	2.46	0
						±0.001	±0.001	±0.02		±0.18	
35 [8]	2.3	0.25	0	0.31	0.44	0.021	0.021	0.14	0.008	3.80	0
						±0.001	±0.001	±0.02	±0.006	±0.24	
36 [8]	2.3	0.30	0	0.28	0.43	0.021	0.021	0.09	0.025	5.12	0
						±0.001	±0.001	±0.01	±0.004	±0.35	
37 [8]	2.3	0.28	0	0.29	0.43	0.021	0.021	0.08	0.054	7.57	0
						±0.001	±0.001	±0.01	±0.014	±0.55	

D.2. Biomass-specific rates

Table D.2: Overview of reconciled data. Consumption is specified with negative rates and production with positive rates. Sources: Heffernan et al., 2020 [1], Valgepea et al., 2018 [2], Valgepea, de Souza Pinto Lemgruber, et al., 2017 [3], de Lima et al., 2022 [4], Elisiário et al., 2023 [5], Allaart, 2023 [6], Chen et al., 2018 [7], and Diender et al., 2019 [8]. Abbreviations: Growth rate (μ), biomass-specific CO consumption/production rate (q_{CO}), biomass-specific H_2 consumption/production rate (q_{H_2}),biomass-specific CO_2 consumption/production rate (q_{CO_2}), biomass-specific ethanol production rate (q_{EtOH}),biomass-specific total acetate production rate (q_{AcT}),biomass-specific 2,3-butanediol production rate (q_{BDO}). a: Standard deviation assumed as 5%. b: Not specified, assumed as zero. c: Calculated. d: Experiments performed in bubble column.

SST Number	μ [h^{-1}]	q_{CO} [mmol/(g_{DW} h)]	q_{H_2} [mmol/(g_{DW} h)]	q_{CO_2} [mmol/(g_{DW} h)]	q_{EtOH} [mmol/(g_{DW} h)]	q_{AcT} [mmol/(g_{DW} h)]	q_{BDO} [mmol/(g_{DW} h)]
1 [1]	0.042	-3.73	-109.69	-41.17	11.90	9.75	0
	±0.005	±0.48	±12.24	±4.58	±1.57	±1.35	
2 [1]	0.020	0	-52.19	-20.70	5.44	4.53	0
	±0.004		±8.52	±3.33	±1.05	±0.90	
3 [1]	0.021	-1.52	-64.38	-23.22	8.25	3.712	0
	±0.002	±0.23	±5.87	±2.16	±0.82	±0.61	
4 [2]	0.042	-24.06	0.58	13.53	1.31	3.17	0
	±0.005	±2.41	±0.08	±1.34	±0.15	±0.37	
5 [2]	0.042	-33.76	0.46	19.88	2.75	3.25	0.074
	±0.005	±3.60	±0.12	±2.13	±0.33	±0.40	±0.01
6 [2]	0.042	-23.29	-35.94	2.21	8.63	1.12	0
	±0.007	±3.11	±5.06	±0.39	±1.23	±0.22	
7 [2]	0.042	-24.78	-30.22	4.57	7.39	1.92	0
	±0.005	±2.34	±3.12	±0.48	±0.77	±0.26	
8 [3]	0.040	-21.80	-12.97	5.52	1.20	6.18	0
	±0.005	±2.34	±1.52	±0.70	±0.16	±0.72	
9 [3]	0.040	-20.76	-12.16	5.41	1.20	5.72	0
	±0.005	±2.22	±1.43	±0.69	±0.16	±0.67	
10 [3]	0.040	-25.50	-12.77	8.76	2.47	5.11	0.01
	±0.005	±2.72	±1.53	±1.07	±0.31	±0.62	±0.001
11 [3]	0.040	-30.94	-12.35	13.08	3.74	4.25	0.09
	±0.005	±3.31	±1.53	±1.55	±0.44	±0.53	±0.01
12 [3]	0.040	-29.67	-11.88	12.64	3.70	3.87	0.09
	±0.005	±3.17	±1.46	±1.49	±0.44	±0.49	±0.01
13 [4]	0.043	-34.89	0.28	20.31	2.70	3.63	0.07
	±0.005	±3.48	±0.08	±2.06	±0.36	±0.47	±0.02
14 [4]	0.085	-55.07	0.25	33.13	5.33	3.57	0.23
	±0.009	±5.06	±0.18	±3.07	±0.54	±0.38	±0.05
15 [4]	0.12	-69.45	0.28	41.13	6.32	5.36	0.14
	±0.01	±6.02	±0.15	±3.58	±0.62	±0.64	±0.03
16 [4]	0.042	-25.74	-7.83	11.26	2.24	3.99	0.10
	±0.004	±2.51	±1.09	±1.30	±0.39	±0.58	±0.03
17 [4]	0.084	-55.42	-19.54	25.82	7.55	4.96	0.35
	±0.01	±6.30	±2.68	±3.24	±0.95	±0.65	±0.09
18 [4]	0.12	-68.53	-19.03	34.24	8.79	4.85	0.65
	±0.01	±6.36	±2.25	±3.34	±0.89	±0.61	±0.10
19 [5]	0.009	-16.22	0	8.61	0.36	3.07	0.10
	±0.001	±1.77		±0.93	±0.05	±0.36	±0.01
20 [5]	0.024	-20.77	0	10.45	0.07	4.56	0.04
	±0.003	±2.39		±1.20	±0.01	±0.54	±0.02
21 [5]	0.039	-26.77	0	13.41	0.11	5.83	0
	±0.005	±3.09		±1.55	±0.02	±0.69	
22 [5]	0.04	-24.41	0	13.21	1.10	3.74	0
	±0.005	±2.86		±1.54	±0.15	±0.50	
23 [6]	0.01	-10.87	0.36	5.81	0.22	2.12	0
	±0.001	±1.30	±0.09	±0.69	±0.05	±0.28	
24 [6]	0.01	-9.57	0	4.92	0.16	1.97	0
	±0.001	±1.18		±0.60	±0.03	±0.25	
25 [7]	0.063	-37.00	0	21.87	3.37	2.82	0.09
	±0.009	±4.34		±2.58	±0.43	±0.38	±0.01

Table D.2: Continued

SST Number	μ [h^{-1}]	q_{CO} [mmol/(g_{DW}h)]	q_{H_2} [mmol/(g_{DW}h)]	q_{CO_2} [mmol/(g_{DW}h)]	q_{EtOH} [mmol/(g_{DW}h)]	q_{AcT} [mmol/(g_{DW}h)]	q_{BDO} [mmol/(g_{DW}h)]
26 [7]	0.063	-39.45	0	23.86	4.04	2.25	0.16
	±0.009	±4.65		±2.83	±0.52	±0.28	±0.02
27 [7]	0.063	-38.37	0	23.56	4.30	1.63	0.15
	±0.009	±4.52		±2.80	±0.54	±0.22	±0.02
28 [8]	0.028	-12.98	0	6.44	0.02	2.72	0
	±0.009	±3.20		±1.59	±0.004	±0.68	
29 [8]	0.028	-14.12	0	7.00	0	3.03	0
	±0.01	±4.65		±2.31		±1.01	
30 [8]	0.021	-17.64	0	8.79	0.01	4.02	0
	±0.003	±2.34		±1.16	±0.01	±0.54	
31 [8]	0.021	-20.64	-4.10	8.24	0.02	5.79	0
	±0.004	±2.94	±0.65	±1.22	±0.003	±0.82	
32 [8]	0.021	-18.53	-7.14	5.68	0.03	5.99	0
	±0.004	±2.55	±1.10	±0.86	±0.01	±0.83	
33 [8]	0.021	-15.51	-11.57	2.34	0.42	5.77	0
	±0.003	±1.97	±1.52	±0.35	±0.06	±0.75	
34 [8]	0.028	-32.34	0	16.11	0	7.59	0
	±0.005	±4.86		±2.42		±1.15	
35 [8]	0.028	-33.71	0	16.83	0.04	7.88	0
	±0.006	±5.26		±2.63	±0.03	±1.24	
36 [8]	0.028	-46.29	0	23.25	0.17	10.82	0
	±0.004	±6.07		±3.05	±0.03	±1.43	
37 [8]	0.028	-57.91	0	29.32	0.43	13.34	0
	±0.005	±8.91		±4.50	±0.13	±2.08	

D.3. Gas-Liquid Mass Transfer

Table D.3: Overview of reconciled data. Sources: Heffernan et al., 2020 [1], Valgepea et al., 2018 [2], Valgepea, de Souza Pinto Lemgruber, et al., 2017 [3], de Lima et al., 2022 [4], Elisiário et al., 2023 [5], Allaart, 2023 [6], Chen et al., 2018 [7], and Diender et al., 2019 [8]. Abbreviations: Dissolved CO concentration (c_{CO}), dissolved H_2 concentration (c_{CH_2}), dissolved CO_2 concentration (c_{CO_2}), CO volumetric mass transfer coefficient (k_La_{CO}), H_2 volumetric mass transfer coefficient ($k_La_{H_2}$), CO_2 mass transfer coefficient ($k_La_{CO_2}$). a: Experiments performed in bubble column.

SST Number	c_{CO} [mmol/L]	c_{H_2} [mmol/L]	c_{CO_2} [mmol/L]	k_La_{CO} [h^{-1}]	$k_La_{H_2}$ [h^{-1}]	$k_La_{CO_2}$ [h^{-1}]
1 [1]	0.016	0.453	8.73	824.6	1227.7	801.9
2 [1]	0	0.504	10.29	133.0	198.0	129.3
3 [1]	0.024	0.418	9.30	352.1	524.2	342.4
4 [2]	0.554	0	1.98	149.1	221.9	145.0
5 [2]	0.212	0.002	9.38	260.1	387.3	253.0
6 [2]	0.074	0.302	0.349	248.0	369.2	241.2
7 [2]	0.033	0.306	0.991	719.8	1071.7	700.0
8 [3]	0.487	0.120	10.96	143.0	212.9	139.1
9 [3]	0.479	0.117	11.12	143.0	212.9	139.1
10 [3]	0.330	0.068	15.44	202.4	301.3	196.8
11 [3]	0.202	0.061	19.60	248.0	369.2	241.2
12 [3]	0.195	0.059	19.84	248.0	369.2	241.2
13 [4]	0.164	0.002	10.41	285.0	424.4	277.2
14 [4]	0.075	0.001	12.84	433.3	645.2	421.4
15 [4]	0.039	0.002	16.64	933.2	1389.5	907.6
16 [4]	0.225	0.102	18.17	272.2	405.3	264.7
17 [4]	0.017	0.037	25.61	416.8	620.5	405.3
18 [4]	0.034	0.083	28.06	908.4	1352.5	833.5
19 [5]	0.147	0	10.56	167.2	248.9	162.6
20 [5]	0.078	0	11.84	167.2	248.9	162.6
21 [5]	0.094	0	11.43	167.2	248.9	162.6
22 [5]	0.268	0	7.67	167.2	248.9	162.6
23 [6]	0.052	0.001	0.920	252.7	376.2	245.7
24 [6]	0.052	0	0.888	252.7	376.2	245.7
25 [7][a]	0.047	0	19.04	546.9	814.2	531.8
26 [7][a]	0.044	0	18.97	630.0	938.0	612.7
27 [7][a]	0.052	0	18.44	669.0	996.0	650.6
28 [8]	-0.065	0	23.02	100.5	149.6	97.7
29 [8]	0.089	0	18.62	100.5	149.6	97.7
30 [8]	-0.065	0	46.40	75.7	112.6	73.6
31 [8]	0.101	0.014	38.85	78.4	116.8	76.3
32 [8]	0.160	0.086	32.24	81.0	120.6	78.8
33 [8]	0.116	0.236	24.91	85.1	149.6	82.8
34 [8]	0.207	0	15.38	100.5	149.6	97.7
35 [8]	0.252	0	14.15	100.5	149.6	97.7
36 [8]	0.302	0	12.80	100.5	149.6	97.7
37 [8]	0.278	0	13.51	100.5	149.6	97.7

E

ATP yields for the synthesis of fermentation products

The adenosine triphosphate (ATP) yields for the synthesis of acetate ($Y_{ATP,R1}$) and ethanol ($Y_{ATP,R3}$) with carbon dioxide (CO) as electron donor in *Clostridium autoethanogenum* (*C. autoethanogenum*) (Eq. (E.1) - (E.3)) were calculated using the energy balancing method. For calculations, it was assumed that ethanol production occurs via aldehyde:ferredoxin oxidoreductase (AOR) and alcohol dehydrogenase (ADH), and methylene-THF reductase is electron bifurcating (Diender et al., 2019; Liew et al., 2017; Munoz and Philips, 2023; Valgepea, de Souza Pinto Lemgruber, et al., 2017). Furthermore, the ATP yield for the synthesis of ethanol ($Y_{ATP,R2}$) through acetate reduction (Eq. (E.2)) was determined according to the same method.

$$4CO + 2H_2O \longrightarrow AcT + 2CO_2 + Y_{ATP,R1}ATP \quad \text{(E.1)}$$

$$2CO + AcT + H_2O \longrightarrow EtOH + 2CO_2 + Y_{ATP,R2}ATP \quad \text{(E.2)}$$

$$6CO + 3H_2O \longrightarrow EtOH + 4CO_2 + Y_{ATP,R3}ATP \quad \text{(E.3)}$$

E.1. ATP yield for acetate and ethanol production from CO

E.1.1. CO distribution in catabolism

The production of 1 mol of acetate or ethanol requires a total of 4 and 6 mol CO, respectively (Eq. (E.1) - (E.3)). Part of the CO enters the Wood-Ljungdahl pathway via the carbonyl branch to serve as the carbonyl group of acetyl-CoA (Ac-CoA), while CODH/ACS oxidizes the rest of the CO (Fernández-Blanco et al., 2023). The amount of CO used to form the carbonyl group of acetyl-CoA is determined by the amount of acetyl-CoA required to create the desired product, which was calculated by dividing the number of carbons in the product ($N_{C,i}$) by the number of carbons in acetyl-CoA ($N_{C,Acetyl-CoA}$). Subsequently, the amount of oxidized CO was determined by subtracting the CO used as the carbonyl group of acetyl-CoA from the total amount of CO used during catabolism (Eq. (E.4)). Acetate, ethanol and acetyl-CoA all contain 2 carbons per molecule, which means that only 1 mol of CO is required to form the carbonyl group of acetyl-CoA and the residual 3 and 5 CO are oxidized by CODH/ACS.

$$CO_{ox} = CO_{tot} - \frac{N_{C,i}}{N_{C,acetyl-CoA}} \quad \text{(E.4)}$$

with CO_{ox} the oxidized amount of CO, CO_{tot} the total catabolized amount of CO, $N_{C,i}$ the number of carbons in acetate or ethanol, and $N_{C,i}$ the number of carbons in acetyl-CoA.

Acetate production:

$$CO_{ox} = 4 - \frac{2}{2} = 3 \text{ mol CO}$$

Ethanol production:

$$CO_{ox} = 6 - \frac{2}{2} = 5 \text{ mol CO}$$

E.1.2. Derivation of the CO oxidation reaction by CODH/ACS

During CO-oxidation, the electrons from CO are used to reduce oxidized ferredoxin, leading to the generation of its reduced form (Fd^{2-}_{red}) (Eq. (E.5)) (Katsyv and Müller, 2020). Overall, 3 and 5 mol CO is oxidized during acetate and ethanol production, generating 3 and 5 mol Fd^{2-}_{red}, respectively.

$$CO_{ox} + H_2O \rightarrow CO_2 + Fd^{2-}_{red} \tag{E.5}$$

Acetate production:

$$3CO_{ox} + 3H_2O \rightarrow 3CO_2 + 3Fd^{2-}_{red}$$

Ethanol production:

$$5CO_{ox} + 5H_2O \rightarrow 5CO_2 + 5Fd^{2-}_{red}$$

E.1.3. Derivation of the product reaction

The product reaction has two parts: 1) acetyl-CoA production from CO and 2) product production from acetyl-CoA. First, the second part of the reaction was derived, as the first part requires the required amount of acetyl-CoA to be known. Both acetate and ethanol production require 1 mol of acetyl-CoA and generate 1 mol of ATP per mol of product. However, ethanol production requires the additional consumption of 1 mol Fd^{2-}_{red} and NADH.

Acetate production:

$$Ac\text{-}CoA \rightarrow ATP + AcT$$

Ethanol production:

$$Ac\text{-}CoA + Fd^{2-}_{red} + NADH \rightarrow ATP + EtOH$$

As 1 mol acetyl-CoA is required for acetate and ethanol production, the same reaction from CO to acetyl-CoA (Eq. (E.6)) was used to derive the acetate and ethanol product reactions.

$$H_2 + CO + CO_2 + ATP + NADPH + 2NADH \rightarrow Ac\text{-}CoA + Fd^{2-}_{red} + H_2O \tag{E.6}$$

Acetate product reaction:

$$H_2 + CO + CO_2 + NADPH + 2NADH \rightarrow Fd^{2-}_{red} + H_2O + AcT$$

Ethanol product reaction:

$$H_2 + CO + CO_2 + NADPH + 3NADH \rightarrow H_2O + EtOH$$

E.1.4. Derivation of the hydrogen production reaction by the HytA-E/FdhA complex

The electron-bifurcating hydrogenase-formate dehydrogenase (HytA-E/FdhA) reduces Fd^{2-}_{red} and NADPH to produce hydrogen (Eq. (E.7)) (Katsyv and Müller, 2020). In the acetate and ethanol product reaction, only 1 mol of H_2 is consumed, so 1 mol H_2 is produced by the HytA-E/FdhA complex for acetate and ethanol production, respectively.

$$0.5Fd^{2-}_{red} + 0.5NADPH \rightarrow H_2 \tag{E.7}$$

Acetate production:

$$0.5Fd^{2-}_{red} + 0.5NADPH \rightarrow H_2$$

Ethanol production:

$$0.5Fd^{2-}_{red} + 0.5NADPH \rightarrow H_2$$

E.1.5. Derivation of the NADPH balancing reaction by the Nfn complex

The consumed NADPH is balanced by an electron-bifurcating and ferredoxin-dependent transhydrogenase (Nfn) (Eq. (E.8)) (Katsyv and Müller, 2020). NADPH is consumed in the product and the hydrogen production reaction, resulting in a total of 1.5 mol consumed NADPH for both acetate and ethanol production. To balance the consumed NADPH, the Nfn complex generated 1.5 mol NADPH.

$$0.5Fd_{red}^{2-} + 0.5NADH \rightarrow NADPH \tag{E.8}$$

Acetate production:

$$0.75Fd_{red}^{2-} + 0.75NADH \rightarrow 1.5NADPH$$

Ethanol production:

$$0.75Fd_{red}^{2-} + 0.75NADH \rightarrow 1.5NADPH$$

E.1.6. Derivation of the electron transfer reaction by the Rnf complex

The Rnf complex uses the residual Fd_{red}^{2-} to generate NADH and build a H^+-gradient over the cell-membrane by using the released energy from Fd_{red}^{2-} oxidation to export protons (Eq. (E.9)) (Katsyv and Müller, 2020). During acetate production, 4 mol Fd_{red}^{2-} is generated in the CO-oxidation reaction and acetate product reaction. However, the hydrogen production and NADPH balancing reaction use 0.5 and 0.75 mol Fd_{red}^{2-}, respectively. Therefore, 2.75 mol Fd_{red}^{2-} remained to generate NADH and export a total of 5.5 mol H^+. During ethanol production, Fd_{red}^{2-} is produced in only the CO-oxidation reaction, and consumed in the hydrogen production and NADPH balancing reaction. The residual 3.75 mol Fd_{red}^{2-} is used to generate NADH and export 7.5 H^+ outside the cell.

$$Fd_{red}^{2-} \rightarrow NADH + 2H_{out}^{+} \tag{E.9}$$

Acetate production:

$$2.75Fd_{red}^{2-} \rightarrow 2.75NADH + 5.5H_{out}^{+}$$

Ethanol production:

$$3.75Fd_{red}^{2-} \rightarrow 3.75NADH + 7.5H_{out}^{+}$$

E.1.7. Calculation of the ATP yield

The exported protons enter the cell through the membrane-bound ATP synthase (ATPase), which uses the potential of the H^+-gradient over the membrane to generate ATP. Here, it is assumed that 3.6 mol H^+ are required to generate 1 mol ATP (Eq. (E.10)) (Katsyv and Müller, 2020). Overall, an $Y_{ATP,R1}$ and $Y_{ATP,R3}$ of 1.5 and 2.1 was found.

$$3.6H_{out}^{+} \rightarrow 3.6H_{in}^{+} + ATP \tag{E.10}$$

Acetate production:

$$5.5H_{out}^{+} \rightarrow 5.5H_{in}^{+} + 1.5ATP$$

Ethanol production:

$$7.5H_{out}^{+} \rightarrow 7.5H_{in}^{+} + 2.1ATP$$

E.2. ATP yield for ethanol production from acetate

The reaction for ethanol production from CO (Eq. (E.3)) is the sum of the reaction for acetate production from CO (Eq. (E.1)) and acetate reduction to ethanol (Eq. (E.2)). Therefore, the ATP yield of acetate reduction can be determined by subtracting the ATP yield during acetate production from the ATP yield during ethanol production, resulting in an ATP yield of 0.6 ATP per mol ethanol. The ATP yield was also calculated using the energy balancing method for validation.

E.2.1. Derivation of the CO oxidation reaction by CODH/ACS

In the acetate reduction reaction, acetate is the precursor for ethanol. Therefore, all catabolized CO is oxidised by the CODH/ACS complex, yielding 2 mol of Fd_{red}^{2-}.

$$2CO_{ox} + 2H_2O \rightarrow 2CO_2 + 2Fd_{red}^{2-}$$

E.2.2. Derivation of the product reaction

The product reaction of acetate reduction consists of only one part, namely ethanol production from the acetate precursor.

$$AcT + Fd_{red}^{2-} + NADH \rightarrow EtOH$$

E.2.3. Derivation of the electron transfer reaction by the Rnf complex

During acetate reduction, 2 mol Fd_{red}^{2-} is produced during CO-oxidation, while 1 mol Fd_{red}^{2-} is consumed in the product reaction. Therefore, 1 mol Fd_{red}^{2-} remains for NADH generation, resulting in 2 exported protons.

$$1Fd_{red}^{2-} \rightarrow 1NADH + 2H_{out}^{+}$$

E.2.4. Calculation of the ATP yield

The $Y_{ATP,R2}$ of acetate reduction is 0.6, assuming the ATPase having a yield of 1 mol ATP per 3.6 mol H^+.

$$2H_{out}^{+} \rightarrow 2H_{in}^{+} + 0.6ATP$$

F

Thermodynamic determination of kinetic parameters

To get an impression of the order of magnitude of the kinetic parameters of *Clostridium autoethanogenum* (*C.autoethanogenum*) grown on carbon monoxide (CO), a bioenergetic analysis of the system based on the methods described by Heijnen and Kleerebezem (2010), Kleerebezem (2022) and Kleerebezem and Van Loosdrecht (2010) was performed.

F.1. Metabolism

The metabolism of *C. autoethanogenum* consists of the catabolic and anabolic reactions. In catabolism, energy for growth and maintenance processes is produced. In *C. autoethanogenum* acetate and ethanol are the two major catabolic products, which are represented by two separate catabolic reactions (Eq. (F.2) - Eq. (F.3)). During CO-fermentation, CO is the only carbon and energy source. Therefore, it acts as both an electron donor and acceptor in the catabolic reaction. The anabolic reaction describes biomass production from CO and ammonium (NH_4^+) (Eq. (F.1)), which serve as carbon and nitrogen sources, respectively.

Anabolic reaction:

$$1.88CO + 0.34H_2O + 0.28NH_4^+ \rightarrow CH_{1.52}O_{0.46}N_{0.28} + 0.88CO_2 + 0.28H^+ \quad \text{(F.1)}$$

Catabolic reactions:

$$CO + 0.5H_2O \rightarrow 0.17C_2H_5OH + 0.67CO_2 \quad \text{(F.2)}$$

$$CO + 0.5H_2O \rightarrow 0.25C_2H_3O_2^- + 0.5CO_2 + 0.25H^+ \quad \text{(F.3)}$$

The metabolism is obtained by combining the anabolic reaction with both catabolic reactions. As the analysis serves to find estimates of the kinetic parameters, the situations in which solely acetate or ethanol is produced were analyzed. This means that two metabolisms were derived and serve as a range in which the kinetic parameters fall, depending on the produced ratio of acetate and ethanol. The metabolic reaction is a function of the catabolic and anabolic reaction, with λ_{Cat} the number of cycles required for the catabolic reaction to yield enough Gibbs energy to produce one C-mol of biomass. Assuming that all Gibbs energy generated in the catabolic reaction is used for biomass production, Equation (F.4) can be written in terms of Gibbs energy (Eq. (F.5)), such that λ_{Cat} can be determined.

$$Met = \lambda_{Cat} \cdot Cat + 1 \cdot An \quad \text{(F.4)}$$

$$\Delta G_{Met} = \lambda_{Cat} \cdot \Delta G_{Cat} + 1 \cdot \Delta G_{An} \quad \text{(F.5)}$$

with λ_{Cat} the number of cycles required for the catabolic reaction to yield enough Gibbs energy to produce one C-mol of biomass, ΔG_{Met} the Gibbs free energy change of the metabolic reaction in kJ/mol, ΔG_{Cat} the Gibbs free

energy change of the catabolic reaction in kJ/mol and ΔG_{An} the Gibbs free energy change of the anabolic reaction in kJ/mol.

To determine the standard Gibbs energy change at biological relevant conditions (ΔG_R^{01}) of the catabolic and anabolic reactions, the standard Gibbs energy change (ΔG_R^0) (Eq. (F.6)) was first determined from the Gibbs energy of formation (ΔG_f^0) of the compounds participating in the catabolic and anabolic reactions (Table F.1). Subsequently, the ΔG_R^0 were corrected for pH to obtain the ΔG_R^{01} (Eq. (F.7)). Finally, the standard Gibbs energy changes were corrected for the process temperature of 37 ^oC (310.15 K) (Eq. (F.8)). The steady states in the dataset have a pH ranging from 5 to 6.2 (Table C.1). Therefore, for this analysis, the mean pH of 5.6 is used. All in all, the ΔG_{Cat}^{01} of the catabolic reaction with ethanol and acetate production were determined as -41.3 and -46.4 kJ/mol$_{CO}$, respectively. Furthermore, a $\Delta G_{An}^{01,T}$ of -69.0 kJ/mol$_x$ was found.

$$\Delta G_R^0 = \sum_{i=1}^{n} Y_i^R \cdot Gf_i^0 \tag{F.6}$$

$$\Delta G_R^{01} = \Delta G_R^0 + R \cdot T_s \cdot \ln\left(c_{H^+}{}^{Y_{H^+}^R}\right) \tag{F.7}$$

$$\Delta G_R^{01,T} = \Delta G_R^{01} \cdot \frac{T}{T_s} + \Delta H^{01} \cdot \frac{T - T_s}{T_s} \tag{F.8}$$

with ΔG_R^0 the standard Gibbs energy change in kJ/mol, Y_i^R the stoichiometric coefficient of compound i, Gf_i^0 the Gibbs energy of formation of compound i in kJ/mol ,ΔG_R^{01} the standard Gibbs energy change at biological relevant conditions in kJ/mol, $\Delta G_R^{01,T}$ the standard Gibbs energy change at process conditions in kJ/mol, ΔH^{01} the standard enthalpy change at biological relevant conditions in kJ/mol, R the gas constant of 8.31 $\cdot 10^{-3}$ kJ/(K mol), T the process temperature in K, T_s the standard temperature of 298.15 K, and c_{H^+} the proton concentration in mol/L.

Table F.1: Standard Gibbs energy (ΔG_f^0) and enthalpy (ΔH_f^0) of formation (Kleerebezem and Van Loosdrecht, 2010)
* From Norman et al. (2019)

Compound	Chemical formula	ΔG_f^0 [kJ/mol]	ΔH_f^0 [kJ/mol]
Carbon monoxide	CO	-137.2	-110.5
Carbon dioxide	CO_2	-394.4	-393.5
Ethanol	C_2H_5OH	-181.8	-288.3
Acetate	$C_2H_3O_2^-$	-369.4	-485.8
Biomass	$CH_{1.52}O_{0.46}N_{0.28}$*	-67.0	-91.0
Water	H_2O	-237.2	-285.8
Ammonium	NH_4^+	-79.4	-133.3
Proton	H^+	0	0

Catabolic reaction with ethanol as the product:

$$\Delta G_{Cat}^0 = Y_{CO}^{Cat} \cdot G_{f,CO}^0 + Y_{H_2O}^{Cat} \cdot G_{f,H_2O}^0 + Y_{EtOH}^{Cat} \cdot G_{f,EtOH}^0 + Y_{CO_2}^{Cat} \cdot G_{f,CO_2}^0$$
$$\Delta G_{Cat}^0 = -1 \cdot -137.2 + -0.5 \cdot -237.2 + 0.17 \cdot -181.8 + 0.67 \cdot -394.4$$
$$\Delta G_{Cat}^0 = -37.5\ kJ/mol_{CO}$$
$$\Delta H_{Cat}^0 = Y_{CO}^{Cat} \cdot H_{f,CO}^0 + Y_{H_2O}^{Cat} \cdot H_{f,H_2O}^0 + Y_{EtOH}^{Cat} \cdot H_{f,EtOH}^0 + Y_{CO_2}^{Cat} \cdot H_{f,CO_2}^0$$
$$\Delta H_{Cat}^0 = -1 \cdot -110.5 + -0.5 \cdot -285.8 + 0.17 \cdot -288.3 + 0.67 \cdot -393.5$$
$$\Delta H_{Cat}^0 = -57.0\ kJ/mol_{CO}$$
$$\Delta G_{Cat}^{01} = -37.5 + 8.31 \cdot 10^{-3} \cdot 298.15 \cdot \ln\left((3 \cdot 10^{-6})^0\right) = -37.5\ kJ/mol_{CO}$$
$$\Delta H_{Cat}^{01} = -57.0 + 8.31 \cdot 10^{-3} \cdot 298.15 \cdot \ln\left((3 \cdot 10^{-6})^0\right) = -57.0\ kJ/mol_{CO}$$
$$\Delta G_{Cat}^{01,T} = -37.5 \cdot \frac{310.15}{298.15} + -57.0 \cdot \frac{310.15 - 298.15}{298.15} = -41.3\ kJ/mol_{CO}$$

Catabolic reaction with acetate as the product:

$$\Delta G^0_{Cat} = Y^{Cat}_{CO} \cdot G^0_{f,CO} + Y^{Cat}_{H_2O} \cdot G^0_{f,H_2O} + Y^{Cat}_{Ac^-} \cdot G^0_{f,Ac^-} + Y^{Cat}_{H^+} \cdot G^0_{f,H^+} + Y^{Cat}_{CO_2} \cdot G^0_{f,CO_2}$$
$$\Delta G^0_{Cat} = -1 \cdot -137.2 + -0.5 \cdot -237.2 + 0.25 \cdot -369.4 + 0.25 \cdot 0 + 0.5 \cdot -394.4$$
$$\Delta G^0_{Cat} = -33.8\ kJ/mol_{CO}$$
$$\Delta H^0_{Cat} = Y^{Cat}_{CO} \cdot H^0_{f,CO} + Y^{Cat}_{H_2O} \cdot H^0_{f,H_2O} + Y^{Cat}_{Ac^-} \cdot H^0_{f,Ac^-} + Y^{Cat}_{H^+} \cdot H^0_{f,H^+} + Y^{Cat}_{CO_2} \cdot H^0_{f,CO_2}$$
$$\Delta H^0_{Cat} = -1 \cdot -110.5 + -0.5 \cdot -285.8 + 0.25 \cdot -465.8 + 0.25 \cdot 0 + 0.5 \cdot -393.5$$
$$\Delta H^0_{Cat} = -64.8\ kJ/mol_{CO}$$
$$\Delta G^{01}_{Cat} = -33.8 + 8.31 \cdot 10^{-3} \cdot 298.15 \cdot \ln\left((3 \cdot 10^{-6})^{0.25}\right) = -41.8\ kJ/mol_{CO}$$
$$\Delta H^{01}_{Cat} = -64.8 + 8.31 \cdot 10^{-3} \cdot 298.15 \cdot \ln\left((3 \cdot 10^{-6})^{0.25}\right) = -72.8\ kJ/mol_{CO}$$
$$\Delta G^{01,T}_{Cat} = -41.8 \cdot \frac{310.15}{298.15} + -72.8 \cdot \frac{310.15 - 298.15}{298.15} = -46.4\ kJ/mol_{CO}$$

Anabolic reaction:

$$\Delta G^0_{An} = Y^{An}_{CO} \cdot G^0_{f,CO} + Y^{An}_{NH_4^+} \cdot G^0_{f,NH_4^+} + Y^{An}_{H_2O} \cdot G^0_{f,H_2O} + Y^{An}_{x} \cdot G^0_{f,x} + Y^{An}_{H^+} \cdot G^0_{f,H^+} + Y^{An}_{CO_2} \cdot G^0_{f,CO_2}$$
$$\Delta G^0_{An} = -1.88 \cdot -137.2 + -0.28 \cdot -79.4 + -0.34 \cdot -237.2 + 1 \cdot -67.0 + 0.28 \cdot -0 + 0.88 \cdot -394.4$$
$$\Delta G^0_{An} = -53.3\ kJ/mol_{CO}$$
$$\Delta H^0_{An} = Y^{An}_{CO} \cdot H^0_{f,CO} + Y^{An}_{NH_4^+} \cdot H^0_{f,NH_4^+} + Y^{An}_{H_2O} \cdot H^0_{f,H_2O} + Y^{An}_{x} \cdot H^0_{f,x} + Y^{An}_{H^+} \cdot H^0_{f,H^+} + Y^{An}_{CO_2} \cdot H^0_{f,CO_2}$$
$$\Delta H^0_{An} = -1.88 \cdot -110.5 + -0.28 \cdot -133.3 + -0.34 \cdot -285.8 + 1 \cdot -91.0 + 0.28 \cdot -0 + 0.88 \cdot -393.5$$
$$\Delta H^0_{An} = -95.0\ kJ/mol_{CO}$$
$$\Delta G^{01}_{An} = -53.3 + 8.31 \cdot 10^{-3} \cdot 298.15 \cdot \ln\left((3 \cdot 10^{-6})^{0.28}\right) = -62.3\ kJ/mol_{CO}$$
$$\Delta H^{01}_{An} = -95.0 + 8.31 \cdot 10^{-3} \cdot 298.15 \cdot \ln\left((3 \cdot 10^{-6})^{0.28}\right) = -104.0\ kJ/mol_{CO}$$
$$\Delta G^{01,T}_{An} = -62.3 \cdot \frac{310.15}{298.15} + -104.0 \cdot \frac{310.15 - 298.15}{298.15} = -69.0\ kJ/mol_{CO}$$

The Gibbs free energy change of the metabolic reaction (ΔG^{01}_{Met}) is estimated by the correlation obtained by Heijnen and Van Dijken (1992) (Eq. (F.9)), which depends on the number of carbons (NoC) and the degree of reduction (γ) of the used carbon source. Here, CO is used as the carbon source, and thus are the NoC_{CO} and γ_{CO} 1 and 2 (Table 2.2), respectively. Using this correlation, the ΔG^{01}_{Met} was estimated as -651.08 kJ/C-mol$_x$.

$$-\Delta G^{01}_{Met} = 200 + 18 \cdot (6 - NoC)^{1.8} + \exp\left(((3.8 - \gamma)^2)^{0.16} \cdot (3.6 + 0.4 \cdot NoC)\right) \quad \text{(F.9)}$$

with ΔG^{01}_{Met} the Gibbs free energy change of the metabolism in kJ/mol, NoC_{CO} the number of carbons in the used carbon source, and γ the degree of reduction of the used carbon source.

$$-\Delta G^{01}_{Met} = 200 + 18 \cdot (6 - 1)^{1.8} + \exp\left(((3.8 - 2)^2)^{0.16} \cdot (3.6 + 0.4 \cdot 1)\right) = -651.08\ kJ/C\text{-}mol_x$$

Finally, the λ_{Cat} for the metabolic reaction with ethanol and acetate production were determined as 15.7 and 14.1, respectively. The metabolic reactions were derived according to Eq. (F.5).

Metabolic reaction with ethanol as the product:

$$\lambda_{Cat} = \frac{\Delta G^{01}_{Met} - \Delta G^{01}_{An}}{\Delta G^{01}_{Cat}} = \frac{(-651.08) - (-62.3)}{-37.5} = 15.7$$
$$17.59CO + 0.28NH_4^+ + 8.20H_2O \rightarrow CH_{1.52}O_{0.46}N_{0.28} + 2.62C_2H_5OH + 11.36CO_2 + 0.28H^+$$

Metabolic reaction with acetate as the product:

$$\lambda_{Cat} = \frac{\Delta G^{01}_{Met} - \Delta G^{01}_{An}}{\Delta G^{01}_{Cat}} = \frac{(-651.08) - (-62.3)}{-41.8} = 14.1$$
$$15.97CO + 0.28NH_4^+ + 7.39H_2O \rightarrow CH_{1.52}O_{0.46}N_{0.28} + 3.52C_2H_3O_2^- + 7.93CO_2 + 3.80H^+$$

F.2. Maintenance coefficient

The maintenance coefficient (m_{CO}) depends on the Gibbs energy required for biomass maintenance (m_G), the Gibbs free energy change of the catabolic reaction (ΔG^{01}_{Cat}), and the process temperature (T) (Eq. (F.10)). The m_G is approximately -4.5 kJ/(C-mol$_x$ h). Furthermore, the ΔG^{01}_{Cat} for both the catabolic reactions have been previously determined as -37.5 and -41.8 kJ/mol for the ethanol and acetate production, respectively (see Section F.1). The steady states in the dataset are all carried out at a temperature of 37 ^{o}C (310.15 K) (Table C.1), therefore this temperature was used to determine the maintenance coefficient estimates. The maintenance coefficients for the reaction with ethanol and acetate production were determined as 0.35 and 0.32 mol$_{CO}$/(mol$_x$ h), respectively.

$$m_{CO} = \frac{m_G}{-\Delta G^{01}_{Cat}} \cdot \exp\left(\frac{-69}{R} \cdot \left(\frac{1}{T} - \frac{1}{298.15}\right)\right) \tag{F.10}$$

with m_{CO} the maintenance coefficient in mol$_{CO}$/(mol$_x$ h), m_G the Gibbs free energy required for biomass maintenance in kJ/(mol$_x$ h), ΔG^{01}_{Cat} the Gibbs free energy change of the catabolic reaction under biological relevant conditions in kJ/mol, R the gas constant of 8.31 $\cdot 10^{-3}$ kJ/(K mol), and T the process temperature in K.

Maintenance coefficient for ethanol production:

$$m_{CO} = \frac{-4.5}{-(-37.5)} \cdot \exp\left(\frac{-69}{8.31 \cdot 10^{-3}} \cdot \left(\frac{1}{310.15} - \frac{1}{298.15}\right)\right) = 0.35\ mol_{CO}/(mol_x h)$$

Maintenance coefficient for acetate production:

$$m_{CO} = \frac{-4.5}{-(-41.8)} \cdot \exp\left(\frac{-69}{8.31 \cdot 10^{-3}} \cdot \left(\frac{1}{310.15} - \frac{1}{298.15}\right)\right) = 0.32\ mol_{CO}/(mol_x h)$$

F.3. Maximum growth rate

The maximum growth rate (μ^{max}) depends on the maximum electron capacity in the catabolism (q_e^{Cat}), the number of electrons involved in the catabolism (NoEln), the maintenance coefficient (m_{CO}), the stoichiometric coefficient of CO in the catabolism (Y_{CO}^{Cat}), the stoichiometric coefficient of CO in the anabolism (Y_{CO}^{An}), the stoichiometric coefficient of CO in the metabolism (Y_{CO}^{Met}), and the process temperature (T) (Eq. (F.10)). The q_e^{Cat} is approximately -3 e-mol/(mol$_x$ h) at 298.15 K. Additionally, the number of electrons involved in the catabolism has been determined by Korkontzelos (2022) as 6.08 e-mol and 6.625 e-mol for ethanol and acetate production, respectively. Furthermore, the Y_{CO}^{Cat}, Y_{CO}^{An}, Y_{CO}^{Met} and m_{CO} have been determined in the previous sections (see Section F.1 and F.2). The process temperature of the steady states in the database is 37 ^{o}C (310.15 K), therefore this temperature was used to calculate the maximum growth rate. For ethanol production, a maximum growth rate of 0.070 h^{-1} was determined. The maximal growth rate for acetate production was 0.072 h^{-1}.

$$\mu^{max} = \frac{\frac{q_e^{Cat}}{NoEln} - Y_{CO}^{Cat} \cdot m_{CO}}{Y_{CO}^{Met} - Y_{CO}^{An}} \cdot \exp\left(\frac{-69}{R} \cdot \left(\frac{1}{T} - \frac{1}{298.15}\right)\right) \tag{F.11}$$

with μ^{max} the growth rate in h^{-1}, q_e^{Cat} the maximum electron capacity in the catabolism at 298.15 K in e-mol/(mol$_x$ h), NoEln the number of electrons involved in the catabolism in e-mol, m_{CO} the maintenance coefficient in mol$_{CO}$/(mol$_x$ h), Y_{CO}^{Cat} the stoichiometric coefficient of CO in the catabolism, Y_{CO}^{An} the stoichiometric coefficient of CO in the anabolism, Y_{CO}^{Met} the stoichiometric coefficient of CO in the metabolism, R the gas constant of 8.31 $\cdot 10^{-3}$ kJ/(K mol), and T the process temperature in K.

Maximum growth rate for ethanol production:

$$\mu^{max} = \frac{\frac{-3}{6.08} - (-1) \cdot 0.35}{(-17.59) - (-1.88)} \cdot \exp\left(\frac{-69}{8.31 \cdot 10^{-3}} \cdot \left(\frac{1}{310.15} - \frac{1}{298.15}\right)\right) = 0.070\ h^{-1}$$

Maximum growth rate for acetate production:

$$\mu^{max} = \frac{\frac{-3}{6.625} - (-1) \cdot 0.32}{(-15.97) - (-1.88)} \cdot \exp\left(\frac{-69}{8.31 \cdot 10^{-3}} \cdot \left(\frac{1}{310.15} - \frac{1}{298.15}\right)\right) = 0.072\ h^{-1}$$

F.4. Maximum CO uptake rate

The maximum CO uptake rate (q_{CO}^{max}) depends on the stoichiometric coefficient of CO in the metabolism (Y_{CO}^{Met}), the maximum growth rate (μ^{max}), the maintenance coefficient (m_{CO}), the stoichiometric coefficient of CO in the catabolism (Y_{CO}^{Cat}), and the process temperature (T) (Eq. (F.12)). The Y_{CO}^{Met}, Y_{CO}^{Cat}, m_{CO} and μ^{max} have been determined in the previous sections (see Section F.1, F.2 and F.3). The process temperature of the steady states in the database is 310.15 K (37 ^{o}C), therefore this temperature was used to calculate the maximum CO uptake rate. The resulting q_{CO}^{max} for ethanol and acetate production were -1.58 and -1.46 mol_{CO}/(mol_x h), respectively.

$$-q_{CO}^{max} = (Y_{CO}^{Met} \cdot \mu^{max} + Y_{CO}^{Cat} \cdot m_{CO}) \cdot \exp\left(\frac{-69}{R} \cdot \left(\frac{1}{T} - \frac{1}{298.15}\right)\right) \quad \text{(F.12)}$$

with q_{CO}^{max} the maximum CO uptake rate in mol_{CO}/(mol_x h), Y_{CO}^{Met} the stoichiometric coefficient of CO in the metabolism, μ^{max} the growth rate in h^{-1}, Y_{CO}^{Cat} the stoichiometric coefficient of CO in the catabolism, m_{CO} the maintenance coefficient in mol_{CO}/(mol_x h), R the gas constant of 8.31 $\cdot 10^{-3}$ kJ/(K mol), and T the process temperature in K.

Maximum CO uptake rate for ethanol production:

$$-q_{CO}^{max} = ((-17.59)\cdot 0.070 + (-1)\cdot 0.35)\cdot \exp\left(\frac{-69}{8.31 \cdot 10^{-3}} \cdot \left(\frac{1}{310.15} - \frac{1}{298.15}\right)\right) = 1.58\ mol_{CO}/(mol_x h)$$

Maximum CO uptake rate for acetate production:

$$-q_{CO}^{max} = ((-15.97)\cdot 0.072 + (-1)\cdot 0.32)\cdot \exp\left(\frac{-69}{8.31 \cdot 10^{-3}} \cdot \left(\frac{1}{310.15} - \frac{1}{298.15}\right)\right) = 1.46\ mol_{CO}/(mol_x h)$$

F.5. Maximum biomass yield on CO

The maximum biomass yield on CO ($Y_{x/CO}^{max}$) was determined using the the Herbert-Pirt equation (Eq. (F.13)), resulting in an estimated $Y_{x/CO}^{max}$ for ethanol and acetate production of 0.057 and 0.063 mol_x/mol_{CO}, respectively.

$$-q_{CO}^{max} = \frac{\mu_{CO}^{max}}{Y_{x/CO}^{max}} + m_{CO} \quad \text{(F.13)}$$

with $Y_{x/CO}^{max}$ the maximum biomass yield on CO in mol_x/mol_{CO}, μ^{max} the growth rate in h^{-1}, q_{CO}^{max} the maximum CO uptake rate in mol_{CO}/(mol_x h), and m_{CO} the maintenance coefficient in mol_{CO}/(mol_x h).

Maximum biomass yield on CO for ethanol production:

$$Y_{x/CO}^{max} = \frac{0.070}{1.58 - 0.35} = 0.057\ mol_x/mol_{CO}$$

Maximum biomass yield on CO for acetate production:

$$Y_{x/CO}^{max} = \frac{0.072}{1.46 - 0.32} = 0.063\ mol_x/mol_{CO}$$

F.6. Overview

Table F.2: Overview of Gibbs free energy changes, and estimated kinetic parameters

Parameter	Unit	Only ethanol production	Only acetate production
ΔG^{0}_{Cat}	kJ/mol	-37.5	-33.8
ΔG^{01}_{Cat}	kJ/mol	-37.5	-41.8
$\Delta G^{01,T}_{Cat}$	kJ/mol	-41.3	-46.4
ΔG^{0}_{An}	kJ/mol	-53.5	-53.3
ΔG^{01}_{An}	kJ/mol	-62.3	-62.3
$\Delta G^{01,T}_{An}$	kJ/mol	-69.0	-69.0
ΔG^{01}_{Met}	kJ/mol	-651.08	-651.08
m_{CO}	mol_{CO}/(mol_x h)	0.35	0.32
μ^{max}	h^{-1}	0.070	0.072
q^{max}_{CO}	mol_{CO}/(mol_x h)	-1.58	-1.46
$Y^{max}_{x/CO}$	mol_x/mol_{CO}	0.057	0.063

G

Derivation of the rewritten Herbert-Pirt equation

The Herbert-Pirt equation rewritten for ATP production and consumption is given by Eq. (G.1).

$$q_{R1}Y_{ATP,R1} + q_{R2}Y_{ATP,R2} = \frac{1}{Y_{x/ATP}^{max}}\mu + m_{ATP} \tag{G.1}$$

with μ the growth rate in h^{-1}, q_R the reaction rate of catabolic reaction R in $mol_p/(g_{DW}\ h)$, $Y_{ATP,R}$ the ATP yield of catabolic reaction R in mol_{ATP}/mol_p, $Y_{ATP/x}^{max}$ the maximum biomass yield on ATP in g_{DW}/mol_{ATP}, and m_{ATP} the ATP required for maintenance in $mol_{ATP}/(g_{DW}\ h)$.

Rewritten in terms of μ:

$$\mu = \left(q_{R1}Y_{ATP,R1} + q_{R2}Y_{ATP,R2} - m_{ATP}\right)Y_{x/ATP}^{max}$$
$$\mu = q_{R1}Y_{ATP,R1}Y_{x/ATP}^{max} + q_{R2}Y_{ATP,R2}Y_{x/ATP}^{max} - m_{ATP}Y_{x/ATP}$$

Assuming a hypothetical case with ATP production in reaction R1 only yields Eq. (G.2):

$$q_{R1}Y_{ATP,R1} = \frac{1}{Y_{x/ATP}^{max}}\mu + m_{ATP} \tag{G.2}$$

with μ the growth rate in h^{-1}, q_{R1} the reaction rate of catabolic reaction R1 in $mol_p/(g_{DW}\ h)$, $Y_{ATP,R1}$ the ATP yield of catabolic reaction R1 in mol_{ATP}/mol_p, $Y_{x/ATP}^{max}$ the maximum biomass yield on ATP in g_{DW}/mol_{ATP}, and m_{ATP} the ATP required for maintenance in $mol_{ATP}/(g_{DW}\ h)$.

Rewritten:

$$q_{R1} = \frac{1}{Y_{x/ATP}^{max}Y_{ATP,R1}}\mu + \frac{1}{Y_{ATP,R1}}m_{ATP}$$

With $4q_{R1} = q_{CO,R1}$:

$$q_{CO,R1} = \frac{4}{Y_{x/CO,R1}^{max}}\mu + 4m_{CO,R1}$$

The Herbert-Pirt equation would be:

$$q_{CO,R1} = \frac{1}{Y_{x/CO,R1}^{max}}\mu + m_{CO,R1}$$

Therefore:

$$0.25Y_{x/ATP}^{max}Y_{ATP,R1} = Y_{x/CO,R1}^{max} \text{ and } \frac{1}{4Y_{ATP,R1}}m_{ATP} = m_{CO,R1}$$

Assuming a hypothetical case with ATP production in reaction R2 only yields Eq. (G.3):

$$q_{R2} Y_{ATP,R2} = \frac{1}{Y_{x/ATP}^{max}} \mu + m_{ATP} \tag{G.3}$$

with μ the growth rate in h^{-1}, q_{R_2} the reaction rate of catabolic reaction R2 in $mol_p/(g_{DW}\ h)$, $Y_{ATP,R2}$ the ATP yield of catabolic reaction R2 in mol_{ATP}/mol_p, $Y_{x/ATP}^{max}$ the maximum biomass yield on ATP in g_{DW}/mol_{ATP}, and m_{ATP} the ATP required for maintenance in $mol_{ATP}/(g_{DW}\ h)$.

Rewritten:

$$q_{R2} = \frac{1}{Y_{x/ATP}^{max} Y_{ATP,R2}} \mu + \frac{1}{Y_{ATP,R2}} m_{ATP}$$

With $2q_{R2} = q_{CO,R2}$:

$$q_{CO,R2} = \frac{2}{Y_{x/CO,R2}^{max}} \mu + 2m_{CO,R2}$$

The Herbert-Pirt equation would be:

$$q_{CO,R2} = \frac{1}{Y_{x/CO,R2}^{max}} \mu + m_{CO,R2}$$

Therefore:

$$0.5 Y_{x/ATP}^{max} Y_{ATP,R2} = Y_{x/CO,R2}^{max} \text{ and } \frac{1}{2Y_{ATP,R2}} m_{ATP} = m_{CO,R2}$$

With respect to the parameter names derived in both hypothetical cases, Eq. (G.1) can be simplified to:

$$\mu = 4 q_{R1} Y_{x/CO,R1}^{max} + 2 q_{R2} Y_{x/CO,R2}^{max} - m_{ATP} Y_{x/ATP}$$

With $m_{ATP}\ Y_{x/ATP}$ being the loss of growth due to maintenance and called m_x from now on, the equation can be further simplified to yield the rewritten Herbert-Pirt equation to estimate the growth rate of *Clostridium autoethanogenum* based on the growth gain due to ATP production in catabolic reactions R1 and R2 and growth loss due to ATP consumption for maintenance (Eq. (G.4)).

$$\mu = \underbrace{4 \cdot Y_{x/CO,R1}^{max} \cdot q_{R1} + 2 \cdot Y_{x/CO,R2}^{max} \cdot q_{R2}}_{\text{gain in growth}} - \underbrace{m_x}_{\text{loss in growth}} \tag{G.4}$$

with μ the growth rate in h^{-1}, $Y_{x/CO,R}^{max}$ the maximum biomass yield on CO for catabolic reaction R in g_{DW}/mol_{CO}, q_R the reaction rate in $mol_{CO}/(g_{DW}\ h)$, and m_x the loss of growth due to maintenance in h^{-1}.

H

Maintenance requirements due to acetic acid inhibition

H.1. Intracellular pH correlation

A certain pH difference between the environment and the cell cytosol is required to maintain a certain proton motive force (PMF) across the cell membrane. Therefore, it was assumed that the intracellular pH of *Clostridium autoethanogenum* (*C. autoethanogenum*) is linearly dependent in the extracellular pH range of 5 to 6.2. Here, it was assumed that at an extracellular pH of 5, the intracellular pH is 6 (Abrini et al., 1994), and at an extracellular pH of 6.2 the intracellular pH is 6.8 (Diender, 2019). The derivation of the equation is given below.

Assume:

$$pH_{in} = a \cdot pH_{out} + b$$

With $pH_{out,1}$ = 5, $pH_{in,1}$ = 6, $pH_{out,2}$ = 6.2 and $pH_{in,2}$ = 6.8, gives:

$$1)\ 6 = 5 \cdot a + b \text{ and } 2)\ 6.8 = 6.2 \cdot a + b$$

Rewriting 1) gives:

$$b = 6 - 5 \cdot a$$

Substitution of 1) in 2) gives:

$$6.8 = 6.2 \cdot a + (6 - 5 \cdot a) \rightarrow a = \frac{2}{3}$$

Substitution of a in rewritten 1) gives:

$$b = 6 - 5 \cdot a \rightarrow b = 2\frac{2}{3}$$

Which results in:

$$pH_{in} = \frac{2}{3} pH_{out} + 2\frac{2}{3}$$

H.2. Calculation of the maintenance increase by Valgepea et al. (2017)

Valgepea, de Souza Pinto Lemgruber, et al. (2017) reported calculating the extra maintenance requirements due to acetic acid inhibition at a total acetic acid concentration (c_{AcT}) of 8 g/L assuming an intracellular pH (pH_{in}) of 6, a cell surface (a_{cell}) of $3.9 \cdot 10^{-12}$ m^2, an acetic acid permeability coefficient (P_{HAc}) of $6.9 \cdot 10^{-5}$ m/s and a cost of 0.25 mole ATP per mole of acetic acid based on an assumed

H^+/ATP stoichiometry for the ATP synthase of 4. Furthermore, a cell diameter of 0.5 μm, a cell height (h_{cell}) of 2.1 μm (Abrini et al., 1994), a cell density of 1100 kg/m^3 (Almeida Benalcázar, 2023), and a molecular biomass weight (Mw_x) of 24 g/mol were assumed. This resulted in a cell surface of 206.36 m^2/mol$_x$.

$$V_{mol_x} = \frac{Mw_x}{\rho_{cell}} = \frac{24 \cdot 10^{-3}\left[\frac{kg}{mol}\right]}{1100\left[\frac{kg}{m^3}\right]} = 2.18 \cdot 10^{-5}\ m^2/mol_x$$

$$V_{cell} = \pi \cdot \left(\frac{d_{cell}}{2}\right)^2 \cdot h_{cell} = \pi \cdot \left(\frac{0.5 \cdot 10^{-6}[m]}{2}\right)^2 \cdot 2.1 \cdot 10^{-6}[m] = 4.12 \cdot 10^{-19}\ m^3$$

$$a_{cell} = a_{cell} \cdot \frac{V_{mol_x}}{V_{cell}} = 3.9 \cdot 10^{-12}[m^2] \cdot \frac{2.26 \cdot 10^{-5}\left[\frac{m^3}{mol_x}\right]}{4.12 \cdot 10^{-19}[m^3]} = 206.36\ m^2/mol_x$$

Subsequently, the intracellular and extracellular concentrations of undissociated acetic acid ($c_{HAc,in}$ & $c_{HAc,out}$) were calculated using an intracellular pH of 6, and extracellular pH (pH_{ext}) of 5, an acetic acid pK_a of 4.76, and a total acetate concentration of 133.2 mol/m^3 (8 g/L).

$$c_{AcT,in} = \frac{1 + 10^{pH_{out} - pK_a}}{1 + 10^{pH_{in} - pK_a}} \cdot c_{AcT,out} = \frac{1 + 10^{5-4.76}}{1 + 10^{6-4.76}} \cdot 133.2 = 19.85\ mol/m^3$$

$$c_{HAc,in} = \frac{c_{AcT}}{1 + 10^{pH_{in} - pK_a}} = \frac{19.85\left[\frac{mol}{m^3}\right]}{1 + 10^{6-4.76}} = 1.08\ mol/m^3$$

$$c_{HAc,out} = \frac{c_{AcT}}{1 + 10^{pH_{out} - pK_a}} = \frac{133.2\left[\frac{mol}{m^3}\right]}{1 + 10^{5-4.76}} = 48.66\ mol/m^3$$

Next, the acetic acid diffusion rate ($r_{HAc,in}$) was determined as 2522.6 mol/mol$_x$/h. With an H^+/ATP stoichiometry of 4, this results in an m_{ATP} of 630 mol$_{ATP}$/mol$_x$/h.

$$\begin{aligned} r_{HAc,in} &= P_{HAc} \cdot a_{cell} \cdot \left(c_{HAc,out} - c_{HAc,in}\right) \\ &= 6.9 \cdot 10^{-5}\left[\frac{m}{s}\right] \cdot 3600\left[\frac{s}{h}\right] \cdot 206.36\left[\frac{m^2}{mol_x}\right] \cdot \left(48.66\left[\frac{mol}{m^3}\right] - 1.08\left[\frac{mol}{m^3}\right]\right) \\ &= 2438.93\ mol/mol_x/h \end{aligned}$$

$$m_{ATP} = \frac{r_{HAc,in}}{Y_{H^+/ATP}} = \frac{2438.93\left[\frac{mol}{mol_x \cdot h}\right]}{4\left[\frac{mol_{H^+}}{mol_{ATP}}\right]} \frac{1}{24\left[\frac{g}{mol}\right]} = 25.41\ mol_{ATP}/(g_{DW}h)$$

Calculation of maximum rates

Allaart et al. (2024) reported a biomass-specific CO uptake rate (q_{CO}) of -119 ±1 mmol/(g_{DW} h). This has been the highest reported q_{CO} and was therefore treated as the maximum biomass-specific CO uptake rate (q_{CO}^{max}) to obtain an indication of the maximum growth rate (μ^{max}) and the maximum rates of catabolic equations R1 (q_{R1}^{max}) and R2 (q_{R2}^{max}).

I.1. Maximum growth rate

The maximum growth rate (μ^{max}) was determined according to the Herbert-Pirt equation for CO fermentation (Eq. (I.1)). The fitted parameters of the maximum biomass yield on CO ($Y_{x/CO}^{max}$) and the maintenance coefficient for growth on CO (m_{CO}) were 1.76 ±0.17 and 1.85 ±0.15 g_{DW}/mol and 5.07 ±2.73 and 6.42 ±2.20 mmol/(g_{DW} h) for the experimental and reconciled data, respectively. Assuming a q_{CO}^{max} of 119 ±1 mmol/(g_{DW} h), a μ^{max} of 0.20 and 0.21 h^{-1} was calculated for the experimental and reconciled data, respectively.

$$-q_{CO}^{max} = \frac{1}{Y_{x/CO}^{max}}\mu^{max} + m_{CO} \tag{I.1}$$

with q_{CO}^{max} the maximum biomass-specific CO consumption rate in mol/(g_{DW} h), $Y_{x/CO}^{max}$ the maximum biomass yield on CO in g_{DW}/mol, μ^{max} the maximum growth rate in h^{-1}, and m_{CO} the maintenance coefficient for growth on CO in mol/(g_{DW} h).

Experimental:

$$\mu^{max} = (119 - 5.07) \cdot 0.00176 = 0.20\ h^{-1}$$

Reconciled:

$$\mu^{max} = (119 - 6.42) \cdot 0.00185 = 0.21\ h^{-1}$$

I.2. Maximum catabolic reaction rates

The maximum rates of catabolic equations R1 (q_{R1}^{max}) and R2 (q_{R2}^{max}) were determined according to Eq. (I.2). The fitted maximum biomass yield on CO for catabolic reactions R1 and R2 were 1.25 ±0.18 and 1.27 ±0.16 g_{DW}/mol and 4.57 ±0.80 and 3.90 ±0.68 g_{DW}/mol for the experimental and reconciled data, respectively. Furthermore, a $q_{R2}^{max}/q_{R1}^{max}$ ratio of 0.6 was assumed. Overall, this yielded a q_{R1}^{max} and q_{R2}^{max} of 19.1 and 21.4 mmol/(g_{DW} h) and 11.5 and 12.8 mmol/(g_{DW} h) for the experimental and reconciled data, respectively.

$$\mu_{max} = 4 \cdot Y_{x/CO,R1}^{max} \cdot q_{R1}^{max} + 2 \cdot Y_{x/CO,R2}^{max} \cdot q_{R2}^{max} \tag{I.2}$$

with μ^{max} the maximum growth rate in h^{-1}, $Y_{x/CO,R}^{max}$ the maximum biomass yield on CO for catabolic reaction R in g_{DW}/mol, and q_R^{max} the maximum reaction rate of catabolic reaction R1 in mol/(g_{DW} h).

Experimental:

$$q_{R1}^{max} = \frac{0.20}{4 \cdot 0.00125 + 2 \cdot 0.00457 \cdot 0.6} = 19.1\ mmol/(g_{DW}h)$$

$$q_{R2}^{max} = 19.1 \cdot 0.6 = 11.5\ mmol/(g_{DW}h)$$

Reconciled:

$$q_{R1}^{max} = \frac{0.21}{4 \cdot 0.00127 + 2 \cdot 0.00390 \cdot 0.6} = 21.4\ mmol/(g_{DW}h)$$

$$q_{R2}^{max} = 21.4 \cdot 0.6 = 12.8\ mmol/(g_{DW}h)$$

I.3. Maximum growth rate Cotter et al. (2009)

Cotter et al. (2009) performed batch cultivations of *Clostridium autoethanogenum* on syngas (50% N_2, 20% CO, 20% CO_2 and 10% H_2) with an gas inflow rate of 10 mL/min. From the exponential growth phase in the growth curve, the maximal growth rate was obtained and yielded 0.093 h^{-1}.

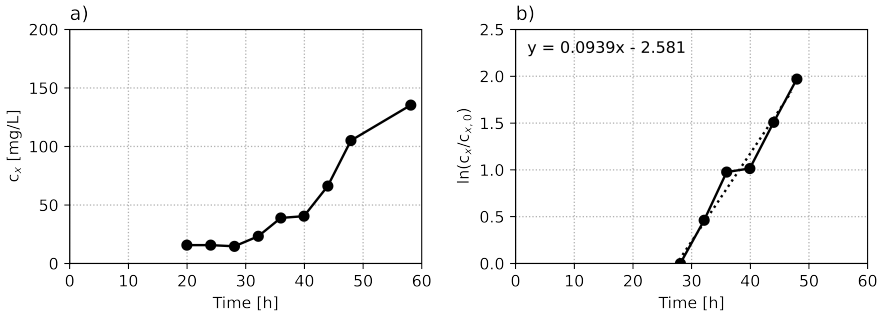

Figure I.1: Biomass concentration (c_x) plotted as a function of time (t) for batch cultivation of *Clostridium autoethanogenum* grown on syngas (50% N_2, 20% CO, 20% CO_2 and 10% H_2) with an gas inflow rate of 10 mL/min. The data is extracted from Figure 5A (Cotter et al., 2009). With a) the growth curve of *C. autoethanogenum* and b) the fitted exponential growth phase.